Alma Mater Studiorum – Università di Bologna

DOTTORATO DI RICERCA IN

SCIENZE FARMACEUTICHE

Ciclo XXI

Settore scientifico disciplinare di afferenza: CHIM/08

TITOLO TESI

CHARACTERIZATION OF L-TYPE CALCIUM CHANNEL BINDING-SITE OF A NEW CLASS OF CALCIUM MODULATORS BY A MULTIDISCIPLINARY APPROACH

Presentata da: Dott. Maria Paola Ugenti

Coordinatore Dottorato **Relatore**

Prof. Maurizio Recanatini **Prof. Alberto Chiarini**

Esame finale anno 2009

a Emanuele

TABLE OF CONTENTS

1. INTRODUCTION

Ca^{2+} ions play crucially important roles in regulating a variety of cellular functions. They provide the basis for excitability in nerve and muscle cells. In neurons, they trigger the release of neurotransmitters from nerve the terminal. In heart and skeletal muscle, they regulate excitability and transform the action potential in mechanical contraction. In addition, Ca^{2+} ions are involved in a broad range of cell regulatory processes – e.g. hormone secretion and volume regulation, gene expression and mediating cell death. Several hereditary diseases have been linked to mutations in genes encoding ion channels. Timothy's syndrome [1], which is a novel disorder characterized by multiorgan dysfunction including lethal arrhythmias, webbing of fingers and toes, congenital heart disease, immune deficiency, intermittent hypoglycemia, cognitive abnormalities, and autism. In every case, Timothy syndrome results from the identical, de novo $Ca_V1.2$ missense mutation G406R in exon 8a. $Ca_V1.2$ is expressed in all affected tissues. Functional expression reveals that G406R produces maintained inward Ca^{2+} currents by causing nearly complete loss of voltage-dependent channel inactivation. This likely induces intracellular Ca^{2+} overload in multiple cell types. In the heart, prolonged Ca^{2+} current delays cardiomyocyte repolarization and increases risk of arrhythmia, the ultimate cause of death in this disorder. These discoveries establish the importance of $Ca_V1.2$ in human physiology and development and implicate Ca^{2+} signaling in autism. Molecular electrophysiological investigation of these so-called channelopathies elucidate the pathophysiology of these rare diseases and help to understand disease-causing mechanisms in other, more common disorders with similar symptoms. Furthermore, insight into the molecular basis of these disorders allows a more rational approach to therapy. On the other hand, disease-causing mutations point to functional important parts of the protein and help to understand ion channel gating on a molecular level.

1.1. Cardiac L-VDCC Structure

The L-VDCCs are heterotetrameric polypeptide complexes comprised of the α_1, α_2/δ, and β (and in some tissues γ) subunits (See Figure 1 [2]) that allow depolarization-induced calcium influx into the cytosol. In all excitable tissues, Ca^{2+} channels invariably contain α_1, α_2/δ, and β subunits. These are considered the functional minimum "core" for Ca^{2+} channel assembly. The accessory subunits (β, α_2/δ) are tightly, but not covalently, bound to the α_1 subunit and modulate the biophysical properties and trafficking of the α_1 subunit to the membrane. The stoichiometric ratio between the α_1,α_2/δ and the β_2 subunits is 1:1:1 [3].

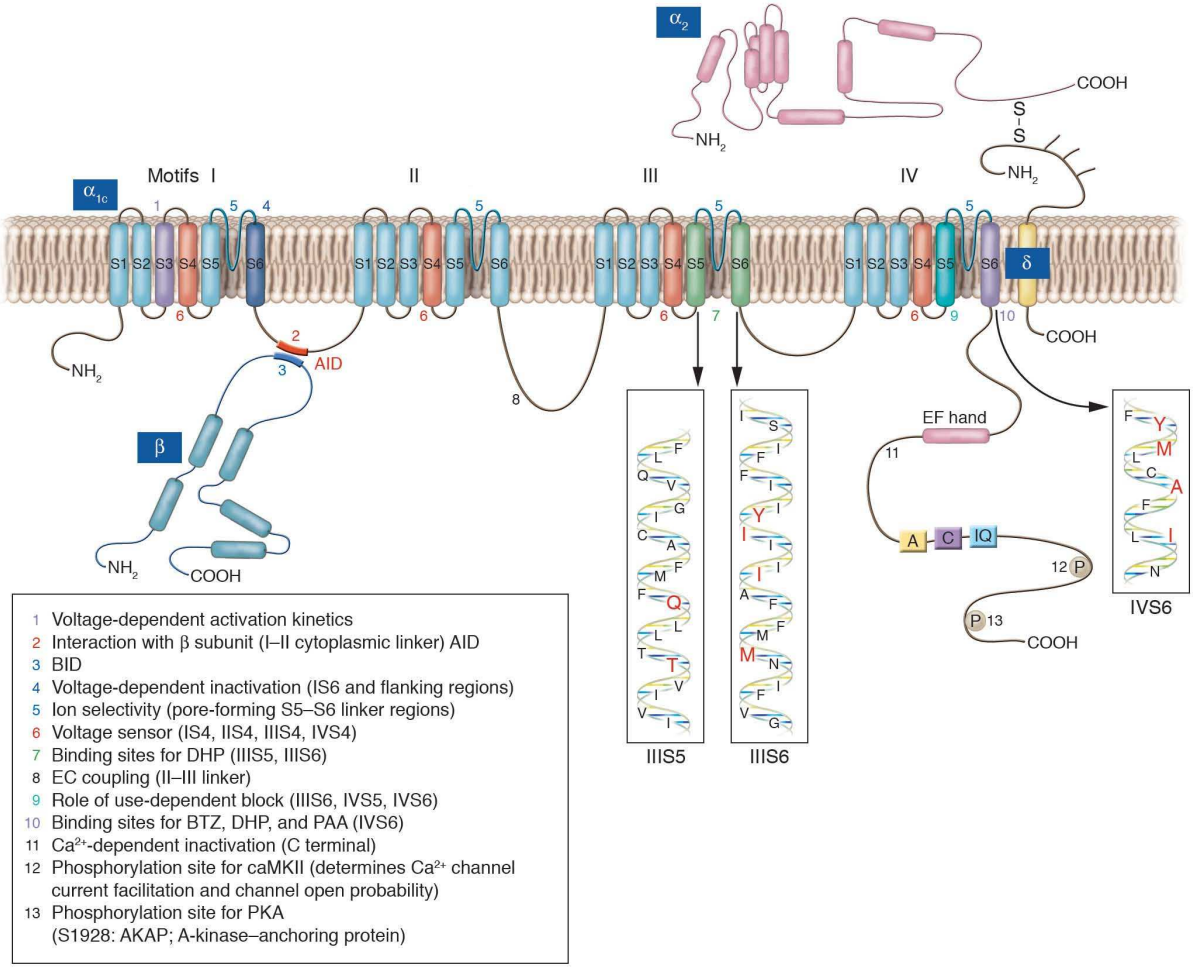

Figure 1. Structural organization of L-VDCC. Sites of interaction between subunits are indicated. The numbers point to areas found to be important to specific channel functions. The EF hand, A, c, and IQ motifs represent specific peptide sequences involved in CaM binding. Key amino acids required for Ca^{2+} antagonist binding are represented in red letters. At least 5 consensus sites for phosphorylation by cAMP-dependent PKA have been discovered within the C-terminal tail of α_{1C}. AKAP79 (79 kDa A-kinase-anchoring protein) helps to target PKA to its specific substrate. COOH, carboxy-terminal.

1.1.1. α_1 subunits

The founding members of this superfamily are the voltage-gated sodium channels (Na^+). The Ca^{2+} channel α_1 subunit (170-240 kDa) consists of four homologous motifs (I-IV) each composed of six membrane-spanning α-helices (termed S1 to S6) linked by variable cytoplasmic loops (linkers) between the S6 and S1 segments. The different types of α_1-subunits differ most strikingly in two principal regions: the cytoplasmic loop linking motifs II and III and the carboxy-terminal region. The currents that are supplied by the voltage-dependent calcium channels (VDCCs) are called: L-, N-, P-, Q- (or P/Q) - R- and T-types. To date 10 α_1 subunit genes have been identified (Table 1 and 2 [4,5]), separated into four classes. The first class is the L-type channels, consisting of $Ca_v1.1$ (α_{1S}), 1.2 (α_{1C}), 1.3 (α_{1D}), 1.4 (α_{1F}). Only the α_{1C} (DHP-sensitive) is expressed in high levels in cardiac muscle. The second class contains $Ca_v2.1$ (α_{1A}), 2.2 (α_{1B}), 2.3 (α_{1E}) which form P/Q-, N- and possibly R-type channels, respectively and are all found in brain. They are primarily responsible for initiation of synaptic transmission at fast synapses in the nervous system. They have a larger intracellular loop connecting domains II and III, which contains a synaptic protein interaction site that binds SNARE proteins involved in exocytosis [6]. The third class of channels are the T-type channels, $Ca_v3.1$ (α_{1G}), 3.2 (α_{1H}), 3.3 (α_{1I}) which are localized to the brain, kidney and heart and originally called low voltage activated (LVA) channels and unlike L-type channels, they are relatively insensitive to DHPs. Ca_v3 channels conduct T-type Ca^{2+} currents which are important in wide variety of physiological functions, including neuronal firing, hormone secretion, smooth muscle contraction, cell proliferation of some cardiac tissue and myoblast fusion. In the heart, T-type channels are abundant in sino-atrial pacemaker cells and Purkinje fibers of many species and are important in pacemaker activity by setting the frequency of action potential firing. It has been reported that the T- type channels are re-expressed in the ventricle of some animal models of heart failure (HF) suggesting that T-channels play a role in cardiac disease. The neuronal T-type channels can generate low-threshold spikes that lead to burst firing and oscillations which are prominent in the thalamus and implicated in variety of neurological disorders [5]. In addition to these well characterized Ca^{2+} channels, the cloning of a single Ca_v-like protein suggest the

existence of a fourth subfamily [7]. This novel protein contains conserved amino acids found in Ca^{2+} (EEEE) or Na^{+} channels (DEKA), including EEKE residues in the corresponding region of its pore loops. However, this new putative channel has not been functionally expressed in a heterologous expression system (*Xenopus leavis* oocytes).

The α_1 subunit incorporates the ion-selective pore, voltage sensor, gating machinery, and the binding sites for channel-modulating drugs [3,8,9], and is autoregulatory. The α_1-subunit is a substrate for protein kinase A, protein kinase C, and Ca^{2+}-calmodulin dependent kinase. The pore is asymmetric, with conserved glutamate (EEEE) or aspartate residues comprising the ion-selectivity filter(s) [10-13], located between segments S5 and S6 of each motif. Cloning and analysis of the VDCC have revealed that the positively charged fourth transmembrane segment (S4) of each motif is highly conserved and is likely to form an α-helix in which every third or fourth residue is basic (Arg or Lys). It is thought that the S4 α-helices traverse the membrane electric field and that, as a response to a depolarizing stimulus, they move outward into the extracellular space and initiate conformational changes from non-conducting to conducting states of the channel ('sliding –helix model') (reviewed in ref. [14]). However, the emerging models are still controversial. Most structure-function studies support a spiral or rotational motion of the S4 or S3 plus S4 α-helices through the channel protein in order to move gating charges across the membrane electric field.

Table 1. Physiological function and pharmacology of calcium channels

Channel	Current	Localization	Specific Antagonists	Cellular Functions
$Ca_v1.1$	L	Skeletal muscle; transverse tubules	Dihydropyridines; phenylalkylamines; benzothiazepines	Excitation-contraction coupling
$Ca_v1.2$	L	Cardiac myocytes; smooth muscle myocytes; endocrine cells; neuronal cell bodies; proximal dendrites	Dihydropyridines; phenylalkylamines; benzothiazepines	Excitation-contraction coupling; hormone release; regulation of transcription; synaptic integration
$Ca_v1.3$	L	Endocrine cells; neuronal cell bodies and dendrites; cardiac atrial myocytes and pacemaker cells; cochlear hair cells	Dihydropyridines; phenylalkylamines; benzothiazepines	Hormone release; regulation of transcription; synaptic regulation; cardiac pacemaking; hearing; neurotransmitter release from sensory cells
$Ca_v1.4$	L	Retinal rod and bipolar cells; spinal cord; adrenal gland; mast cells	Dihydropyridines; phenylalkylamines; benzothiazepines	Neurotransmitter release from photoreceptors
$Ca_v2.1$	P/Q	Nerve terminals and dendrites; neuroendocrine cells	ω-Agatoxin IVA	Neurotransmitter release; dendritic Ca^{2+} transients; hormone release
$Ca_v2.2$	N	Nerve terminals and dendrites; neuroendocrine cells	ω-Conotoxin-GVIA	Neurotransmitter release; dendritic Ca^{2+} transients; hormone release
$Ca_v2.3$	R	Neuronal cell bodies and dendrites	SNX-482	Repetitive firing; dendritic calcium transients
$Ca_v3.1$	T	Neuronal cell bodies and dendrites; cardiac and smooth muscle myocytes	None	Pacemaking; repetitive firing
$Ca_v3.2$	T	Neuronal cell bodies and dendrites; cardiac and smooth muscle myocytes	None	Pacemaking; repetitive firing
Cav3.3	T	Neuronal cell bodies and dendrites	None	Pacemaking; repetitive firing

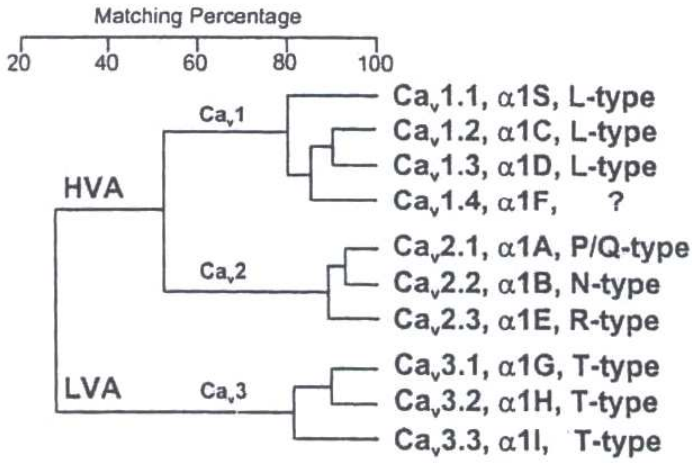

Table 2. Nomenclature and relationships of voltage-gated calcium channels.

Channel name	$Ca_V1.2$
Description	Voltage-gated calcium channel α_1 subunit
Other names	α_{1C}, cardiac or smooth muscle L-type Ca^{2+} channel, cardiac or smooth muscle dihydropyridine receptor
Molecular information	Human: 2169aa, L29529 (cardiac; PMID: 8392192), 2138aa, Z34815 (fibroblast; PMID: 1316612); 2138aa, AF465484 (jejunum; PMID: 12176756); chr. 12p13.3, *CACNA1C*, LocusID: 775 Rat: 2169aa, M59786 (aortic smooth muscle; PMID: 2170396); 2140/2143aa, M67516/M67515 (brain; PMID: 1648941); chr. 4q42, Cacna1c, LocusID: 24239 Mouse: 2139aa, L01776 (brain; PMID: 1385406); chr. 6, Cacna1c, LocusID: 12288 (see 'Comments')
Associated subunits	$\alpha_2\delta$, β, γ[1,2]
Functional assays	Patch-clamp (whole-cell, single-channel), calcium imaging, cardiac or smooth muscle contraction hormone secretion
Current	$I_{Ca,L}$
Conductance	Ba^{2+} (25pS) > Sr^{2+} = Ca^{2+} (9pS)[3]
Ion selectivity	$Ca^{2+} > Sr^{2+} > Ba^{2+} \gg Mg^{2+}$ from permeability ratios
Activation	V_a = −17 mV (in 2 mM Ca^{2+}; HEK cells)[4]; −4 mV (in 15 mM Ba^{2+}; HEK cells) to −18.8 mV (in 5 mM Ba^{2+}; HEK cells and *Xenopus* oocytes)[5–7]; τ_a = 1 ms at +10 mV[5]
Inactivation	V_h = −50 to −60 mV (in 2 mM Ca^{2+}; HEK cells),[4] −18 to −42 mV (in 5–15 mM Ba^{2+}; HEK cells)[5,7,8,9]; τ_{fast} = 150 ms, τ_{slow} = 1100 ms; 61% inactivated after 250 ms in HEK cells[8] (at V_{max} in 15 mM Ba^{2+})[4]; ~70% inactivation after 1 s (at V_{max} in 2 mM Ca^{2+})[4]; inactivation is accelerated with Ca^{2+} as charge carrier (calcium-dependent inactivation: 86% inactivated after 250 ms[8,10])
Activators	BayK8644, dihydropyridine agonists, FPL64176[10,11]
Gating modifiers	Dihydropyridine antagonists (e.g., isradipine, IC_{50} = 7 nM at −60 mV; nimodipine, IC_{50} = 139 nM at −80 mV)[6,9]
Blockers	Nonselective: Cd^{2+} [12]; selective for $Ca_V1.x$: devapamil (IC_{50} = 50 nM in 10 mM Ba^{2+} at −60 mV) and other phenylalkylamines; diltiazem (IC_{50} = 33 μM in 10 mM Ba^{2+} at −60 mV and 0.05Hz)[12]
Radioligands	(+)-[^{3}H]isradipine (K_d < 0.1 nM) and other dihydropyridines; (−)-[^{3}H]devapamil (K_d = 2.5 nM), (+)-*cis*-[^{3}H]diltiazem (K_d = 50 nM)[11]
Channel distribution	Cardiac muscle, smooth muscle (including blood vessels, intestine, lung, uterus); endocrine cells (including pancreatic β-cells, pituitary); neurones[13]; subcellular localization: concentrated on granule-containing side of pancreatic β-cells[14]; neurons (preferentially somatodendritic)[15]
Physiological functions	Excitation-contraction coupling in cardiac or smooth muscle, action potential propagation in sinoatrial and atrioventricular node, synaptic plasticity, hormone (e.g., insulin) secretion[10,13,16,17]
Mutations and pathophysiology	Required for normal embryonic development (mouse, zebrafish)[18,19]; de novo G406R mutation in alternative exon 8A in 1 allele causes Timothy syndrome[20]
Pharmacological significance	Mediates cardiovascular effects of clinically used Ca^{2+} antagonists[17]; high concentrations of dihydropyridines exert antidepressant effects through $Ca_V1.2$ inhibition[17]
Comments	Tissue-specific splice variants exist—in addition to cardiac channels, smooth muscle and brain channels have been cloned[7,21,22]; the gene for $Ca_V1.2$ was first isolated and characterized in rabbit heart (2171aa, P15381, X15539)

1.1.2. Accessory subunits

α_2/δ subunits

The $\alpha_2\delta$ subunits are closely associated with the α_1 subunit by surface interaction and intracellularly linked through a disulfide bridge to a small protein, the δ subunit. The α_2 subunit is entirely extracellular and δ has a single transmembrane region with a very short

intracellular part. The α_2 and δ subunits are encoded by the same gene which is separated by proteolytic cleavage [15]. Ellis *et al.* [16] first cloned the α_2/δ subunit from rabbit skeletal muscle thinking there was only one product from the gene. Presently, at least 4 isoforms encoded by separate genes and have been identified ($\alpha_2/\delta_{1, 2, 3, 4}$) [15,17,18]. The issue of *in vivo* structure-function has yet to be resolved. In heterologous expression systems, co-expression of the α_2/δ subunit affects α_1 function by increasing channel density, charge movement and B_{max} of drug binding (e.g. the DHP, isradipine), with smaller effects on K_D and variable minor effects on channel kinetics [19-21] (and references cited therein). It is probable that α_2/δ and β subunits "drive" the α_1 subunit to the membrane in the correct insertion mode. The α_2/δ_1 subunit is ubiquitously distributed, and possesses a stereo-selective high-affinity binding site for certain GABA-antagonists, such as the drug gabapentin, (1-aminomethyl cyclohexane acetic acid) which is widely used to treat epilepsy, pain, sleep disorders, and many other paroxysmal neurological conditions [22-24]. The α_2/δ_2 subunit also binds gabapentin but at a low affinity, while α_2/δ_3 and α_2/δ_4 do not bind this drug. Mice deficient in α_2/δ_2 exhibit neurological dysfunction such as enhanced seizure susceptibility and cardiac abnormalities, viz. a tendency to bradycardia [25]. The recently cloned human α_2/δ_4 [17] is localized to fetal liver, colon, pituitary, and adrenal gland, and is associated with the α_{1C}-subunit (Ca_v 1.2) and the β_3 subunit. This reinforces the complexity of L-VDCCs, since subunit association appears to confer biophysical properties [10,20]. This rich diversity opens avenues for exciting physiological and pathological discoveries [26].

The γ subunits

It was originally thought that the γ subunit was the product of a single gene and only existed in skeletal muscle [18]. It is interesting that characterization of a genetic defect that induces epileptic seizures in *stargazer* mice [27] led to the detection of a family of at least 5 novel isoforms of the γ subunit that are almost exclusively expressed in brain. To date, 8 genes, encoding a variety of γ subunit isoforms have been identified [28]. Although $Ca_v\gamma_1$ is associated specifically with skeletal muscle $Ca_v1.1$ channels, there is evidence that the γ_2 subunit interacts with AMPA receptor subunits [29] and possibly other membrane-

signaling proteins. Unlike other auxiliary subunits (β and α_2/δ), the γ subunits do not have a significant role in the membrane trafficking of the calcium channels. γ_1 modulates the biophysical properties of the Ca^{2+} channel. Clearly this is a very important subunit, but since it does not appear to be expressed in heart, it is not discussed further.

β Subunit structure

Four β subunit (β_1–β_4) isoforms have been described. All are hydrophilic, non-glycosylated, and located within the cell and only β_2 has been reproducibly shown to form cardiac L-VDCCs. The β subunit does not have a membrane spanning region. It is tightly bound to a highly conserved motif in the cytoplasmic linker between repeats I and II of all cloned high voltage-activated α_1 subunit isoforms, called the α-interacting domain (AID) [30,31], and also to a secondary site [32]. Just recently, elucidation of the high-resolution 3D structure [32-34] of a β subunit has shed light on the molecular mechanism of binding of the α_1 to β subunits. Previous work suggested that the β subunit interacts with α_1 primarily through a highly conserved 30 amino acid motif within the β-subunit, called the β-interaction domain (BID), which binds directly to the AID. However, Van Petegem and colleagues [33] reported that the BID engages the AID through a conserved hydrophobic cleft, and named the α-binding pocket (ABP). Interference with AID-ABP binding might provide a novel way to modulate Ca^{2+} channel function in pathological states. The I-II loop of the α_1-subunit contains an endoplasmic reticulum retention signal that restricts cell surface expression. The β-subunit reverses the inhibition imposed by the retention signal [35].

The roles of the β auxiliary subunits in influencing channel function

Though much knowledge has been accumulated about the multiple roles for the β-subunit in the processing and functioning of L-VDCC using heterologous recombinant co-expression of the different subunits [20,36], the physiological significance of subunit interaction in the context of native tissue is only just beginning to be studied via transgenic approaches and adenovirus-mediated intracellular incorporation of genes, encoding Ca^{2+} channel β-subunits into single cells [3,37,38]. In general, co-expression of the β-subunits modulates the

biophysical properties of the L-VDCC α_1 subunit, producing a substantial increase in Ca^{2+} current amplitude and/or changes in the current kinetics (leftward shift of the current-voltage (*I-V*) relationship) which is consistent with the involvement of the S4 region of the α_1 subunit voltage sensor region. Moreover, it has been shown that α_1 subunits expressed in the absence of β subunits are not regulated by the β-adrenergic system [39] or by pH changes [40]. Frequency- and prepulse-dependent facilitation of L-VDCC activity is regulated by certain classes of β subunits [41]. By employing an antisense strategy to lower the numbers of endogenous β subunits in oocytes, leaving only α_1 subunits intact, a loss of current occurred, implying that the β subunit functions in the assembly and expression of the α_1 subunit [42]. Dr. Schwartz's group provided evidence that the β subunits have a chaperone-like role, in trafficking α_{1C} subunits from the ER to the plasma membrane, and inserting in its proper geometry [43]. Viard *et al.* [44] demonstrated that a region of this β_{2a} subunit is involved in phosphatidylinositol 3 kinases (PI3K)-induced increases of $Ca_v1.2$ (rat brain) channel density. The PIK3-induced regulation is mediated by PIP3–activated Akt/PKB and requires phosphorylation of $Ca_v\beta_2$ subunits on Ser574, which is common to all splice variants of the β_2 subunits. These results indicate that PIK3 regulates Ca^{2+} channel trafficking to the plasma membrane and may be a general mechanism for the regulation of Ca^{2+} entry into excitable cells [44]. The β_1-subunit also has a crucial role in EC coupling as proven by β_1-KO mice with impaired EC coupling and early lethality [45]. The exact mechanism for the lack of EC coupling is not known but it is possible that the deficiency in the assembly process of the α_1/β complex results in the degradation of the α_1 subunit. The role of the β_2 subunit in EC coupling is unclear [46]. β_3 null mice have no detectable abnormalities in the heart [47].

Hullin *et al.* [48] cloned two distinct β subunits, β_2 and β_3, from rabbit heart and showed an association with the α_1 subunit of the L-VDCC. The amino acid homology of these subunits was similar to that of β_1, originally cloned from skeletal muscle [9]. It should be noted that β_{2a}, an important subtype of this subunit, is palmitoylated [49,50]. This modification is

associated with membrane targeting of non-transmembrane proteins (such as the β subunit) to specific areas including the plasma membrane. The role of the β subunits in L-VDCC expression is well characterized although we still do not know how the β subunits modulate preexisting α_1 subunit expression. Colecraft *et al.* [51] devised a novel system in which recombinant adenoviruses were used to express GFP-fused β_{1-4} subunits in cultured adult rat cardiomyocytes. While all four subunits (β_{1b}, β_{2a}, β_3, β_4) increased I_{Ca} density, their effects on inactivation kinetics were non-uniform. The conclusion of this study was that overexpression of the newly cloned rat splice variant of a β_{2b} in adult rat heart cells yielded channels that were identical to that in the native unmodified rat heart cells.

β_3 is most abundant in brain but also is expressed in heart, aorta, lung, trachea, and skeletal muscle. Expression levels of various β subunit isoforms [48,51,52] indicate that altered single-channel behavior in human heart may be due to differential effects and changes in β subunit gene products.

1.1.3. Regulation of intracellular Ca^{2+}: Cardiac Dysfunction

The control of myocardial Ca^{2+} is crucial for the maintenance of normal rhythm, regulation of contraction, enzymatic reactions, as well as, growth and development. For many years, drugs modifying cardiac function by affecting myocardial Ca^{2+} have been used to modulate Ca^{2+} fluxes, levels of Ca^{2+} at storage sites, or increase the Ca^{2+} sensitivity of the contractile proteins. In general, drugs that reduce Ca^{2+} loading of the cardiac myocyte serve to "protect" the heart from the ultimate cause of myocardial cell death, *i.e.*, Ca^{2+} overload. Among the many problems that arise from Ca^{2+} overload, ventricular tachycardia is the most prominent and is often life threatening. Both early and delayed after-depolarizations can be treated with Ca^{2+} channel-blockers (CCBs). Likewise, arrhythmias ascribable to disorders of conduction are also treated with CCBs that function presumably by inhibiting conduction disturbances in the sinoatrial or atrioventricular junction. Clinical trials show that CCB's do not reduce mortality of heart failure. The state of art in pharmacotherapy of heart failure, considering its epidemic nature in the world, is very disappointing. Recent reviews have

emphasized that we are dealing with a highly complex, multifaceted disease almost similar to the cancers [53-57].

Although considerable information is known regarding the L-VDCC and its role in EC coupling, the consequence of increased Ca^{2+} channel density remains speculative and controversial. In Dr. Schwartz's laboratory a transgenic mouse model was designed overexpressing the L-VDCC α_{1C} subunit (α_{1C}-Tg) as a way to increase $[Ca^{2+}]_i$. The transgenic mouse model exhibits a sustained, low level $[Ca^{2+}]_i$ increase in cardiac cells throughout the life of the animal; hypertrophy develops slowly and the ensuing failure occurs at 9-12 months. This model mimics human dilated, hypertrophic-(ischemic) cardiomyopathy.

1.1.4. Ca^{2+} channel antagonists (blockers, "CCB") and Ca^{2+} binding domains

L-VDCC is an important pharmacologic target in the treatment of a number of conditions. In the late 1960s, Fleckenstein showed that Ca^{2+}-antagonists like verapamil protected the rat heart against structural damage associated with prolonged $[Ca^{2+}]_i$ overload. Among the many problems that arise from Ca^{2+} overload, ventricular ectopic rhythm is the most prominent (ventricular fibrillation). In pharmacological models, the CCBs are considered promising drugs to treat supraventricular arrhythmias, hopefully preventing lethal ventricular fibrillation (VF).

Using a variety of techniques, several laboratories have identified individual amino acids within the L-VDCC α_1 subunit that participate in the formation of the major drug-binding domains. Three classes of organic CCBs, include: Dihydropyridines (DHPs), phenylalkylamines (PAAs), and benzothiazepines (BTZs). Each drug type, DHP, PAA and BTZ has separate but overlapping, or allosterically-linked, Ca^{2+} channel-binding sites at IIIS6 and IVS6, IVS6 and IIIS6, and IVS6 motifs (Figure 2), respectively. Nine amino acid residues in segments IIIS5 [58], IIIS6 [59] and IVS6 contribute to the "DHP pocket". The four amino acid region (YMAI) in motif IVS6 is a common binding site for both BTZ [60] and PAA [61,62].

DHPs block the calcium channel at the extracellular level and have greater vascular selectivity than other classes of CCBs. When used clinically, as a result of vigorous peripherial vasodilatation, they tend to cause reflex tachycardia and often increase

contractility, as catecholamines activate the calcium channel intracellularly, on a different site from that blocked by DHPs. Tissue selectivity is considered to be one of the most beneficial properties of CCBs as it diminishes the likelihood of undesirable side-effects. In general, vascular selectivity permits coronary and peripherial dilatation in the absence of significant myocardial depression. Nifedipine is at least 10 times more vascular than myocardial-selective compared to Verapamil and Diltiazem. Nisoldipine and felodipine are at least 1000 times more selective than nifedipine. On the other hand it can be a disadvantage, causing adaptive reactions. Verapamil and Diltiazem have prominent effects on nodal tissues. The BTZs are thought to approach their binding site on $Ca_v1.2$ from the extracellular face of the plasma membrane [63]. Verapamil and Diltiazem have a use-dependent or a frequency-dependent effect. The more frequently the calcium channel opens, the better the penetration to the binding site. This explains their effect on nodal tissue in paroxysmal supraventricular tachycardia. The general absence of 'use-dependence' and the presence of voltage-sensitivity of DHP binding explain their vascular selectivity. The use-dependent blockade by diltiazem of L-VDCCs would be expected to inhibit large increases in Ca^{2+} influx accompanying a sudden increase in heart rate. In addition, the acceleration of inactivation would be expected to reduce Ca^{2+} influx during action potentials that arise from normal negative resting potentials. Both of these effects likely contribute to the beneficial effect of Diltiazem when used as a prophylactic or depressant of supraventricular tachycardia [64,65]. Diltiazem facilitates the inactivation of the channel both by accelerating the transition from the activated state to the inactivated state and by decelerating the transition from the inactivated state to the available state. However, these drugs have not emerged unequivocally favorable in all clinical studies to date. Verapamil and Diltiazem can, in some cases, prevent episodes of acute ischemic VF in humans, but they do not have much of a beneficial effect on overall mortality as do the β-blockers, and the ACE inhibitors. The clinical implications of this finding reported in different clinical trials are similar to that reported for encaidine and flecainidine in the Cardiac Arrhythmia Suppression Trial [66]. Patients suffering from coronary disease may die of either heart failure or arrhythmias. Likewise, arrhythmias ascribable to disorders of conduction are also treated with CCBs that function, presumably, by inhibiting conduction disturbances in the sinoatrial or atrioventricular junction. Although CCBs bind specifically to regions of the α_{1C} subunit of

the L-VDCC, these drugs are not currently judged as being helpful in the setting of congestive heart failure. In fact, all clinical trials to date, with the exception of the Prospective Randomized Amlodipine Survival Evaluation (PRAISE I) study in where the patents had congestive heart failure, were a failure. However, a sub-group analysis (PRAISE II) revealed that improved clinical symptoms were seen only in patients with heart failure of a non-ischemic cardiomyopathic nature. A favorable effect on survival was found only in patients without a history of angina [67]. In the Third Vasodilator-Heart Failure Trial [68] (V-HeFT III), felodipine was administered to patients with congestive heart failure in a setting of stable therapy with enalapril, diuretics and digoxin. The drug had neither a beneficial or deteriorating effect despite the improvement in exercise performance and LV function, as reported previously in the V-HeFT II trial in patients with chronic CHF [69]. Chronic Nifedipine (has a strong peripheral vasodilating effects) therapy caused a higher incidence of clinical deterioration and worsening of HF [70,71]. The DEFIANT-I study (Doppler Flow and Echocardiography in Functional Cardiac Insufficiency: Assessment of Nisoldipine Therapy) was a double-blind randomized study of the effects of the DHP nisoldipine on left ventricular (LV) size and function after acute myocardial infarction (MI). Diastolic LV function improved in patients recovering from acute MI [72]. The Danish Verapamil Infarction Trial II (DAVIT II) demonstrated that long term treatment with verapamil significantly improved reinfarction survival after acute MI. Verapamil significantly reduced (35%) the 18 month mortality rate, but produced no change in mortality in the heart failure (HF) group [73]. Hypertensive patients are often treated with CCBs to reduce cardiovascular disease risk, but the overall benefit compared with atenolol and hydrochlorothiazide and ACE inhibitors is controversial and problematic. The Controlled Onset Verapamil Investigation of Cardiovascular End Points (CONVINCE) trial indicated that the effectiveness of CCB therapy was comparable to diuretic and β-blocker treatment in reducing cardiovascular disease [74]. According to the Multicenter Diltiazem Postinfarction Trial [75] analysis diltiazem exerted no overall effect on mortality or cardiac events in a large population of patients with previous infarction, but in patients with pulmonary congestion diltiazem was associated with an increased number of cardiac events and mortality. Interestingly, the increase in mortality was not accompanied by a worsening of HF. Despite these concerns, in the Studies of Left Ventricular Dysfunction Trial

(SOLVD), 3-35% of the patients were treated with CCBs in addition to digitalis and diuretics. CCB use was associated with significantly increased risks of fatal and nonfatal MI [76]. CCBs have a favorable systemic vasodilator effect and should improve diastolic relaxation. One would assume that CCBs inhibiting Ca^{2+} influx into myocardial cells might be beneficial because theoretically they could reduce Ca^{2+} overload, an important trigger for activating certain downstream Ca^{2+}-dependent pathways involved in hypertrophy and cardiac dysfunction. Clinical trials to date however have been disappointing. In fact, it has been suggested that the effects of CCBs on mortality in patients with HF may be associated with increased sympathetic activity. Summing up the therapy of heart failure, the β-AR blockers, ACE Inhibitors (angiotensin-converting enzyme inhibitors)), diuretics, and aldosterone receptor(s) inhibitors (spironolactone and new derivatives) have achieved therapeutic success probably through multiple actions that culminate in a positive "remodeling" of the diseased heart ([77] Review). The state of art in the pharmacotherapy of heart failure, considering its epidemic nature in the world, is also disappointing.

As discussed above, although CCBs bind specifically to regions of the α_{1C} subunit of the L-VDCC, these drugs are not currently judged as being helpful in the setting of congestive heart failure, and should be if used at all, with caution. All clinical trials underscore the use of drugs that inhibit the sympathetic nervous system and reduce the load on the heart.

Use-dependence

Less detailed structural information is known regarding the mechanism of use-dependent block, a feature that is critical to the activity of therapeutically successful L-VDCC antagonists. The modulated receptor theory states that drug affinity for a specific receptor on the channel is modulated by the channel state. The model has been proposed (modulated receptor hypothesis) that can account for the voltage and use-dependent block of Na^+ channels by local anesthetics [78,79]. Each channel (sodium and calcium) blocker has a characteristic association and dissociation rate constant for channels in each of these states. The more frequently the Ca^{2+} channel opens, the better penetration is for the drug to reach the binding site. Verapamil and Diltiazem preferentially interact with the open and inactivated states of the channel (reviewed in ref.[80], explaining their preferential effect on nodal tissue. Single amino acids have now been identified as inactivation determinants in

motifs IIIS6, IVS6 and IVS5 with some of them also serving as high affinity determinants for the DHP receptor site [80-82].

Diltiazem is the prototype benzothiazepine and is the only drug of this type currently in clinical use (Cardizem). Diltiazem exhibits modest selectivity for block of vascular muscle over cardiac muscle L-type channels, but is also useful in treatment of arrhythmias due to the block of L-type channels in the heart. The BTZ binding site on L-VDCCs is allosterically linked to the binding sites for PAAs and DHPs. BTZ binding inhibits PAA binding but stimulates DHP binding to L-type channels in a temperature dependent manner. Diltiazem was found to produce more tonic block than methoxyverapamil but less than nifedipine and nitrendipine. The frequency-dependent block by Diltiazem is due to rapid binding to the open state and preferential binding to the inactivated channel.

1.1.5. Voltage-gated cation channels

The gating of most ion channels is regulated by different specific mechanisms, which change their permeation properties: membrane potential (voltage-gated ion channels), specific chemical signals such as Ca^{2+} or synaptic transmitters (ligand gated ion channels), or changes in the membrane conformation (mechanosensitive or volume sensitive ion channels etc.). Voltage-gated cation channels are responsible for the generation and propagation of action potentials. Whereas potassium channels form tetramers of four identical domains, the main molecule of the Na^{+} and Ca^{2+} channels is one large subunit. The pore of the voltage-gated cation channels is formed by the loops, which are located in between the S5 and S6 transmembrane regions of the four domains/motifs. The S4 segments contain four to eight positively charged residues conferring voltage dependence to the channel protein (for a review see [3,83]. At the resting membrane potential (-60 to –90mV) the channels usually reside in closed state and are not permeable for ions (Figure 2 [83]). At very hyperpolarized potentials, where the channels are in their resting state, inactivation is removed (steady-state inactivation curve). This means that the inactivation gate is not occluding the channel and if nothing else was in the way ions could flow through the pore. However at those very negative potentials, the activation gates are all closed. Those closed gates block the pore and prevent conduction. Upon depolarization, they open their gate and can conduct ions, a process called activation. This is triggered by the movement of the voltage sensors. Some

of the channels, after the opening of the activation gate, can close another existing gate upon ongoing depolarization a process called inactivation. The inactivation gates begin to close, but with a slower time course than the activation gates. The inactivated channels require time at hyperpolarized potentials before they can be activated again (recovery from inactivation). During this refractory period the channels recover from the inactivated state. Voltage gated ion channels can have more inactivated states which are kinetically distinct. Upon hyperpolarization, the opened activation gate closes in a process called deactivation. In general, voltage-gated ion channels are characterized by at least one open (O) and one closed (C) state and may have one or more inactivated (I) states (Figure 2A [83]).

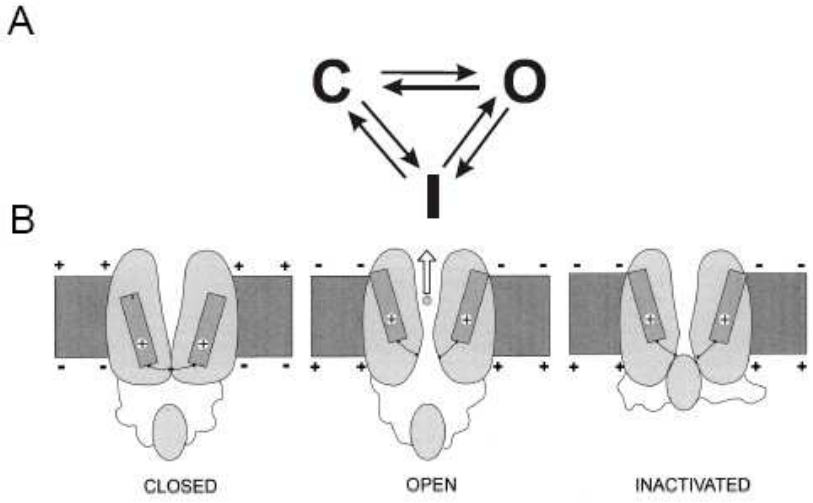

Figure 2. Gating transitions in voltage-gated cation channels. **(A)** Schematic representation of the main conformational states of voltage-gated channels and the transitions between them. **(B)** Mechanistic view of channel gating [83].

2. MOLECULAR BIOLOGICAL METHODS

2.1. cDNA constructs and mRNA

Restriction enzymes were used to linearize plasmid cDNA for in vitro cRNA synthesis. All restriction enzymes were used according to the manuals of the suppliers. The cDNA for the human heart α_{1C} (HHT-α_{1C}, Accession number L04569) [84] subunit used in this project was subcloned into the HindIII/NotI sites of the pBS SK- (Stratagene) vector. Rabbit lung α_{1Cb} (VSM-α_{1Cb} Accession number X55763) [85] was subcloned into the pSP72 vector (Promega). The cDNAs must be linearized prior to generating mRNA. This allows the RNA polymerase to transcribe the cDNA only once, at the end of the cDNA the RNA polymerase "falls off" the DNA.

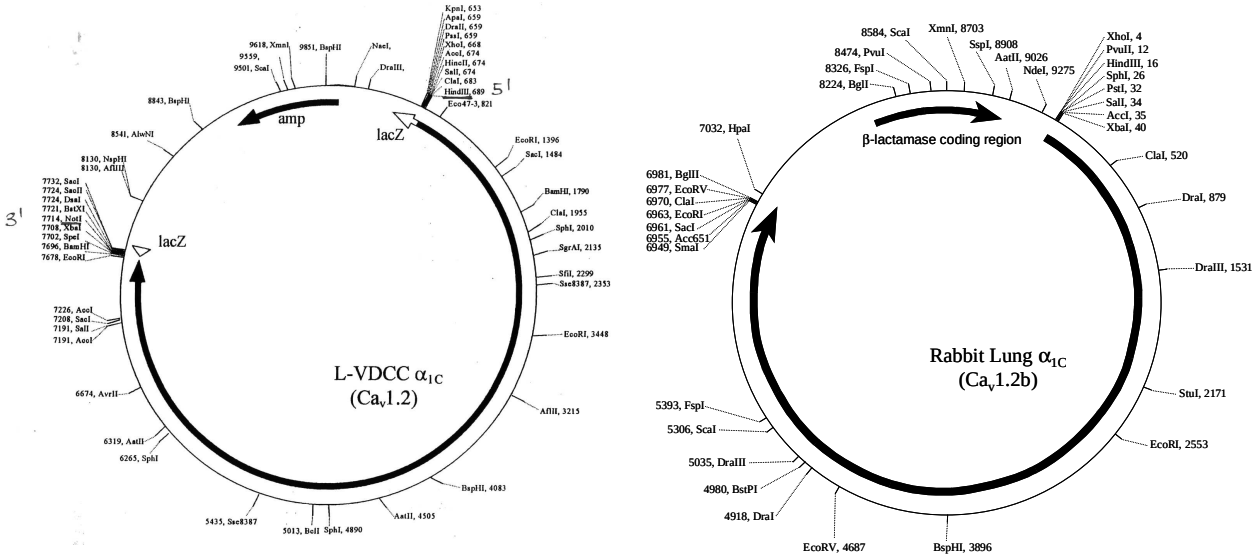

Figure 3. The map of pBS SK-vector and the pSP72-vector with the insertion of recombinant HHT-α_{1C} and Lung-α_{1Cb}, respectively. The vectors are showing the positions of the ampicillin resistance gene or the β–lactamase coding region and selection of the most important restriction sites.

All restriction enzymes that were used to linearize the plasmid cDNAs for in vitro mRNA synthesis were used according to the protocols of the supplier.

For these experiments, 30-50μg of DNA was digested overnight (to a final volume of 400μl) with specific restriction enzymes. HHT-α_{1C} was linearized with XbaI (NEB), VSM-α_{1Cb} linearized with Acc651 (a neoschizomer of KpnI, NEB), rabbit skeletal muscle α_2/δ–1

[16](SK-α_2, Accession number M21948) was linearized with NheI (NEB) and human heart β_3-subunit (Accession number L06112) [86] was linearized with NotI (NEB). These enzymes were chosen because they have unique restriction sites (cut only once) and generate 5′ overhangs (Figure 4).

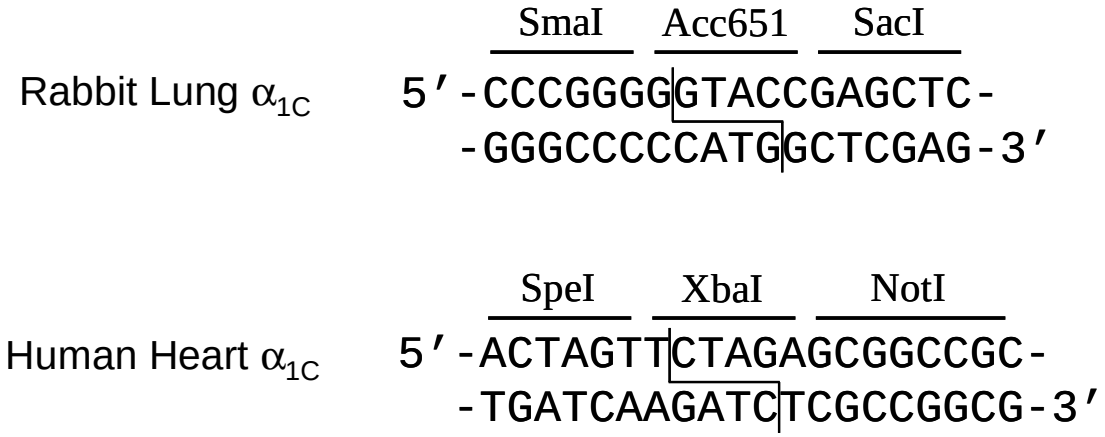

Figure 4. Enzyme restrictions of the Lung-α_{1Cb} and HHT-α_{1C} DNA molecules, respectively. Figure illustrates the detailed positions of the recognition sequences for Acc651 and Xba1, respectively. Before transcription of cDNA to mRNA the circular DNA has to be linerized using restriction enzymes. These endonucleases break the internal phosphodiesterase bonds at a very specific position which is characteristic for every enzyme.

After overnight digestion, the samples were phenol/chloroform extracted and then precipitated with Ammonium Acetate and Ethanol to remove impurities. The DNA pellet was resuspended in 30µl RNase-free water and the concentration was determined by the Optical Density at wavelengths 260 and 280 (OD260/280),

2.1.2. In vitro RNA synthesis

All reagents and materials were kept on ice. The commercial kit mMessage^{TM} mMachine (Ambion) was used to generate mRNA using the T7 promoter for HHT-α_{1C}, α_2-1 [72] and hβ_3 and the SP6 promoter kit was used for RL-α_{1Cb} following the manufacturer's protocol. 1µl GTP was added to the reaction mixture to compensate for the long message. In brief, the linearized plasmid DNA was incubated for 2 hours with the transcription buffer, the ribonucleotide mix and the enzyme mix at 37°C. Additionally 1µl RNAse-free DNAse type I

(2U/μl) was added and the mixture was incubated for 15 more minutes at 37°C to remove DNA. After mRNA synthesis, the mRNA was precipitated with Lithium Chloride (as stated in the manufacturer's protocol) followed by a resuspension in 100μl RNase-free water. The mRNA was then precipitated with Ammonium Acetate and Ethanol to further remove any unincorporated nucleotides. The removal of unincorporated nucleotides is essential because their presence will artificially increase the mRNA concentration as determined by OD260/280. After precipitation with ammonium acetate, the mRNA is resuspended in RNase-free water. The amount of water used depended on the size of the mRNA pellet, usually between 50-80μl. The concentration of mRNA was determined by OD260/280.

3. MATERIALS AND METHODS

3.2. Spectroscopic measurement of nucleic acid concentration

To determine the concentration of the DNA and RNA probes the absorption at 260nm (A_{260}) optical wavelength was measured on an automated spectrophotometer (UV-Visible Spectrophotometer, UV-1650 PC, SHIMADZU). Appropriate nucleic acid dilutions were prepared to obtain absorption between 0 and 1. An Optical Density (OD) of 1 corresponds to a concentration of 50μg/ml for DNA and 40μg/ml for RNA. A qualitative test was done by measuring the ratio A260/A280 (Absorption at 260 and 280nm wavelengths). A ratio between 1.6 and 2 was considered to indicate purified DNA or RNA.

3.1. Agarose gel electrophoresis

The quality of the mRNA is determined by running formaldehyde based RNA gel electrophoresis on the samples. The mRNA is place into a solution containing formaldehyde, formamide and MOPS. This is run on a 1% agarose gel also containing formaldehyde, formamide and MOPS. Staining the gel with ethidium bromide after electrophoresis (followed by destaining with water) allows the mRNA to become visible under UV light. Any unincorporated nucleotides show as a blurry band at a lower molecular weight.

3.3. Oocyte preparation and injection

The use of *Xenopus laevis* oocytes as an expression system for ion channels was first described by Miledi *et al.* [87] in 1983 and since then has become a standard technique for investigation of ion channels. Oocytes are especially suitable for electrophysiological recordings, since they have only a few endogenous channels, and faithfully express foreign RNA that has been injected.

3.3.1 Frog surgery

All the experiments were carried out in accordance with the University of Cincinnati Institutional Animal Care and Use Committee. Adult female *Xenopus laevis* (XenopusI, Ann Arbor, MI) frogs with a length of at least 9cm were anesthetized in 1L 0.5% Tricaine water

solution (3-aminobenzoic acid ethyl ester methanesulfonate salt (MS-222), Sigma-Aldrich, USA) for about 15-20min. The frog was put on its back on ice after achieving the necessary anesthetic grade checked by the loss of the righting response and the loss of response to painful stimuli. Extremities and head were covered with ice in order to prolong the effect of the anesthetic and to prevent excessive bleeding. The surgical area and all surgical instruments were sterilized with 70% ethanol solution. Instruments were kept on a sterile wrap during the procedure. Skin, muscle fascia and muscle tissue were cut at a length of 1cm. A portion of the ovary was removed through this opening with forceps and scissors and placed in OR-2 medium.

3.3.2. Defolliculation and selection

Before defolliculation, oocytes were extensively washed with OR-2 medium (in mM: 82.5 NaCl, 2 KCl, 1 MgCl2, 5 HEPES, pH 7.5). Defolliculation was achieved by treatment with 2mg/ml collagenase (type IA; Sigma-Aldrich, USA) dissolved in OR-2 Ca^{2+} free medium. Usually 2 hours of gently shaking at room temperature were enough to defolliculate the oocytes completely without damaging the vitelline membrane. Defolliculated stage V-VI oocytes were incubated in P/S medium (in mM): 96 NaCl, 2.0 KCl, 1.0 $MgCl_2$, 1.8 $CaCl_2$, 5.0 HEPES, 2.5 sodium pyruvate, and 0.5 theophylline at pH 7.5. The P/S medium was supplemented with 100μg/ml streptomycin and 100 units/ml penicillin at 19°C in low temperature aseptic incubator (VWR Scientific, West Chester, USA). Medium was changed every day. Before injection, a selection was done for healthy stage V and VI oocytes [88].

3.3.4. Oocyte microinjection

In vitro synthesized mRNA can be injected and expressed in *Xenopus laevis* oocytes. Borosilicate glass pipettes (210/310/510, Drummond Scientific, Broomall, PA USA) were pulled on a vertical pipette puller, Model 720 (David Kopf Instruments, Tujunga, California). The tips of the pipettes were broke under a StereoZoom 3 microscope (Nikon,, Japan) to obtain optimal diameter and sharpness (around 20μm tip diameter). Pipettes were filled with heavy mineral oil (Sigma-Aldrich, USA) and were mounted in the head-stage of a Drummond Digital Microdispenser, Cat. #3-000-510 (Drummond Scientific Co., Broomall, PA USA). The pipette tip was filled with 2μl RNA.

A

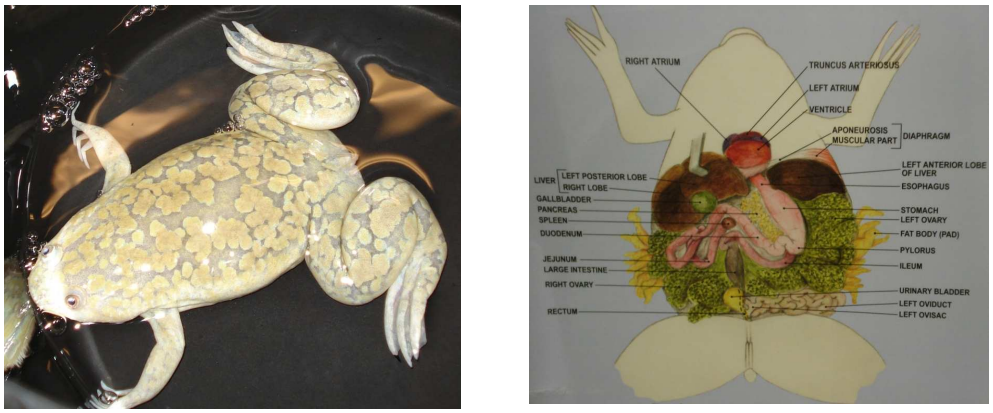

B

Figure 5. The *Xenopus* oocyte expression system. **(A)** Adult female *Xenopus leavis* frog **(B)** Developmental states of *Xenopus leavis* oocyte: healthy stage V and VI oocyte can be recognized by their size and by their clear differentiation of the animal (dark) and vegetal poles (light).

Oocytes were lined up on a plastic grid previously sterilized with 70% ethanol and covered with culture medium. 50nl undiluted mRNA were injected in the vegetal pole of a single oocyte. After injection oocytes were stored in groups of 20 per plates and incubated at 19°C. The amount of the injected RNA correlated well with expression levels, *i.e.* current size was dependent on the expression rate. With a concentration of 1μg/μl mRNA, the amount of mRNA injected to each oocyte is about 50ng. In order to compare current amplitudes of $Ca_v1.2$ L-VDCC channels HHT-α_{1C} [84] and rabbit lung VSM-α_{1Cb} (a generous gift from Dr. R. Hullin) [85], RNA preparations were injected on the same day into the same batch of oocytes and measured in parallel on days 2-4 after injection. In order to increase current density and stabilize gating, the calcium channel α_{1C}-subunit encoding mRNA was co-injected with mRNA encoding the β_3 [86] and $\alpha_2/\delta{-}1$ [16] calcium channel subunits in a 1:1:1 molar ratio (the final concentration remains 1μg/μl or 1ng/nl). To minimize

contamination with chloride current, oocytes were microinjected with 50nl of a 40mM K_4-BAPTA solution (potassium 1,2-bis(2-amino-phenoxy)ethane-N,N,N',N'-tetraacetate in 10mM HEPES, pH 7.05) 60min prior to current recording.

4. ELECTROPHYSIOLOGY

4.1. Reagents and solutions

Solutions for voltage-clamp measurements

All reagents were ordered from Sigma-Aldrich (St. Louis, MO USA).

4.2. General procedures

Most of the current knowledge about ion channels in cell membranes derived from experiments using voltage clamp. In the voltage clamp technique, the membrane potential is held constant with a feedback amplifier while the current flowing through the membrane is measured. Current is measured because the investigator has no direct way of measuring conductance. The method was developed by Cole [89] in 1949 and Hodgkin and Huxley [90]. Since that time many variants of the technique have evolved and voltage clamp measurements have been extended to a wide range of tissues.

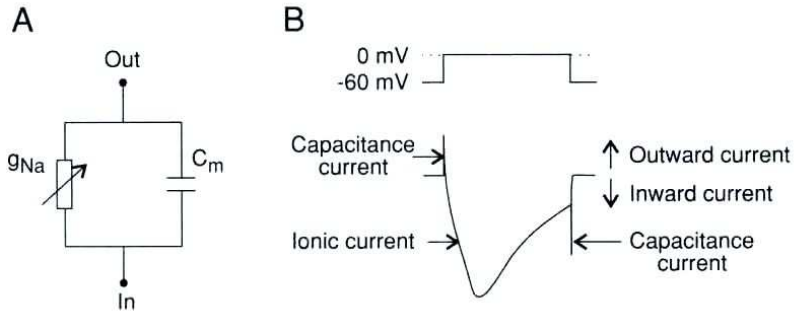

Figure 6. **(A)** Simplified electrical circuit of membrane that contains only voltage-gated Na+ channels. C_m, membrane conductance; gNa, Na^+ conductance. **(B)** The current elicited by a voltage clamp depolarization consist of a brief initial capacity current followed by an ionic current. In this case, the ionic current only flows through voltage-gate channels. The Na^+ current flows from the outside to the inside of the membrane. Edited by Ashcroft FM, Ion Channels and Disease (Book), Academic Press, 2000, UK.

The current that flows through the membrane at any particular potential can be measured (I_t). This current is the sum of the ionic current (I_i), which represents current flow through open ion channels and the capacitive current (I_c), which is largely due to charging of the membrane capacitance. The magnitude of the capacity current is determined by the

capacitance of the cell membrane (C_m), which is normally 1μF/cm^2, and it flows only while the voltage is changing (Figure 6).

Thus, $\mathbf{I_t=I_i+C_m \times dV/dt}$. Since I_C =C dV/dt, once the potential is clamped, no capacitive current flows. Hence, I_C flows only during the membrane-clamping process. Clearly, the ionic current will be the same as the total membrane current. The good voltage clamp requires that the membrane potential be changed rapidly, so that the capacity current is over before the ionic current starts to flow. The speed of the voltage response is limited by the rate at which current can be injected to the microelectrode. This depends on the electrode resistance.

4.2.1. Basic apparatus with electrical and mechanical isolation

A patch-clamp set-up may consist of a chamber, a microscope (for cell visualization) placed on an anti-vibration table (pneumatic support for the patch clamp setup and passive support for the two electrode voltage clamp measurements), a patch clamp amplifier and pulse generator for voltage-clamping the cells, a micromanipulator holding the amplifier probe for positioning the attached patch pipette, and data-recording devices (oscilloscope, computer). A Faraday cage was build around the experimental setup and all metal parts near the head-stage were grounded, using the virtual ground input of the amplifier. An example of patch-clamp set-up is shown in Figure 7.

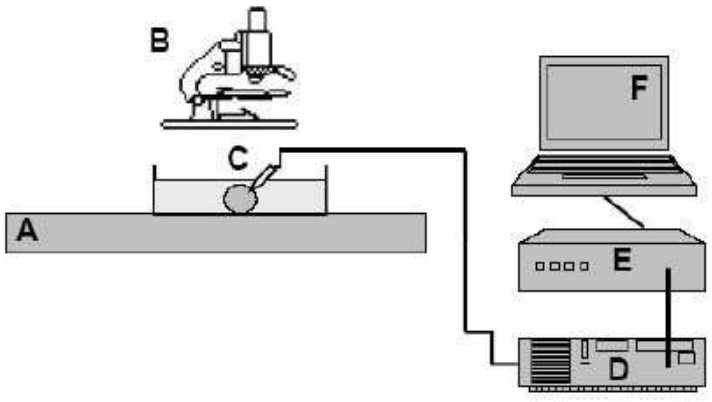

Figure 7. A common electrophysiology setup. To reduce vibration, the microscope with the recording chamber, manipulator and headstage should be mounted on a massive antivibration table **(A and B)**. The glass microelectrode **(C)** is connected to a feedback amplifier **(D)**. The amplified and filtered signal is digitized by the AD converter **(E)**. The digitized signal is visualized and stored on a PC **(F)**. Single-Channel Recording Second Edition (Book), Edited by Sakmann B. and Neher E., Plenum Press, 1995, USA

4.2.2. Glass electrodes

Glass microelectrodes were pulled with David Kopf vertical Pipette Puller Model 720 (David Kopf Instruments, Tujunga, California USA) from thin wall borosilicate glass pipettes with filament (1.2mm OD, 0.90mm ID; A-M Systems, INC. Everett, WA, USA). The microelectrodes for patch-clamp recordings were pulled with Sutter and fire polished (Garner Glass Company, Claremont, CA USA ID 1.10, OD 1.60, Glass type 7052). The resistance of the whole-cell patch clamp electrodes ranged between 2 and 4MΩ. Sharp glass electrodes for two-electrode voltage clamp (TEVC) were pulled in a way to minimize the access resistance while minimizing cell damage – 0.5 to 1.5MΩ with the standard 3M KCl electrode solution.

Ag/AgCl electrodes

Ag/AgCl pellet holder's electrodes were purchased from Warner Instruments (Catalog# 64-1301). The bathing solution was connected to the ground through a 3M KCl/agar bridge (2% agarose in filtered 3M KCl).

4.2.3. Digitizing, recording and analysis

In the cardiomyocytes, the Axopatch-200A patch-clamp amplifier was used to record membrane currents. The voltage clamp amplifier output was digitized by a DIGIDATA 1200 AD/DA converter (Axon Instruments, Union City, USA), connected to a personal computer (PC 486) running Clampex 5.6 (Axon Instruments, Union City, USA) acquisition software under Microsoft DOS 6.2 (Microsoft Corp. Redmond, USA). In the two electrode voltage-clamp experiments in oocytes, we used Axoclamp-2A amplifier with pCLAMP software (version 5.5, Axon Instruments, USA) to generate voltage clamp protocols, acquire data and analyze current traces. Whole cell leakage currents were subtracted on-line using the P/4 procedure. Current were digitized at 1kHz after being filtered 1kHz. The data were stored on the computer hard drive for later analysis and a hard copy record was done for every protocol. Analysis was done on a PC using combination of Clampfit 6.03 (Axon), Origin (Version 7.0 Microcal, Northampton, USA) and Excel (Microsoft XP 2003) software.

4.3. Patch clamp

Instead of using sharp microelectrodes to puncture the membrane and penetrate the cell in traditional voltage clamping, patch-clamping uses a fire-polished pipette of about 1μm that is sealed to a 'patch' of membrane. After forming the cell-attached seal the membrane patch is destroyed by strong suction, electrically or it may be permeabilized with pore-forming antibiotic nystatin. This provides electrical continuity with the cell interior allowing currents through the whole of the cell membrane to be measured under of the whole-cell current. The tightness of the gigaseal prevents the leak currents flowing between the pipette and the reference electrode. However, the current through the series resistance of the pipette and the residual resistance of the ruptured patch is often sufficiently large to introduce significant voltage errors. It has an advantage that the intracellular solution can be manipulated however, but it has a disadvantage since the cytosolic constituents are lost from the cell by dialysis. A typical patch clamp circuit shown in Figure 8. The key difference between the two electrode voltage clamp is that the patch clamp uses a single electrode both to control the membrane potential and to measure the current.

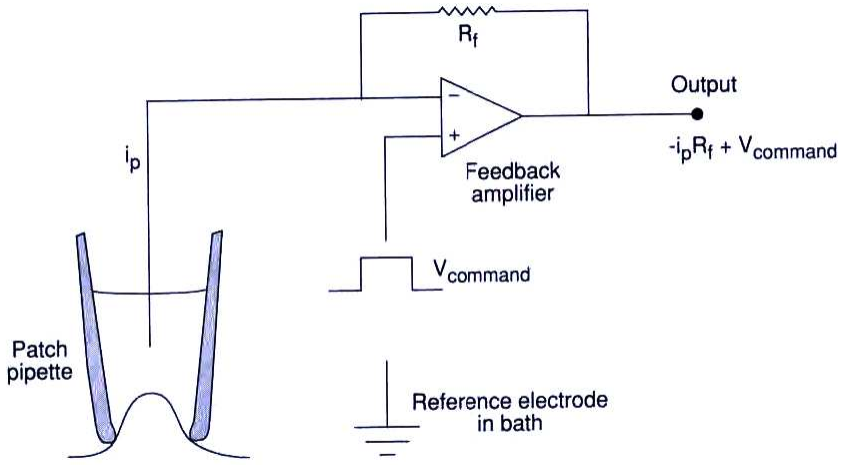

Figure 8. One electrode continuous voltage clamp method (whole cell patch clamp circuit). A typical patch-clamp circuit is shown in Figure. One advantage of this system is that the patch-clamp uses a single electrode both to control the membrane potential and to measure current. The sensitive current-to-voltage converter is fabricated using a high megaohm resistor (R_f) and an operational amplifier (Feedback amplifier, A1). The patch pipette is connected to the inverting input of a feedback amplifier and the command voltage is connected to the positive input. Since the A1 has extremely high gain, the potential at the negative input is forced to follow the command potential (V_{cmd}) at the positive input. All current flowing in the micropipette also flows through R_f. This current is proportional to the voltage across R_f, which is measured at the output of the differential amplifier (A2). Edited by Ashcroft FM, Ion Channels and Disease (Book), Academic Press, 2000, UK)

4.3.1. Two-electrode voltage-clamp on *Xenopus laevis* oocytes

Experimental setup

Figure 9 shows a schematic diagram for the two electrode voltage clamp (TEVC) circuit. The oocyte is penetrated with two microelectrodes filled with electrolyte solution (typically 3M KCl), connected to the recording system through Ag-AgCl electrodes. In the two-electrode voltage clamp recording from oocytes, one intracellular electrode measures the membrane potential (voltage electrode-*ME1*) and the second passes sufficient current (current electrode-*ME2*) to maintain the desired voltage clamp, using a feedback circuit. The amount of current passed through the current electrode is determined by the discrepancy between the membrane potential and the command potential. When these two are equal, no current flows through the current electrode. A good voltage clamp requires that the membrane potential be changed rapidly so that the capacity current is over before the ionic current starts to flow. The main disadvantage of the TEVC is the relative slow response due to the high value of the capacitance of the oocyte membrane. The response time (τ) of a voltage clamp to a step voltage change is: $\tau=R_I C_m/A$ where R_I is the resistance of the current-passing electrode, C_m is the membrane capacitance, and A is the gain of the command amplifier. Since not that much can be done about C_m, the only two things one can do in order to achieve fast clamping of the cell is to use the lowest R_I and the largest A possible. The higher the electrode resistance, the more difficult it is to inject sufficient current fast. When studying voltage gated channels, one wants the fastest clamp attainable. A well-tuned, TEVC can clamp an oocytes fast enough to study the gating kinetics of most voltage-gated channels except Na^+. A faster clamp can be achieved by recording from smaller oocytes.

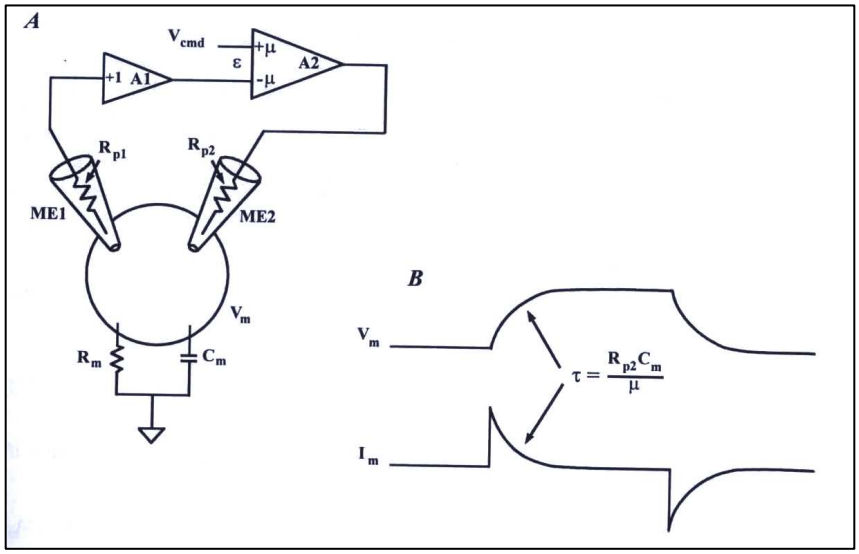

Figure 9. Conventional Two-Electrode Voltage Clamp. **(A)** The membrane potential (V_m) is recorded by a unity-gain buffer amplifier (A1) connected to the voltage recording microelectrode (ME1). V_m is compared to the command potential (V_{cmd}) in a high-gain differential amplifier (A2; gain=μ). The output of A2 is proportional to the difference (ε) between V_m and V_{cmd}. The voltage at the output of A2 forces current to flow through the current-passing microelectrode (ME2) into the cell. The polarity of the gain in A2 is such that the current in ME2 reduces ε. **(B)** unlike the ideal case, there is a finite time is required to charge the cell capacitance. If μ (the gain of the clamp amplifier) was infinite, or if R_{p2} (the resistance of the output ME2) was zero, the response would approach the ideal case. The Axon Guide for Electrophysiology & Biophysics Laboratory Techniques (1993, USA)

In the oocyte set-up, the Plexiglas recording chamber was placed under a stereo microscope (StereoZoom 3, Nikon, Japan). Head-stages (HS-2, Gain: x10MG, Axon Instruments, USA) and pipette holders (MEH3S12 Microelectrode Holder Half-Cells-World Precision Instruments, Inc. Sarasota, FL USA) were fixed on Narishige manipulators. Axoclamp-2A amplifier was used for all TEVC measurements.

Experimental procedures

The voltage electrode was wrapped in aluminum foil in order to reduce the capacity coupling between current and voltage electrodes. In order to minimize the capacity C_m (Figure 9), the recording chamber was filled with solution just enough to cover the oocyte. The cell was fixed on a grid in the recording chamber. The tips of the two electrodes were inserted in the bath solution. Electrode potentials were compensated, while the amplifier was switched to current clamp mode. The voltage electrode was inserted in the oocyte and the resting membrane potential was measured. Cells with a resting membrane potential more negative

than –20mV were only measured. In whole cell patch clamp experiments Series resistance and capacity compensation were performed, using the circuits present in the amplifier.

Advantages of the oocytes system: (Single-Channel Recording Second Edition (Book), Edited by Sakmann B. and Neher E., Plenum Press, 1995, USA)

1. Hundreds of viable cells can be isolated from a given donor frog.
2. The cells are quite hardy and can survive for up to 2 weeks *in vitro*.
3. The cells are big (up to 1.3mm in diameter) and can be easily injected with RNA
4. The oocytes faithfully express foreign RNA that has been injected into them.
5. The oocytes have only a few endogenous channels (the major one being a Ca^{2+}-activated Cl^- channels) that are found in high density at the animal pole, and which usually carry only a small fraction of the current expressed. In voltage-clamp recordings, the Cl^- current shows voltage-dependency, but this is a result of Ca^{2+} influx through endogenous voltage-gated Ca^{2+} channels followed by activation of the Cl^- channels. The Ca^{2+} activated Cl^- current can be inhibited by intracellular injection of Ca^{2+} chelators (BAPTA) or pharmacological blockers (Niflumic acid).

Disadvantages of the oocytes system:

1 Because of its large size, whole-cell patch-clamp experiments, where one can control the intracellular ionic compositions by dialysis across the patch pipette, are not possible.
2. The endogenous channels, although few, can interfere with current measurements if they are small.
3. Posttranslational modifications may be different in the oocytes compared with the native cells. Hence, channels may actually function differently in their native environment.
4. Ocyte exhibit seasonal variation such that channel expression and ability to obtain seals are more difficult in the summer months.
5. *Xenopus* is an amphibian, and the cells should be studied at room temperature (18-23°C). At higher temperatures, the cells rapidly deteriorate.

4.4. Voltage-clamp protocols used to characterize calcium channels

4.4.1. Voltage dependence of activation

Whole-cell Ba^{2+} current recordings

The recording medium was a Ca^{2+}- and Cl^- free solution composed of (in mM): 40 $Ba(OH)_2$, 50 N-methyl-glucamine, 2.0 KOH, 5.0 HEPES, Niflumic acid (282mg/2l) pH adjusted to 7.4, with methanesulfonic acid. The voltage dependence of activation for HHT-α_{1C} and RL-VSM-α_{1Cb} calcium channels was obtained by 350ms depolarizing pulses to different potentials from a holding potential of –60mV for the whole-cell measurements, –80mV for the TEVC experiments) at 15s. The exact holding potential used in the protocol is further specified in the results section. *I-V* curves were obtained by plotting the maximal current amplitude of every trace vs. voltage. *I-V* curves were fitted to standard Boltzmann equation in the form $I_{Ba}= G_{max}(V_m-V_{rev})/(1+\exp(-(V_m-V_{0.5})/K))$, where K is the slope factor, $V_{0.5}$ is the voltage that causes half maximal activation, G_{max} is the maximal conductance, V_m is membrane voltage, I_{Ba} is the current measured at the same voltage , and V_{rev} is the reversal potential of I_{Ba}. In order to avoid the I_{Ba} run-down, we determined the *I-V* curves before and after drugs by using 80ms long test pulse from -50mV to +60mV from a holding potential at -80mV at 10s (0.1Hz). In cardiomyocytes, I_{Ca} currents were activated by depolarizing steps (400ms) from -40mV to +50mV in 10mV increments from a holding potential of -50mV at 40s (0.025Hz) or 5s (0.2Hz).

Voltage dependence of steady state inactivation

Steady-state inactivation was determined using a double pulse protocol: 5s prepulse to the various potentials from -80mV to +50mV at a holding potential of -80mV followed by a 30ms test pulse to –80mV. Finally a 400ms long test pulse was applied at +10 mV at 30s (0.033Hz). The normalized peak current at this potential is proportional to the percentage of calcium channels that are still available for activation. The data points were fit to a standard Boltzmann function: $I/I\max=1/(1+\exp[(V-V_{0.5})/k_V])$, with $V_{0.5}$ being the voltage of half-maximal inactivation and k_V a slope factor. In cardiomyocytes, to measure the voltage

dependence of steady-state I_{Ca} inactivation, a gapped double-pulse voltage-clamp protocol was used. Ca^{2+} currents recorded at +10mV for 200ms after 1-s prepulse to increasing values of voltages between -80mV and +50mV at holding potential of -80mV at a frequency of 0.033Hz (30s). Channel availability was calculated by dividing the remaining current (I) at +10mV by I_{max} and expressed as a function of the prepulse potential.

Inactivation time constants and persistent current

The time course of decay for I_{Ba} in oocytes was determined using least-squares fit of the inactivating section of the current trace (5000ms) with a first exponential function by using the Chebyshev algorithm of Clampfit. C is the non-inactivating current.

$$I(t)=A \exp[-(t-t_0)/\tau] + C$$

The amplitude A of the time constant τ contributes to more than 90% to the total current amplitude.

Recovery from inactivation

Recovery of I_{Ba} from inactivation was studied after depolarizing the calcium channels during a 3s prepulse to +10mV. The time course of I_{Ba} recovery from inactivation was estimated at a holding potential of -80mV by applying a 400ms test pulse to +10mV at various time intervals after the conditioning prepulse (from 20ms to 28s) at 30s. After the double-pulse protocol oocytes were hyperpolarized to -100mV for 3min to permit the channels to recover from inactivation resulting in complete unblock of the channels. Peak I_{Ba} values were normalized to the peak current amplitude measured during the prepulse. The time course of recovery from inactivation was best fit to a second order exponential function with an initial delay.

Use-dependent block

Use-dependent block was determined as the inhibition of peak I_{Ba} during trains of 15 test pulses lasting 80ms applied at 0.5Hz from a holding potential of -60mV to test potentials +10mV positive to the peak potential of the I-V curves. An identical pulse protocol was used in the presence of drugs. Diltiazem (racemic) and the new Diltiazem analogs were perfused

in the bath (for a 3min period) at a concentration of 100μM. This concentration was selected because it provided sufficient block for the use-dependent measurements in *Xenopus* oocytes. In cardiomyocytes, basically the same protocol was used as for the oocytes, except in some experiment the test pulse was 320ms long under UDB protocol.

4.4.2. Isolation of ventricular myocytes and electrophysiology

Cardiomyocytes were dissociated from the ventricles of 4-5 month-old mice (FVB/n), by methods previously described [91]. Briefly, the heart was perfused with Ca^{2+}-free Tyrode's solution for 10 minutes, and with Ca^{2+}-free Tyrode solution containing collagenase type 2 (Worthington Biochemical Corporation, Lakewood, NJ, USA) and 1mg/ml BSA (Bovine Serum Albumin, fatty acid free) for 5-7 minutes by the Langendorff method at 37 °C. At the end of the perfusion, the heart was removed and the ventricles were mechanically disaggregated with a bore pipette. The dissociated cells were filtered through a nylon mesh, and stored at 4 °C in low Cl^- high K^+ Kraft-Bruhe (KB) solution (in mM): L-glutamic-acid 50, KCl 40, taurine 20, KH_2PO_4 20, $MgCl_2$ 3, Glucose 10, EGTA 1, HEPES 10, pH 7.4 with 1 M KOH until the electrophysiological (EP) studies. Only Ca^{2+} tolerant cells with clear cross striations and without spontaneous contractions or significant granulation were selected for the experiments.

All current recordings were obtained in the whole-cell, voltage-clamp configuration of the patch clamp technique by using 1.60 OD borosilicate glass electrodes (Garner Glass Company). Cell capacitance was calculated by integrating the area under an uncompensated capacity transient elicited by a 25mV hyperpolarizing test pulse (25ms) from a holding potential of 0mV. Series resistance was within the range of 2 to 11MΩ. Most of the data presented in these studies were obtained with electrodes having a resistance of 0.5-3MΩ.

After formation of a high resistance seal between the recording electrode and the myocytes membrane, electrode capacitance was fully compensated electronically before breaking the membrane parch.

The recorded current (I_{Ba}) were filtered at 2KHz through a four-pole low-bass Bessel filter and digitized at 5kHz. The experiments were controlled using pClamp 5.6 software (Axon Instruments, USA) and analyzed using Clampfit 6.0.3. Ca^{2+} currents were recorded using an external solution containing (in mM): $CaCl_2$ 2, Tetraethyl-ammonium chloride (TEA- Cl) 135,

4-aminopyridine (4-AP) 5, glucose 10, HEPES 10, pH 7.3. The pipette solution contained(mM): cesium aspartate 100, CsCl 20, $MgCl_2$ 1, Mg-ATP 2, Na_2-GTP 0.5, EGTA 5, HEPES 5, pH 7.3 with 1 N CsOH.

4.4.3. Statistics

All data are shown as means±standard error of the mean (SEM) if not indicated otherwise, n=number of cells of animal tested. Comparisons between two groups were tested for statistically significant differences ($p<0.05$ or better) using a two-tailed unpaired Student's *t*-test. Comparisons of amplitudes of I_{Ba} or I_{Ca} at different times (before and after drug application) in the same groups were done using a paired Student's *t*-test. Comparisons between several groups was done using one-way analysis of variance (ANOVA) followed Turkey's test.

4.5. Isolated retrograde perfused heart preparation

Mice were anesthetized intraperitoneally with a mixture of 8.7mg/ml Ketamine/1.3mg/ml Xylazine and injected with 1.5U heparin to prevent intracoronary microthrombi. The heart was rapidly excised, the aorta was canulated with a 20 gauge needle and perfused in a retrograde fashion at a constant hydrostatic pressure of 55mmHg with a modified Krebs-Henseleit solution (KHS) containing (in mM): 118 NaCl, 4.7 KCl, 2.5 $CaCl_2$, 1.2 $MgSO_4$, 1.2 KH_2PO_4, 25 $NaHCO_3$, 0.5 EDTA 11 glucose. Buffer was equilibrated with 95% O_2 and 5% CO_2, insuring a pH of 7.4. Hearts were bathed in the perfusate in a water-jacketed bath maintained at 37.4 °C. A home-made fluid-filled catheter (PE-50) was inserted into the left atrium through the pulmonary vein, guided through the mitral valve opening, advanced into the left ventricle and forced through the ventricular apex. The proximal end of the catheter remained in the left ventricle. The distal end of the catheter was connected via fluid-filled polyethylene tubing to a further Baxter pressure transducer. Aortic pressure in the aortic outflow catheter was measured through a sidearm. A micrometer clamp was attached to the outflow catheter so that the Starling resistance (aortic pressure) could be monitored. Aortic flow was measured with a graduated burette in milliliters per minute. Coronary flow was allowed to drip from the pulmonary artery and measured by an electronic

balance to determine coronary flow rates. Following instrumentation, hearts were allowed to equilibrate for 30min.

The performance of the heart was evaluated by analyzing the heart rate (HR, beats/min), the left ventricular pressure (LVP, in mmHg), which is an index of contractile activity and the mean coronary perfusion pressure were continuously monitored using a Biobench ('National Instruments') DAQ (Data Acquisition) system and digitized at 1kHz. The pressure curve was used to calculate the maximal values of the first derivative of LVP $[(+dP/dt)_{max}]$ (mmHg s^{-1}), which indicates the maximal rate of left ventricular contraction, the maximal rate of left ventricular pressure decline of LVP $[(-dP/dt)_{min}]$ (mmHg s^{-1}), time to peak pressure (TPP) and time to half of relaxation ($TR_{1/2}$) (s), which is the time required for intraventricular pressure to fall from peak to 50%. TPP and $TR_{1/2}$ were normalized with respect to peak LVP since they are dependent upon the extent of pressure development.

Drug infusion

Identical dose–response curves were obtained by perfusing the heart with KHS containing increasing concentration (from 10^{-10}-10^{-4}M) of the Diltiazem and Diltiazem analogs in 2.0 mM $[Ca^{2+}]_o$. Drugs were added to the cardiac preparation entering the heart using a microperfusion pump (multispeed infusion pump, model 600, Harvard Apparatus). Hearts were exposed to each dose level for 150s for maximal response. Drugs were obtained from Sigma Chemicals (St. Louis, MO, USA).

Statistical analysis

Data are expressed as mean±S.E.M. Between groups statistical comparisons were made using the unpaired Student's *t*-test. The statistical significance of the difference between control and serial hemodynamic changes within groups was determined by one-way ANOVA and multiple comparisons with the Turkey procedure. The differences in the dose response curves were analyzed by two-way ANOVA. $p<0.05$ was considered significant.

4.6. Isolation of adult cardiomyocytes for Ca^{2+} measurements

Cardiomyocytes were isolated for analysis and only Ca^{2+}-tolerant cells with clear cross striations and without spontaneous contractions or significant granulation were selected for experimental studies. In brief, the heart was rapidly excised and placed in Tyrode solution containing (in mmol/l): 120 NaCl, 5.4 KCl, 1.2 NaH_2PO_4, 5.6 glucose, 20 $NaHCO_3$, 1.6 $MgCl_2$, 10 2,3-butanedione monoxime (BDM), and 5 taurine (buffer A), gassed with 95% O_2-5% CO_2. All solutions were filtered and equilibrated with 95% O_2-5% CO_2 for at least 20min before use. The heart was retrogradely perfused with buffer A for 4–5min, then with buffer A containing 1mg/ml collagenase type II (Worthington, Freehold, NJ, USA) and 0.08mg/ml protease type XIV (Sigma) at 37°C. After 2min of enzyme perfusion, 50μM Ca^{2+} was added to the enzyme solution. When the heart became "swollen and soft" after ~5min of digestion, the enzyme was recirculated. The heart was perfused for an additional 8–12min or until flow rate surpassed pre-enzyme flow rate. After perfusion, the ventricles were separated from the atria and minced. Myocytes were incubated with 2μmol/l Fura-2 acetoxymethyl ester (F-1221, Molecular Probes, Eugene, OR, USA) which was dissolved in dimethyl sulfoxide containing 0.02% pluronic acid (Pluronic F-127 20% solution in DMSO, Invitrogen, P3000MP)for 30–35min in buffer C (buffer A with 1mmol/l Ca^{2+} without BDM) at room temperature. After being loaded, the cells were washed and resuspended in buffer C. After three washes (40min), the cell suspension was placed in a plexiglass chamber containing 500μl of fresh buffer C. The Fura-2 fluorescence ratio was determined at room temperature using a Delta Scan dual-bean spectrofluorophotometer (Photon Technology, Birmingham, NJ, USA), operating at an emission wavelength of 510nM with excitation wavelengths of 340 and 380nM. The stimulating frequency for Ca^{2+} transient measurements was 0.5Hz. Baseline amplitude (estimated by 340/380nM ratio) of the Ca^{2+} signal was acquired and data were analyzed using software from Felix 1.1 Software and IonWizard (IonOptix).

5. RESULTS

5.1. Effect of Diltiazem and Diltiazem analogs on the characteristics of Ba^{2+} currents through L-VDCC

The L-type calcium channels play a central role in the maintenance of cardiac and smooth muscle electrical and mechanical activity, and exhibit high affinity for the clinically useful drugs known as L-VDCC blockers (CCBs). Therefore, it is important to investigate the effect of the newly synthesized CCBs on both tissues. It is presumed that these new Diltiazem analogs might possess vascular sensitivity and perhaps differently regulate the electrophysiological and biophysical properties of the cardiac and smooth muscle L-VDCC. As previously discussed, CCBs have been shown to be powerful therapeutic tools in the treatment of a wide variety of disorders including hypertension, angina, and some forms of cardiac arrhythmias. From the therapeutic applications standpoint, the high degree of specificity of these drugs for smooth muscle L-VDCCs is very important. The DHPs are the most selective and potent CCBs and they have high vascular selectivity. However, in general, the vascular selectivity has a disadvantage: a reflex-adrenergic discharge with consequent tachycardia and positive inotropism which increases oxygen demand. A multidisciplinary project has led to a discovery of novel, structurally diverse benzothiazepine analog L-VDCC blockers. This project was developed and the primary results of the pharmacological and binding studies were performed in Bologna, Italy. The long term goal of this project is the continued studies of the new BTZ analogs which will provide new insight into the three dimensional structure of the BTZ binding site. At the beginning of the project a Ligand-Based Virtual Screening (LBVS) procedure was developed in order to search for novel Diltiazem analogs. 340.000 molecules were screened, and selection was made based on selected criteria like molecular weight, etc. As a result, 20 compounds were tested *in vitro*, and functional experiments and binding assays revealed several promising compounds as potential Diltiazem analogs [92]. Therefore, the present study was designed to address whether the new Diltiazem analogs, (5b, M2, M7, M8 and P1), maintained the same biophysical and pharmacology properties as the Diltiazem on the L-VDCCs. We took advantage of the cloning and discovery of tissue-specific expression of the cDNAs for L-

VDCC α_{1C} subunits from human heart [84] and rabbit lung vasculature (VSM-α_{1Cb}) [85]. In our experimental design, the effects of new Diltiazem analogs were extensively examined by electrophysiological and pharmacological methods. For the electrophysiological (EP) analysis the heterologous *Xenopus* oocytes expression system was utilized. The HHT-α_{1C}/ or VSM-α_{1Cb} mRNAs were co-expressed with the auxiliary α_2/δ and β_3 subunits, and the current through the functionally expressed Ca^{2+} channels was measured. Based on a previous report, these experiments could provide evidence for the potential tissue selectivity of these selected Diltiazem analogs. Previously, Welling *et al.* [93] investigated the modulation of nisoldipine (DHP) on recombinant calcium channel activity in CHO (Chinese Hamster Ovary) cells stably transfected with α_1 subunits of cardiac and smooth muscle L-VDCCs using patch clamp techniques. The paper focused on two aspects of the nisoldipine effect on cardiac and smooth muscle α_1 channels. For comparison, native heart L-VDCCs: (1) tonic block at holding potential of -80mV and (2) the onset of the development of block at -40mV were tested. The results demonstrated that under identical experimental conditions the SM α_1 channels were more sensitive to lower DHP concentrations that either native or recombinant α_1 cardiac channels.

The authors speculate that the different IVS3 sequences and the presence of the alternatively spliced exon 8 within the IS6 segment [93] might contribute to the observed difference in DHP sensitivity.

The $Ca_v1.2$ calcium channels in cardiac and smooth muscles have been shown to differ at four alternate spliced sites: (1) exon 1/1a in the N-terminus, (2) exon 8/8a, in the transmembrane segment IS6, (3) exon 9 in the cytoplasmic loop connecting domains I and II, and (4) exon 31/32 in the transmembrane segment IVS3. Notably, both channels share similar activation and inactivation properties [94,95]. In our experimental settings, $Ca_v1.2$ α_{1Cb} displayed a slight hyperpolarizing shift in steady-state inactivation potentials compared with $Ca_v1.2$ α_{1C} ($V_{0.5}$ -15.81±0.48mV and -12.04±0.69mV, respectively). It will be explained in detail later. Furthermore, the α_1 subunit cloned from rat aorta by Koch *et al.* [96] is 93.9% identical to the α_1 subunit from rabbit heart and does not contain the regions caused by splice variations in the lung. Lately, Liao P. *et al.* [97] identified a new smooth muscle splice

variant which possess a biophysical property that can be linked to enhanced state-dependent block by DHP. Exon 33 forms part of the IVS3-S4 linker region (Figure 10) and a previous study showed that the exclusion of exon 33 could shift the activation potential and steady state inactivation of $Ca_v1.2$ channels to a more hyperpolarized direction [98].

Figure 10. Amino acid (a.a.) alignment of various isoforms: human heart GenBank™ NM_000719 and rabbit smooth muscle GenBank™ X55763 are different at 3 sites. A schematic diagram of the $Ca_v1.2$ calcium channel shows exon1/1a (A), exon 9 (B) and Carboxyl-terminal (C). The positively charged S4 segments are the voltage sensors. The detailed localization of exons within motifs I-IV of HHT-α_{1C} and Rabbit lung α_{1Cb} further illustrated. Red boxes indicate the differences between the cardiac and smooth muscle form of $Ca_v1.2$ channel. Black box indicates the α-interaction domain (AID).

Native smooth muscle L-type $Ca_v1.2$ channels have more depolarized resting membrane potential than cardiac cells. Approximately 30% of $Ca_v1.2$ channels within rat aorta lacked exon 33, whereas over 95% of rat heart $Ca_v1.2$ calcium channels do express exon 33. Thus, the arterial smooth muscles contained at least two isoforms of $Ca_v1.2$ calcium channels: one is the traditional $Ca_v1.2b$, and the other is $Ca_v1.2SM$. To determine how such a small subpopulation of $Ca_v1.2SM$ channels contribute sufficiently to vasotone, it will require additional work.

It should be pointed out, however, that in patients suffering from Timothy's syndrome, a mutation found in exon 8a of the $Ca_v1.2$ gene, which accounts for 11.5% of total $Ca_v1.2$ channels, died from arrhythmias and sudden cardiac death [1].

The present experiments compared the effects of Diltiazem analogs on HHT- and VSM-L-VDCCs. EP protocols previously utilized in the oocytes expression system were applied to access the Ca^{2+}-inhibiting characteristics of the new diltiazem analogs. The oocytes were injected with the designated mRNAs, and Ba^{2+} currents were measured using the "two electrode voltage clamp technique". To eliminate Ca^{2+}-dependent inactivation while measuring I_{Ba}, the external (recording) solution contained 40mM Ba^{2+} as the charge carrier. Since α_{1C} subunit was co-expressed with the auxiliary subunits, the expressed I_{Ba} peak current amplitude was around 4-6μA. Only oocytes expressing < 6μA of peak currents were used, this was to minimize errors originating from limitations of the two-electrode whole-cell voltage clamp.

At first the drugs' effect was examined on the voltage-dependence of activation. To generate **current-voltage relationships (*I-V* curve)** of $I_{Ba,}$ oocytes were held at a holding potential of -80mV and depolarized to voltages between -50mV and +60mV in 10mV increments for 400ms at 0.066Hz which allowed neither further accumulation of the use-dependent block nor recovery from the blockade by Diltiazem at this holding potential. Depolarization was then discontinued, drug was applied, and after 3min quiescent period, depolarizing test pulses were resumed. *I-V* curves of wild-type HHT-α_{1C} channels and VSM-α_{1Cb} are shown before and after drug application in Figures 11, 12. In 40mM Ba^{2+} solution, I_{Ba} of the Wild-type HHT $Ca_v1.2$ activated at a threshold of -10 mV and reached peak current values between +10 and 20mV. The *I-V* curves did not show any statistical difference after

drug, compared with that of the absence of drug, with regard to the half maximum activation voltage ($V_{0.5}$), the slope factor (K) and the peak current amplitude (I_{Ba}). Electrophysiological properties of the Diltiazem analogs and Diltiazem on the HHT $Ca_v1.2$ channels compared with VSM $Ca_v1.2$ are summarized in Tables 3, 4, 5. The decrease in peak current amplitude was the most pronounced after application of P1, however, it fell short of statistical significance. In conclusion, none of the compounds, including Diltiazem produced any significant changes in the I-V curve of I_{Ba} at -80mV holding potential. The smooth curves are fit of the data to Boltzmann distribution.

The results were similar using the VSM-α_{1Cb} clone except the half activation potential ($V_{0.5}$) was more hyperpolarized compared with those of HHT-α_{1C} (-8.93±1.04mV vs. 4.12±1.35mV, respectively). However, some of the I-V curves displayed a hyperpolarizing shift (left) yielding a discrepancy compared with the presumed peak value (according to the literature) for the expressed $Ca_v1.2$ channels. This shift is most likely not due to the specific effect of the compound on the L-VDCC activation, but it is rather attributed to experimental technique like serious resistance error. When a current I_{Ba} flows across the membrane the resistance R_S leads to a discrepancy between the measured membrane potential Vm (controlled by the amplifier) and the true potential difference across the membrane, V_t. The size of the error is IxR_S. According to Ohm's law, using this equation, it is possible to predict the distortion brought about by series resistance errors in the I-V curve. Series resistance errors can severely distort I-V curves. As a matter of fact, most of the times, since the transcript mRNA was very pure, oocytes expressed the Ca^{2+} channel very efficiently and it was extremely difficult to adjust the right timing for voltage-clamp measurements. In order to be able to record and measure such huge current (>6μA) without introducing error, it is important to use low- resistance electrodes (around 0.5MΩ) for both the voltage recording and current passing electrodes. The electrodes' low resistance eliminates the need in a negative capacitance circuit, to correct for the frequency response of the voltage recording electrode, thereby removing this potential source of clamp instability. However, we could not completely exclude the possibility that the hyperpolarizing shift in some degree linked associated to the VSM-α_{1Cb} clone.

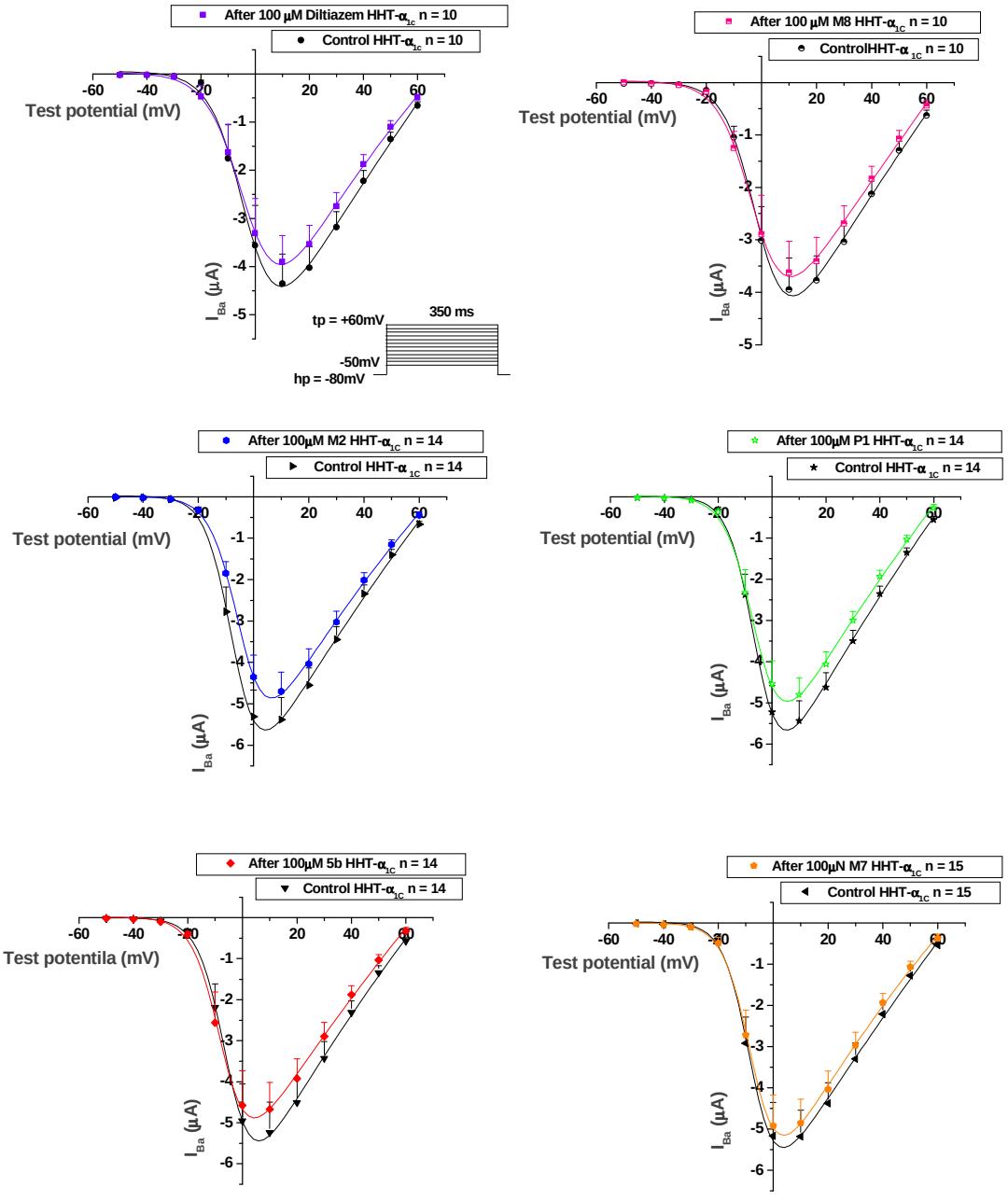

Figure 11. Effect of 100µM of Diltiazem, M8, M2, P1, 5b and M7 on HHT-α_{1C} ($Ca_V1.2$) channel. Figure shows the current (I) -voltage (V) relationships for I_{Ba} before (black line) and after 3 min superfusion with Diltiazem (violet line), M8 (pink line), M2 (blue line), P1 (green line), 5b (red line) and M7 (orange line), respectively. Peak amplitude of Ba^{2+} current elicited by a 400-ms depolarization to the indicated test potentials (-50mV- +60mV) in 10mV increments from a holding potential of -80mV is plotted against the test potential. Smooth line represents the best fit to a Boltzmann equation (See Methods). Each point and vertical bar represents the mean ± S. E. M of 10-15 experiments.

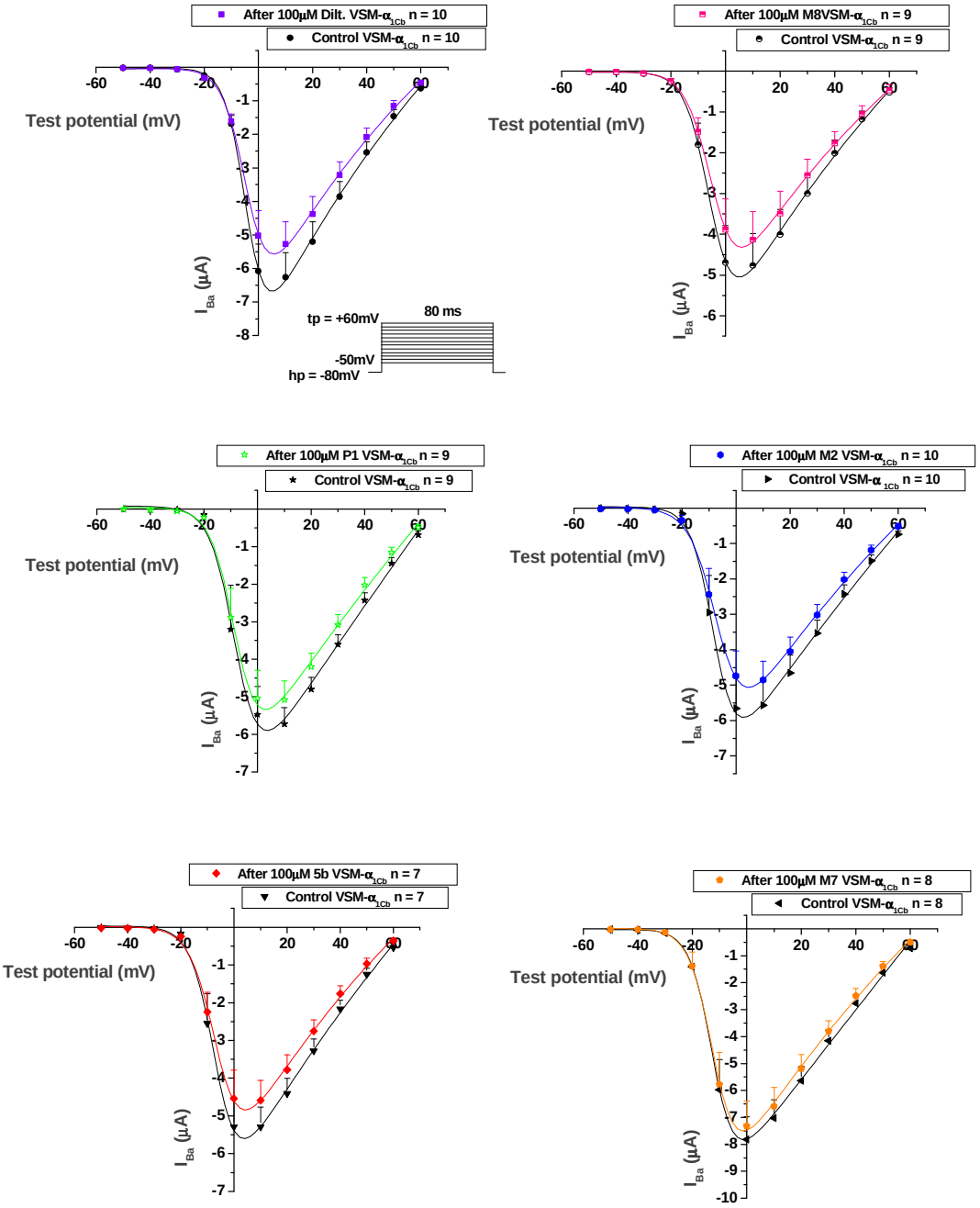

Figure 12. Effect of 100µM of Diltiazem, M8, M2, P1, 5b and M7 on VSM-α_{1Cb} ($Ca_v1.2$) channel. Figure shows the current (*I*) -voltage (*V*) relationships for I_{Ba} before (black line) and after 3min superfusion with Diltiazem (violet line), M8 (pink line), M2 (blue line), P1 (green line), 5b (red line) and M7 (orange line), respectively.

	$V_{0.5\ act.}$ (mV) *Xenopus* oocytes Current-Voltage relationship	K (mV) *Xenopus* oocytes Current-Voltage relationship	Peak current (mV) *Xenopus* oocytes Current-Voltage relationship	Tonic Block (+10mV) *Xenopus* oocytes Current inhibition %
$Control_{HHT}$	4.12 ±1.35 N = 11	5.97 ±0.26 N = 11	-4084.21 ±587.84 N = 10	Run down less than 5%
$Diltiazem_{HHT}$	-0.68 ±2.01 N = 10 NS	5.66 ±0.20 N = 10 NS	-4032.14 ± 580.09 N = 10 NS	-4.92 ±5.26 N = 15 NS
$M8_{HHT}$	0.88 ±1.83 N = 10 NS	6.25 ±0.49 N = 10 NS	-3782.10 ± 666.79 N = 10 NS	-8.23 ±3.10 N = 13 P < 0.05

Tab. 3

	$V_{0.5\ act.}$ (mV) *Xenopus* oocytes Current-Voltage relationship	K (mV) *Xenopus* oocytes Current-Voltage relationship	Peak current (mV) *Xenopus* oocytes Current-Voltage relationship	Tonic Block (+10mV) *Xenopus* oocytes Current inhibition %
$Control_{HHT}$	-5.17 ±1.13 N = 13	4.25 ±0.32 N = 13	-5001.47 ±694.07 N = 13	Run down less than 5%
$M2_{HHT}$	-4.45 ±0.76 N = 12 NS	4.84 ±0.30 N = 12 NS	-5097.05 ±449.76 N = 12 NS	-10.13 ±2.66 N = 16 P < 0.05
$P1_{HHT}$	-4.64 ±1.26 N = 13 NS	4.62 ±0.39 N = 13 NS	-4875.32 ±562.21 N = 12 NS	-6.18 ±3.67 N = 14 NS
$5b_{HHT}$	-4.21 ±1.40 N = 12 NS	4.75 ±0.41 N = 12 NS	-5061.49 ±801.52 N = 12 NS	-3.01 ±1.87 N = 12 NS
$M7_{HHT}$	-5.49 ±1.27 N = 12 NS	4.84 ±0.35 N = 12 NS	-4966.74 ±664.28 N = 12 NS	-3.62 ±3.89 N = 15 NS

Tab. 4

	$V_{0.5\ act.}$ (mV) *Xenopus* oocytes Current-Voltage relationship	K (mV) *Xenopus* oocytes Current-Voltage relationship	Peak current (mV) *Xenopus* oocytes Current-Voltage relationship	Tonic Block (+10mV) *Xenopus* oocytes Current inhibition %
$Control_{VSM}$	-8.93 ± 1.04 N = 10	3.31 ± 0.55 N = 10	-6349.49 ± 644.26 N = 10	Run down less than 5%
$Diltiazem_{VSM}$	-3.08 ± 0.78 N = 10 P < 0.001	4.48 ± 0.29 N = 10 NS	-5314.08 ± 743.64 N = 8 NS	1.60 ± 6.58 N = 7 NS
$M8_{VSM}$	-3.61 ± 1.30 N = 10 NS	4.71 ± 0.71 N = 10 P < 0.05	-4246.55 ± 709.36 N = 9 P < 0.05	-7.46 ± 4.18 N = 7 NS
$M2_{VSM}$	-5.78 ± 1.79 N = 10 NS	3.72 ± 0.43 N = 10 NS	-5131.92 ± 611.96 N = 10 NS	-4.17 ± 8.44 N = 5 NS
$P1_{VSM}$	-5.44 ± 1.71 N = 9 NS	4.05 ± 0.44 N = 9 NS	-5513.10 ± 704.87 N = 8 NS	-1.59 ± 3.39 N = 7 NS
$5b_{VSM}$	-4.78 ± 1.92 N = 7 NS	4.37 ± 0.43 N = 7 NS	-4860.72 ± 609.98 N = 7 NS	1.26 ± 2.82 N = 7 NS
$M7_{VSM}$	-10.19 ± 1.85 N = 8 NS	4.11 ± 0.58 N = 8 NS	-7373.40 ± 896.24 N = 8 NS	-5.61 ± 3.87 N = 5 NS

Tab. 5

Voltage-dependent tonic block of $Ca_v1.2$ channels by Diltiazem and the newly synthesized Diltiazem analogs. After the beginning of whole cell recording, I_{Ba} amplitude was monitored until it was stable, with the use of 80ms test depolarizations to +10mV applied every 15s from a holding potential of -60mV. After the steady state has reached, the control was recorded using the same protocol as above except that the frequency was 2s (0.5Hz). Drugs were then introduced into the bath at 100μM concentrations and I_{Ba} was recorded after 3min during this period of time to reach equilibrium. Tonic ("resting-state dependent") block was defined as peak I_{Ba} inhibition during the first pulse after a 3min equilibration in drug-containing solution at the holding potential. It was previously mentioned that the interaction between Ca^{2+} channel blocker and the L-VDCC is modulated by the state of the channel ("modulated receptor hypothesis") or by the transmembrane potential, thus, showing voltage-dependence, use-dependence or both. Application of the drugs produced little tonic block (Current inhibition % for diltiazem, M8, M2, P1, 5b and M7: -4.92±5.26; -8.23±3.10; -10.13±2.66; -6.18±3.67; -3.01±1.87; -3.62±3.89, respectively) (Table 3, 4), indistinguishable from current "run-down" during a similar period in drug-free solution suggesting that these drugs hardly bind to the resting state of the channel (Figure 11, 12).

Use-dependent block (UDB) by Diltiazem and Diltiazem analogs

During repetitive depolarizations, block by PAAs and BTZs accumulates in a frequency or use-dependent and voltage-dependent manner because additional drug binds (association) during each depolarization and fails to unbind (dissociation) completely at the resting potential between depolarizations. Such a use-dependent block is important for the clinical efficacy of drugs. The use-dependent block develops more rapidly and more strongly at depolarized holding potentials, which is explained by the voltage dependence of dissociation rates of the drugs. To examine the UDB of I_{Ba}, trains of 15 pulses (80ms) applied from a holding potential of -60mV to +10mV (peak potential of the current-voltage relationship) at a frequency of 0.5Hz. The current amplitude for each pulse was normalized relative to that of the first pulse (Figure 17). The final steady-state block represents tonic block plus UDB. Diltiazem progressively decreased I_{Ba} in a use-dependent manner (Figure 13, 14, 15, 16 and 17). M2, M8 and P1 did not show any use-dependency. We can see a slight decrease in I_{Ba} during the train due to the accumulation of inactivation. Based on these results, we might have expected a decreased current decay during the 3s test pulse by M8, M2 and P1, and

this could have explained in part the lack of use-dependency. Despite the significantly faster inactivation kinetics by the new Diltiazem analogs, UDB was not observed in oocytes injected with neither HHT-α_{1C} nor VSM-α_{1Cb} (Figure 14 and 17).

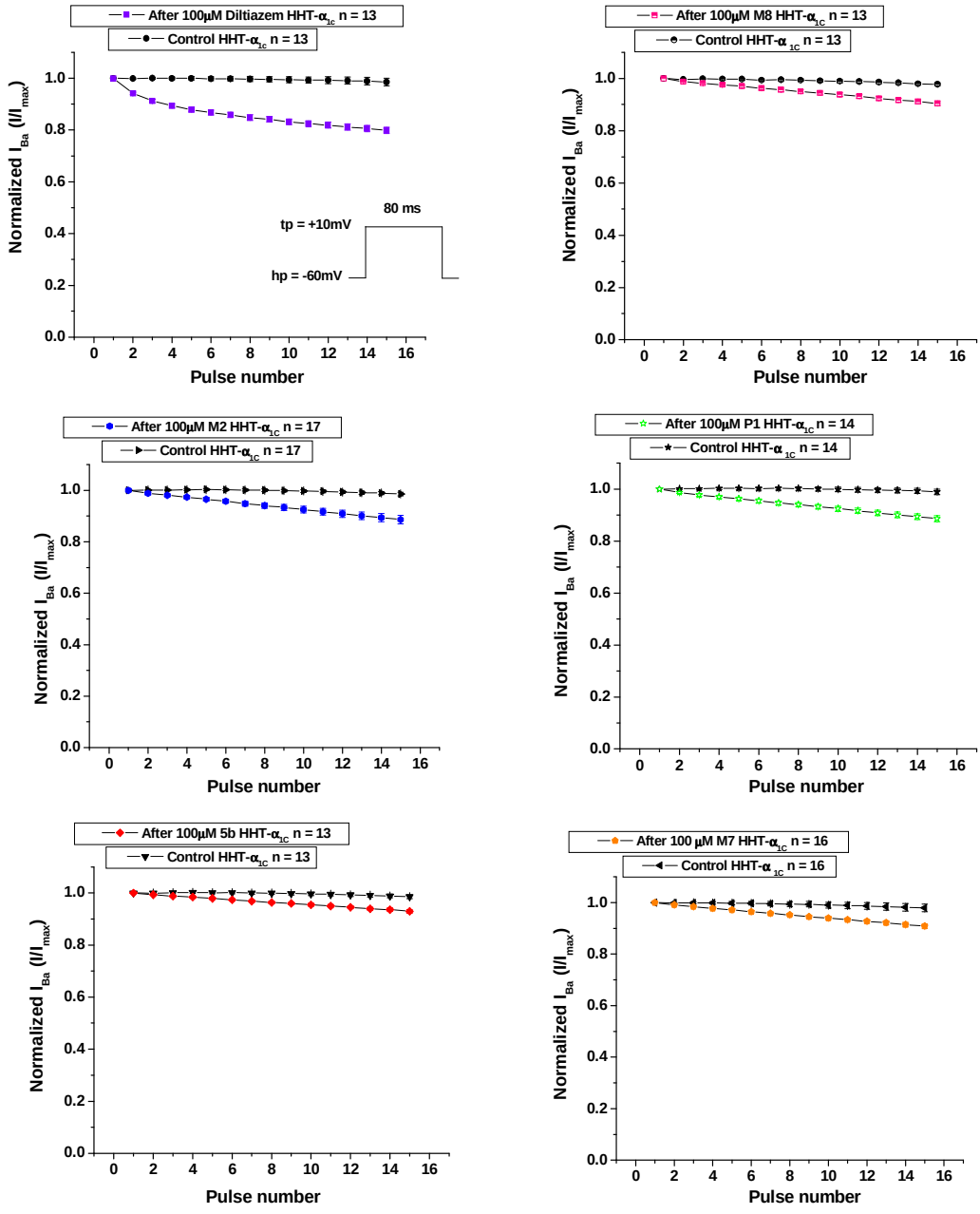

Figure 13. Use-dependent block of $Ca_v1.2$ α_{1C} channel currents. Use dependent I_{Ba} inhibition during fifteen consecutive test pulses by 100μM of Diltiazem, M8, M2, P1, 5b and M7, respectively. Depolarizing pulses (80ms duration) to +10mV test pulse from a holding potential of -60mV were applied at 0.5Hz frequencies. Mean reduction in peak current of I_{Ba} in each successive depolarizing pulse was normalized to that for the peak I_{Ba} during the first pulse and plotted against pulse number. The applied pulse protocol is displayed in the inset. Each point represents the mean of 13-18 experiments.

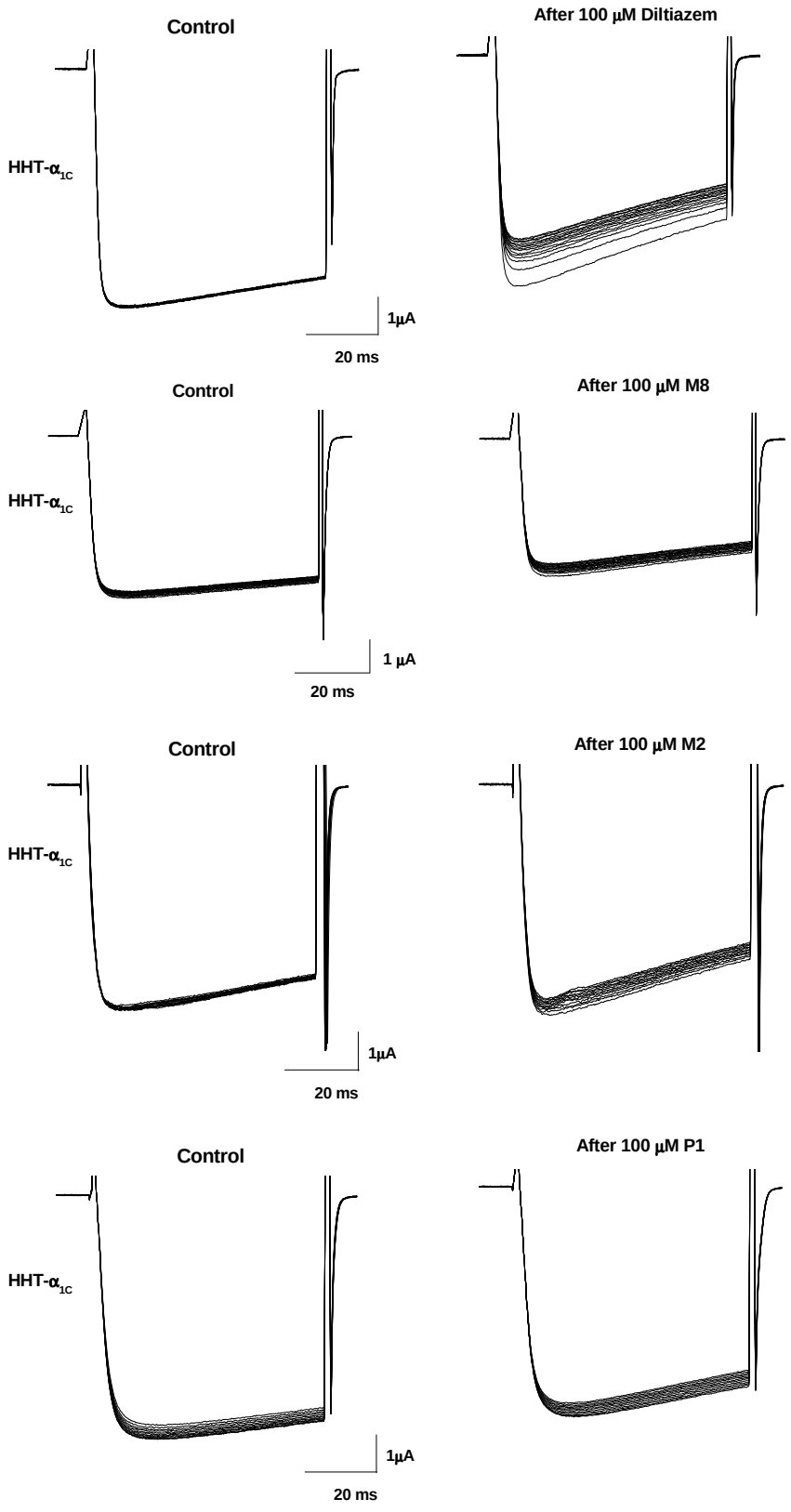
Control
After 100 μM Diltiazem
HHT-α1C
1μA
20 ms
Control
After 100 μM M8
HHT-α1C
1 μA
20 ms
Control
After 100 μM M2
HHT-α1C
1μA
20 ms
Control
After 100 μM P1
HHT-α1C
1μA
20 ms

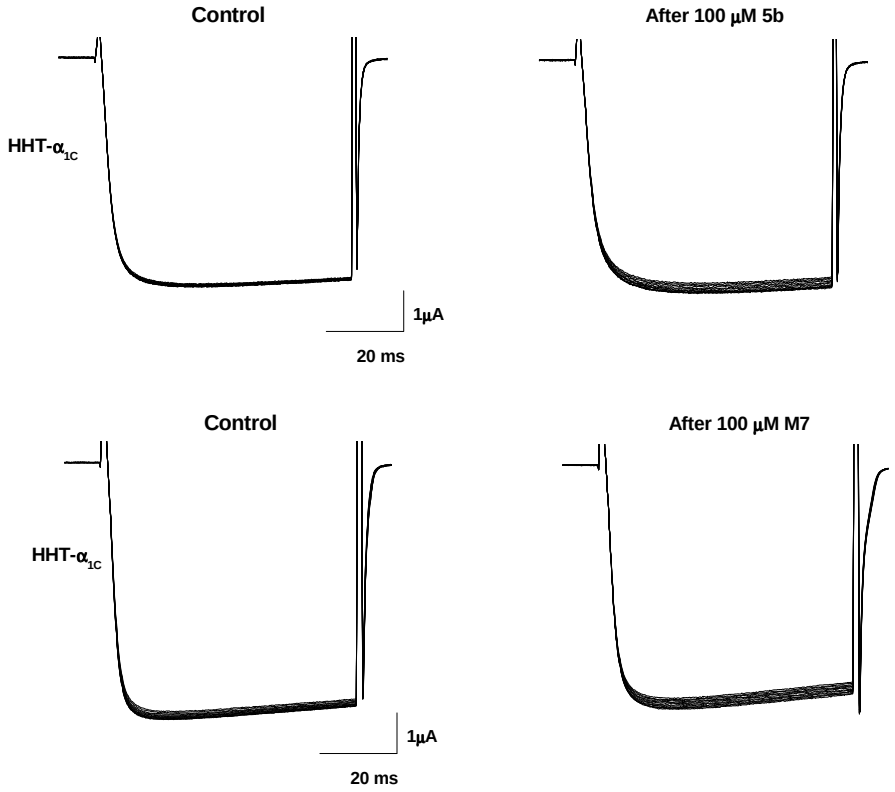

Figure 14. Use-dependent block of $Ca_v1.2$ α_{1C} channel currents. 0.5Hz train consisting of fifteen 80ms depolarizations to +10mV was applied. Representative current traces of I_{Ba}, in the absence and presence of 100μM of diltiazem, M8, M2, P1, 5b and M7, respectively. The small decrease of I_{Ba} after application of M8, M2, P1, 5b and M7 shown in figure 14, is due to combination of the accumulation of voltage-dependent inactivation and "run-down" of I_{Ba} caused by the big current developed in the oocytes.

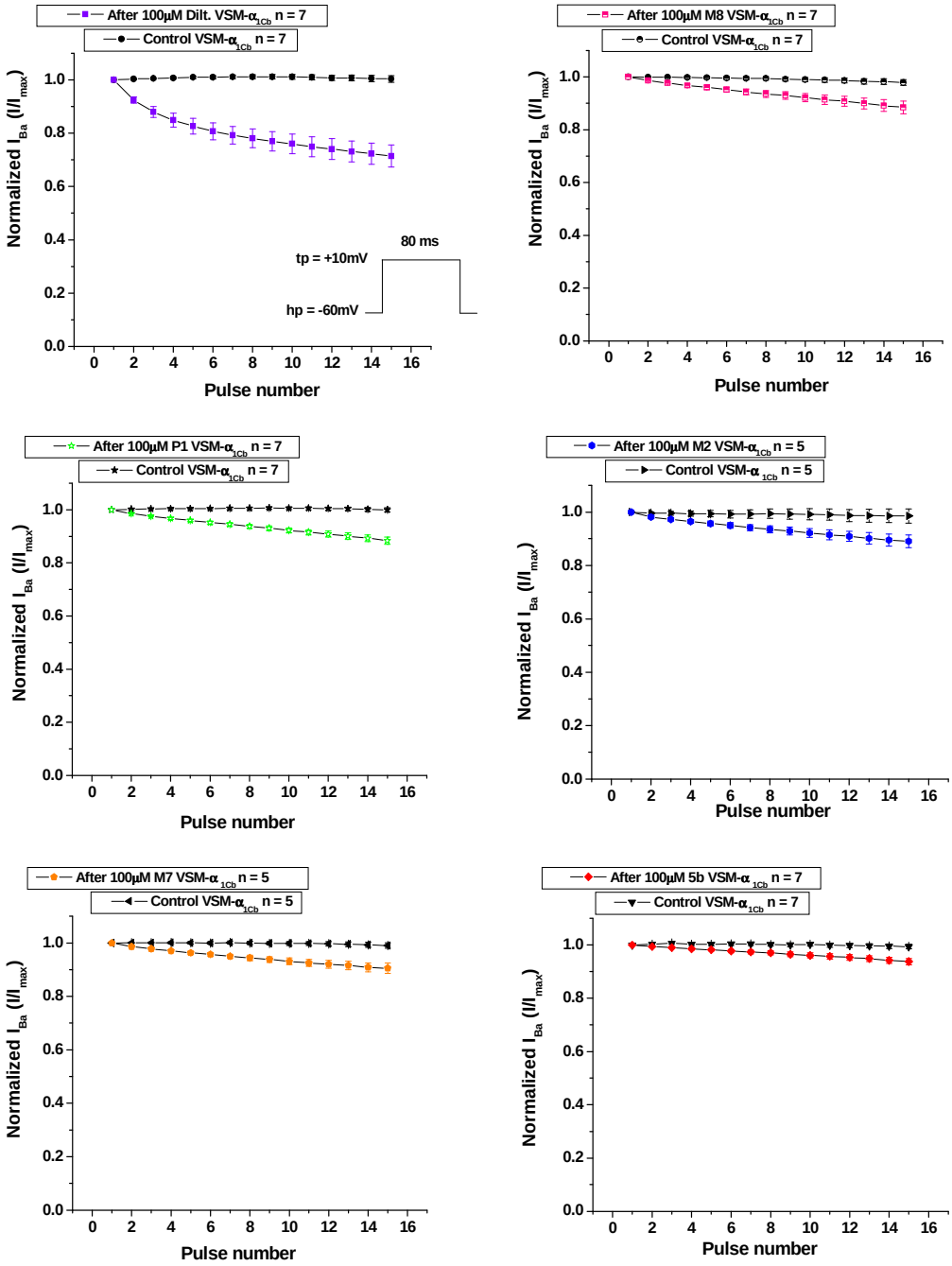

Figure 15.Use-dependent block of VSM-α_{1Cb} ($Ca_v1.2$) channel current. Use dependent I_{Ba} inhibition during fifteen consecutive test pulses by 100µM of Diltiazem, M8, M2, P1, 5b and M7, respectively.

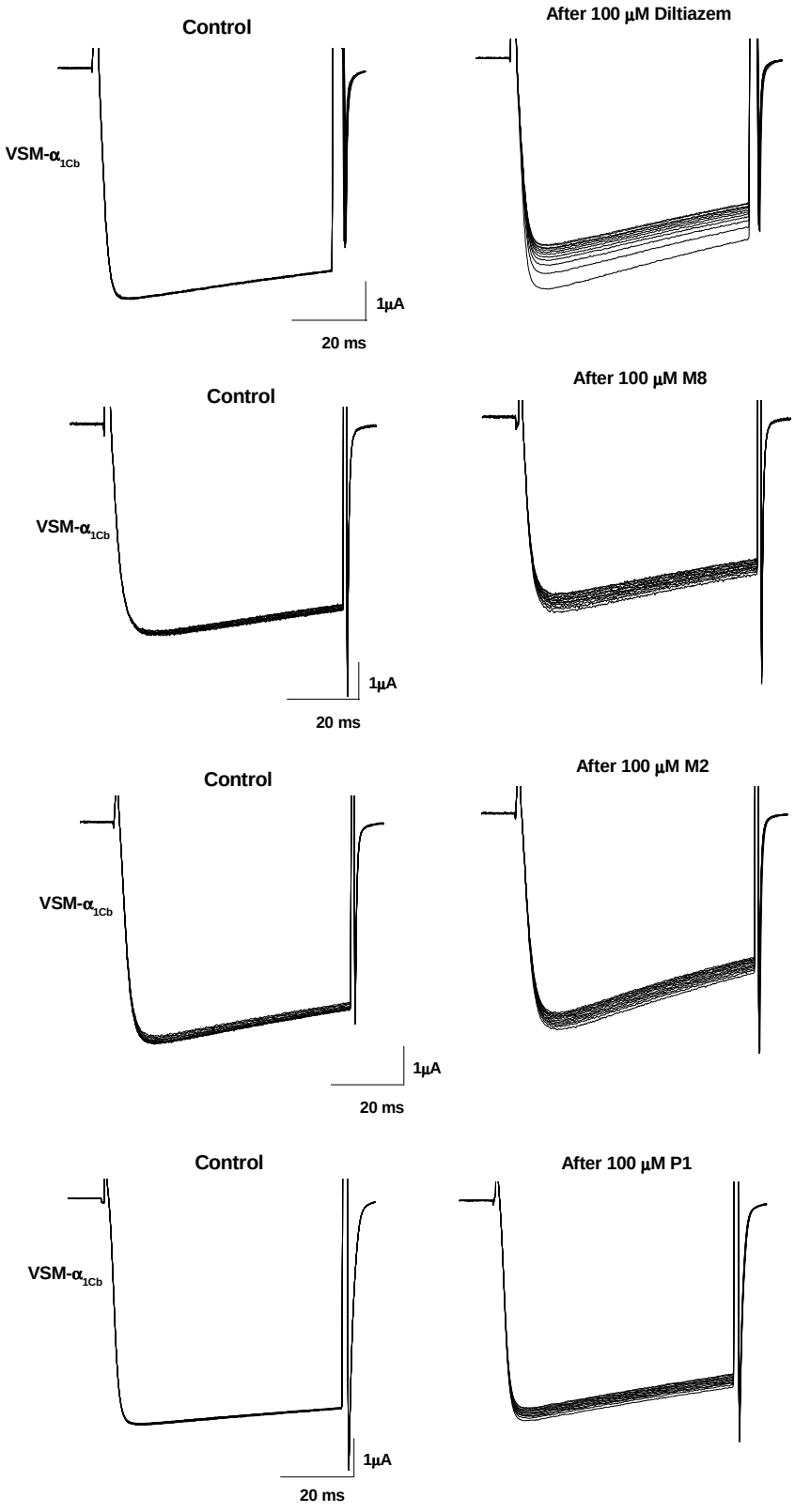
Control
After 100 μM Diltiazem
VSM-α1Cb
1μA
20 ms
Control
After 100 μM M8
VSM-α1Cb
1μA
20 ms
Control
After 100 μM M2
VSM-α1Cb
1μA
20 ms
Control
After 100 μM P1
VSM-α1Cb
1μA
20 ms

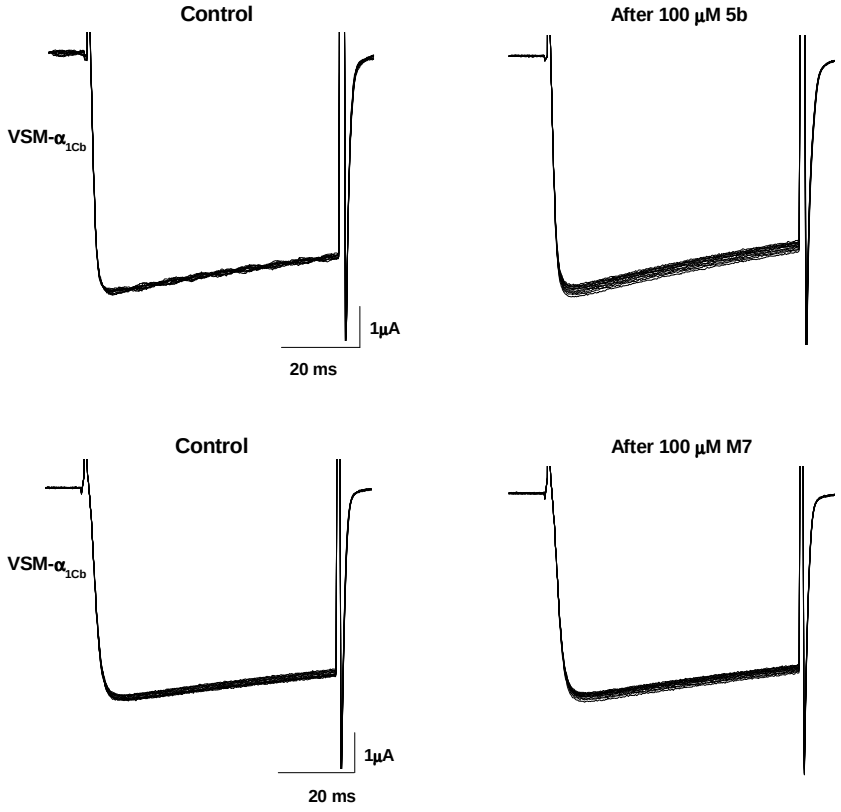

Figure 16. Use-dependent block of VSM-α_{1Cb} ($Ca_v1.2$) channel currents. Representative current traces of I_{Ba}, in the absence and presence of 100µM of Diltiazem, M8, M2, P1, 5b and M7, respectively. The small decrease of I_{Ba} after application of M8, M2, P1, 5b and M7 shown in figure 16, is due to combination of the accumulation of voltage-dependent inactivation and "run-down" of I_{Ba} caused by the big current developed in the oocytes.

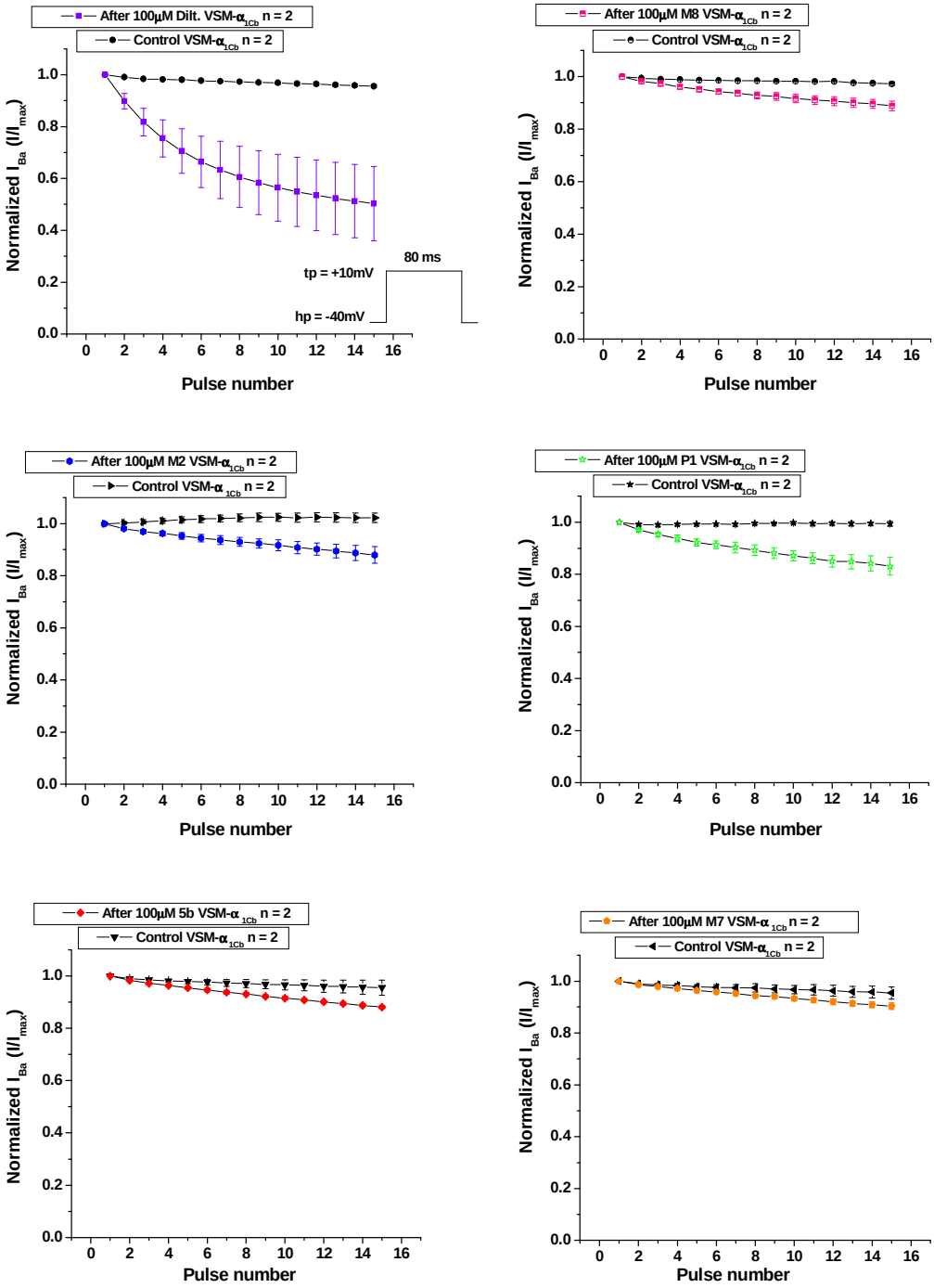

Figure 17.Use-dependent block of VSM-α_{1Cb} ($Ca_v1.2$) channel currents. Use dependent I_{Ba} inhibition during fifteen consecutive test pulses by 100µM of Diltiazem, M8, M2, P1, 5b and M7, respectively. Depolarizing pulses (80ms duration) to +10mV test pulse from a holding potential of -40mV were applied at 0.5Hz frequencies. Mean reduction in peak current of I_{Ba} in each successive depolarizing pulse were normalized to that for the peak I_{Ba} during the first pulse and plotted against pulse number.

Action of Diltiazem and Diltiazem analogs on the time course of I_{Ba}

To understand the reduction of frequency dependent block after the Diltiazem analogs in HHT $Ca_v1.2$ channels, the effect of Diltiazem and the Diltiazem analogs on Ca^{2+} channel inactivation was examined. At first, from the sample traces of *I-V* relations, it was found that the voltage-dependent inactivation of HHT-$Ca_v1.2$ after M2, M8, and P1 was accelerated compared with that of control. To characterize the voltage-dependent inactivation of HHT-$Ca_v1.2$ after drugs, the time-dependent inactivation was analyzed. Hering *et al.* [81] suggested that inactivation is an important determinant for the development of use-dependent block by PAA. If Diltiazem interacts with calcium channels in their open state, the time course of I_{Ba} should be affected during a depolarizing voltage pulse, as has been described for calcium channel currents, when Ba^{2+} was the charge carrier. The effect of Diltiazem and the five Diltiazem analogs on the rate of current decay was determined during a maintained 3s depolarizations. Indeed, Diltiazem accelerated the rate of I_{Ba} decay during the depolarizing pulse. The drug-induced increase of the rate of I_{Ba} is caused by the development of drug block during the depolarization and is characteristic of the compounds that block the open and/or inactivated state of calcium channels that are present at depolarized potentials more potently than the resting state at -80mV. The inactivation process (descending phase of I_{Ba}) was fitted by mono-exponential curves with time constants of 269.11±12.97ms under control conditions and 207.23±10.05ms after exposure of 100μM Diltiazem. An unexpected finding was that M8, M2 and P1 significantly accelerated the time course of inactivation (See Table 6, 7, 8) in both HHT-α_{1C} and VSM-α_{1Cb} channels. Treatment with 5b and M7 did not affect the time course of I_{Ba} significantly (Figure 18, 19 and 20).

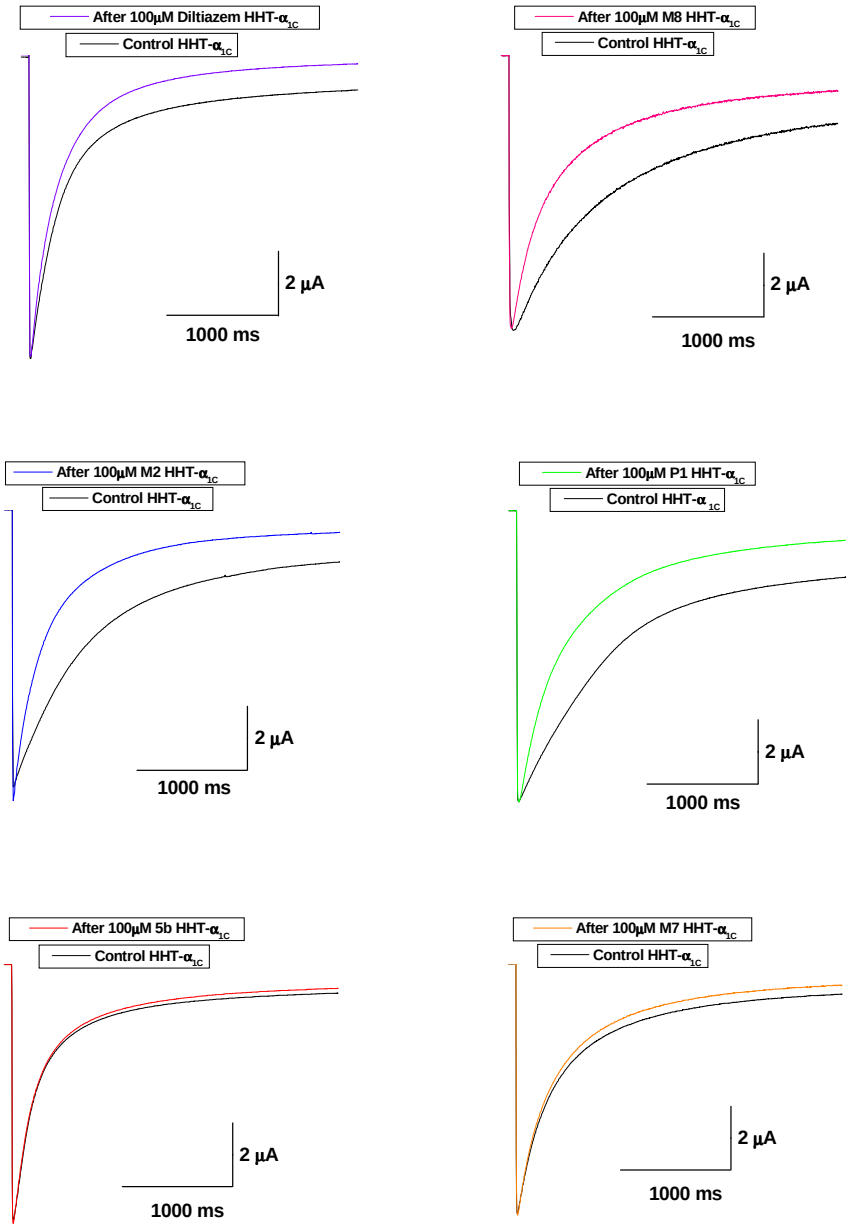

Figure 18. Time course of Diltiazem and Diltiazem analogs block of depolarized channels. Representative traces of Ba^{2+} current through HHT-$Ca_v1.2$ measured during 3s depolarization to +10mV from a holding potential of -80mV in the absence and presence of drugs. For each compound, the original recordings of I_{Ba} under control and under the influence of compounds were superimposed. In some cases, I_{Ba} was normalized to peak current, to facilitate comparison of the rate of current decay in the absence and presence of Diltiazem.

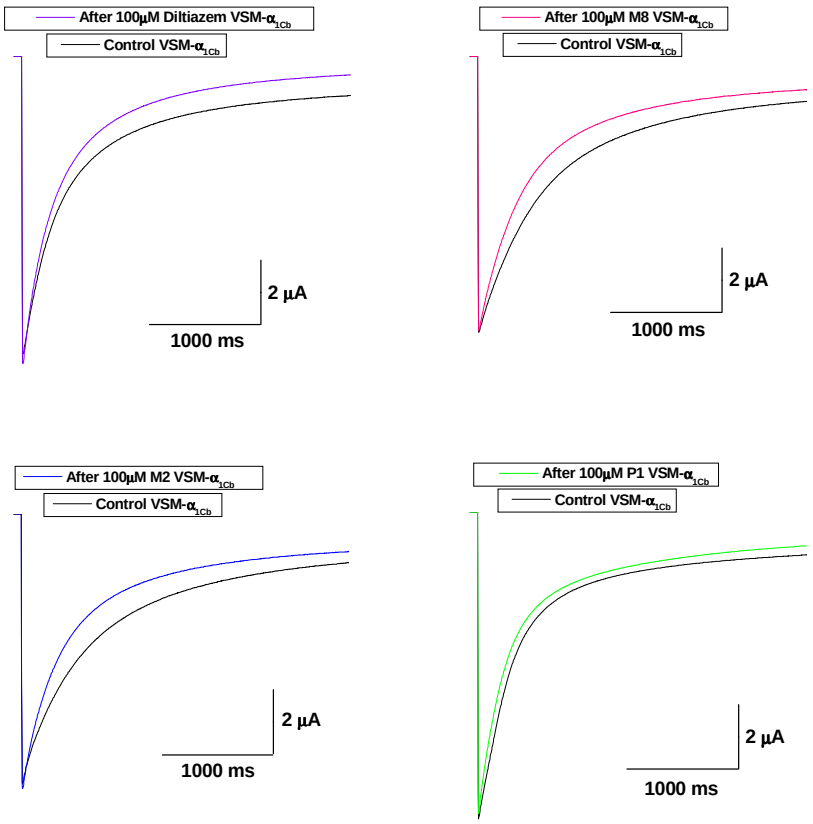

Figure 19. Time course of Diltiazem and Diltiazem analogs block of depolarized VSM-$Ca_v1.2$ channels current. For each compounds the original recordings of I_{Ba} under control and under the influence of compounds were superimposed. In some cases I_{Ba} were normalized to peak current, to facilitate comparison of the rate of current decay in the absence and presence of Diltiazem.

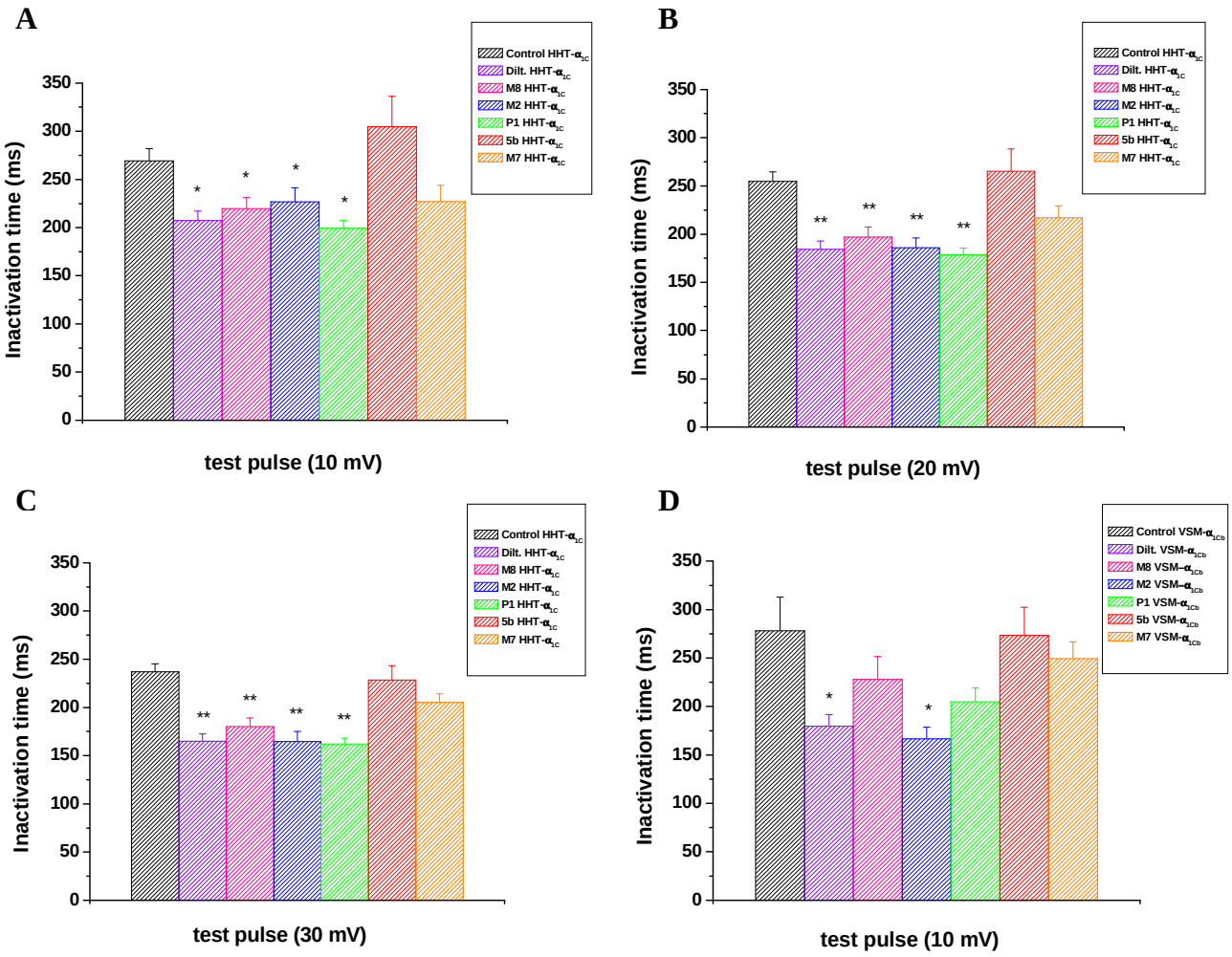

Figure 20. Voltage-dependent inactivation of I_{Ba} of HHT-α_{1C} $Ca_v1.2$ channels (*A*, B, *C*), and VSM-α_{1C} $Ca_v1.2$ channels (D) (*, $p < 0.05$, **, $p < 0.001$, unpaired t test) evoked at test pulse of 10, 20, and 30mV for the HHT-$Ca_v1.2$ channels and at test pulse of 10 mV for the VSM-$Ca_v1.2$ channels. Each column represents the mean ± SEM of the inactivation of I_{Ba} by Diltiazem (violet), M8 (pink), M2 (blue), P1 (green) 5b (red) and M7 (orange).

Effect of drugs on the steady-state inactivation of HHT-$Ca_v1.2$ channel

To study the affinity of M8, M2, P1, 5b, M7 and Diltiazem for the inactivated state of the Ca^{2+} channels, the steady-state inactivation curves were determined using a standard double-pulse protocol. M8, M2, P1 and Diltiazem significantly shifted the steady-state inactivation curves towards the negative potential, suggesting that all of the drugs shift Ca^{2+} channels to the inactivated state (Figure 21, 22). From the Boltzmann's distribution, $V_{0.5}$ (the mid potential) and the K (slope of the curve) were calculated in the control condition and in the presence of 100μM of each six compounds including the reference Diltiazem. The $V_{0.5}$ values are as follows: Control-1, $V_{0.5}$=-12.04±0.69mV; Diltiazem, -19.20±0.78mV; M8, -16.09 ± 0.98mV; Control-2, $V_{0.5}$=-12.50±0.46mV; M2, -15.48±0.64mV; P1, -16.82±1.19mV (Tables 6, 7 and 8). Only M8, M2, 5b and M7 caused a slight change in the slope factor compared with control (Control-1, k=7.93±0.28 mV; M8, k=9.65±0.26mV; Control-2, k=7.38±0.27mV; 5b, k=8.17±0.12mV; M7, K=8.60±0.18mV). The finding is that three of the newly synthesized Diltiazem analogs M2, M8, P1 and the reference Diltiazem shifted the steady state inactivation curves to the hyperpolarizing direction, implying that these drugs have a higher affinity for the inactivated state of the channel than for the resting state.

In the case of analysis of the steady-state inactivation, two different controls (since not every experiment after drug has self control), one for Diltiazem and M8, and another one for M2, P1, 5b and M7, were applied. The reason for that is the difference in the time of the measurements. In fact, at the beginning of the EP studies, the measurements were focused on the comparison between Diltiazem and M8 effects only, and later it was decided to include in the analysis the M2, P1, 5b and M7 compared with Diltiazem. During the latest set of experiments (new mRNAs were transcribed), I_{Ba} current and the number of experiments were bigger than during the first set experiments, so it was impossible to compare all compounds with Diltiazem and only one control for all of them.

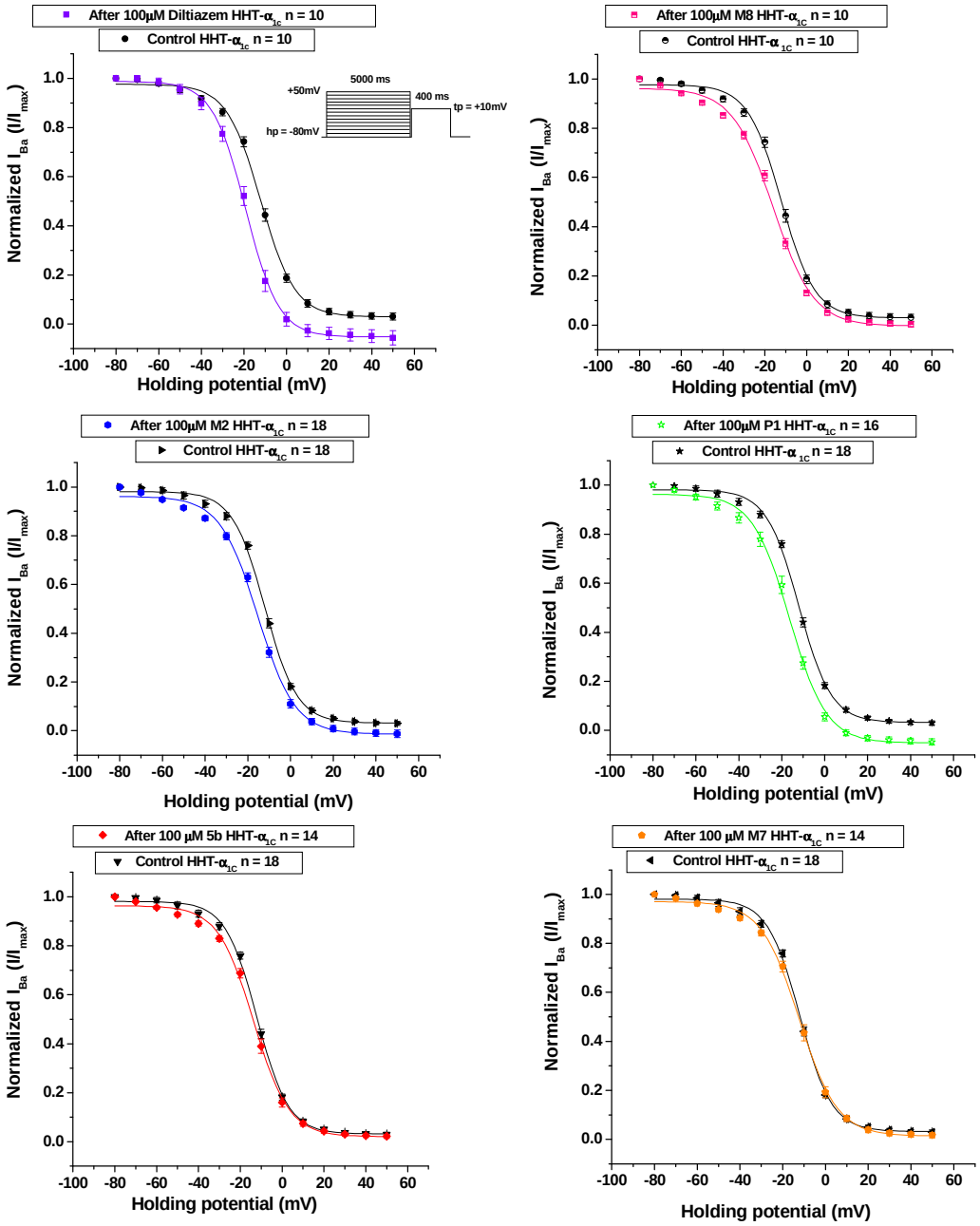

Figure 21. Steady-state inactivation curves for I_{Ba} in the absence (black line) or presence of 100µM of Diltiazem (violet line), M8 (pink line), M2 (blue line), P1 (green line), 5b (red line), and M7 (orange line). Inactivation fraction was determined by using a two-pulse protocol in which a 5s conditioning prepulse to the indicated potentials was followed by a test pulse to peak I_{Ba} potential. Resultant currents were recorded before and 3min after superfusion with Diltiazem, M8, M2, P1, 5b and M7. The steady-state inactivation curves were obtained by normalizing the current values to the peak I_{Ba} at -80mV. The relative peak current at +10mV was plotted against the different prepulse potentials. Inactivation curves were fitted according to the Boltzmann equation (See Methods Section). Each point and vertical bar represents the mean ± S.E.M. of 10-18 experiments.

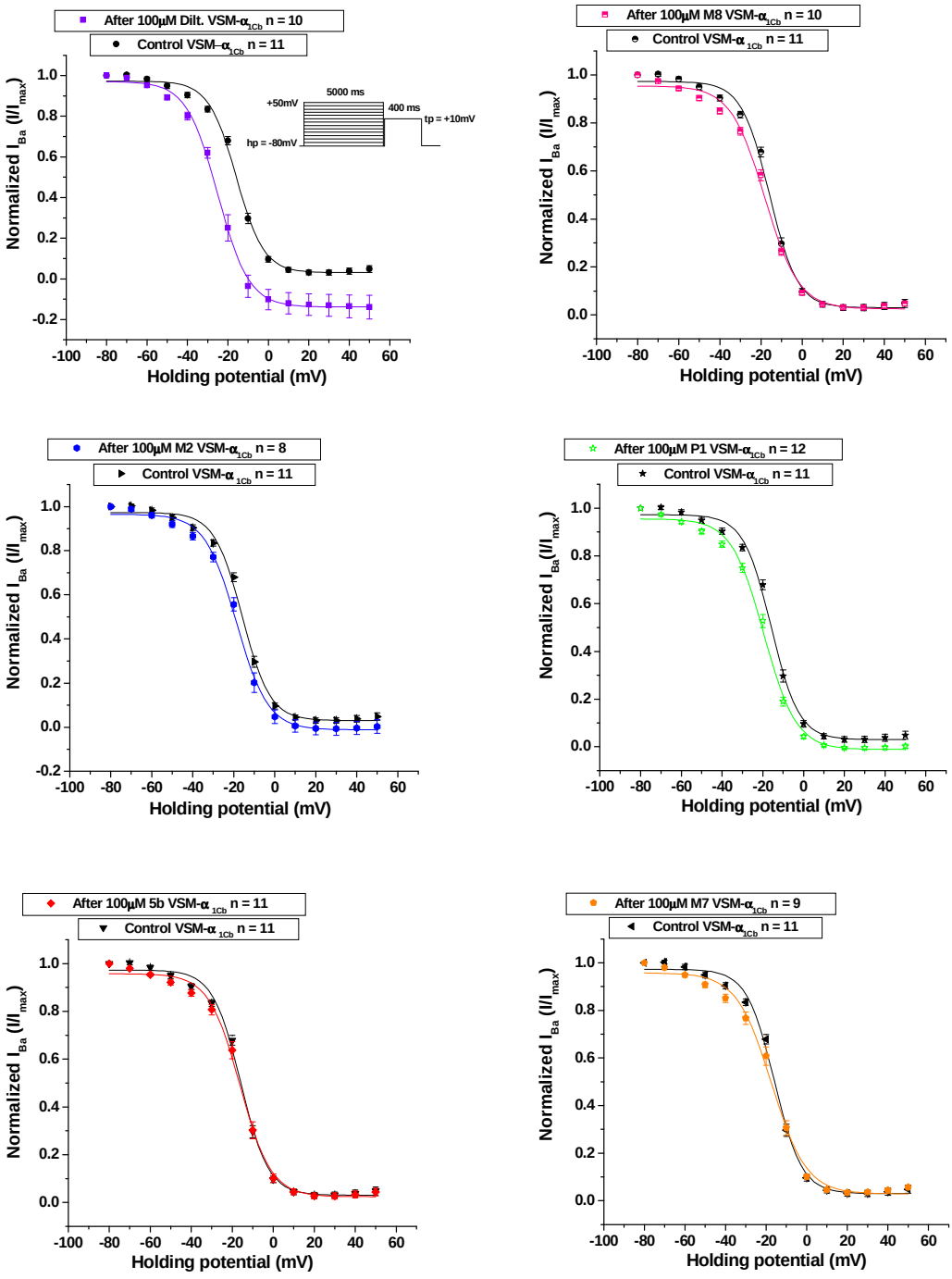

Figure 22. VSM-α_{1Cb} ($Ca_v1.2$) channel steady-state inactivation curves for I_{Ba} in the absence (black line) or presence of 100µM of Diltiazem (violet line), M8 (pink line), M2 (blue line), P1 (green line), 5b (red line), and M7 (orange line).

	$V_{0.5\ inact.}$ (mV) Steady state inactivation *Xenopus* oocytes	K (mV) Steady state inactivation *Xenopus* oocytes	τ_1 (ms) Recovery from inactivation *Xenopus* oocytes	τ_2 (ms) Recovery from inactivation *Xenopus* oocytes	τ_1 (ms) Inactivation time *Xenopus* oocytes
Control$_{HHT}$	-12.04 ± 0.69 N = 10	7.93 ± 0.28 N = 10	48.98 ± 4.20 N = 10	1823.74 ± 221.71 N = 10	269.11 ± 12.97 N = 12
Diltiazem$_{HHT}$	-19.20 ± 0.78 N = 10 P < 0.001	7.82 ± 0.32 N = 10 NS	442.34± 151.85 N = 7 P < 0.05	1951.32 ± 241.70 N = 7 NS	207.23 ± 10.05 N = 12 P < 0.05
M8$_{HHT}$	-16.09 ± 0.98 N = 10 P < 0.05	9.65 ± 0.26 N = 10 P < 0.001	65.88 ± 11.29 N = 11 NS	1636.80 ± 222.64 N = 11 NS	219.60 ± 11.49 N = 12 P < 0.05

Tab. 6

	$V_{0.5\ inact.}$ (mV) Steady state inactivation *Xenopus* oocytes	K (mV) Steady state inactivation *Xenopus* oocytes	τ_1 (ms) Recovery from inactivation *Xenopus* oocytes	τ_2 (ms) Recovery from inactivation *Xenopus* oocytes	τ_1 (ms) Inactivation time *Xenopus* oocytes
Control$_{HHT}$	-12.50 ± 0.46 N = 18	7.38 ± 0.27 N = 18	48.98 ± 4.20 N = 10	1823.74 ± 221.71 N = 10	269.11 ± 12.97 N = 12
M2$_{HHT}$	-15.48 ± 0.64 N = 18 P < 0.001	8.72 ± 0.27 N = 18 P < 0.05	50.20 ± 6.81 N = 8 NS	1854.15 ± 321.68 N = 8 NS	226.86 ± 14.51 N = 10 P < 0.05
P1$_{HHT}$	-16.82 ± 1.19 N = 16 P < 0.05	8.41 ± 0.51 N = 16 NS	94.14 ± 17.97 N = 7 P < 0.05	1350.73 ± 314.01 N = 7 NS	199.28 ± 8.19 N = 9 P < 0.001
5b$_{HHT}$	-13.53 ± 0.83 N = 14 NS	8.17 ± 0.12 N = 14 P < 0.05	ND	ND	304.96 ± 31.28 N = 10 NS
M7$_{HHT}$	-12.19 ± 1.03 N = 14 NS	8.60 ± 0.18 N = 14 P < 0.05	ND	ND	227.02 ± 16.75 N = 8 NS

Tab. 7

	$V_{0.5\ inact.}$ (mV) Steady state inactivation *Xenopus* oocytes	K (mV) Steady state inactivation *Xenopus* oocytes	τ_1 (ms) Recovery from inactivation *Xenopus* oocytes	τ_2 (ms) Recovery from inactivation *Xenopus* oocytes	τ_1(ms) Inactivation time *Xenopus* oocytes
Control$_{VSM}$	-15.81± 0.48 N = 11	6.70± 0.26 N = 11	88.57± 39.46 N = 4	1611.42± 166.29 N = 4	278.14± 34.70 N = 14
Diltiazem$_{VSM}$	-24.80± 0.58 N = 10 P < 0.001	7.59± 0.43 N = 10 NS	625.11± 99.99 N = 2 P < 0.05	1423.56± 191.97 N = 2 NS	180.40± 10.11 N = 14 P < 0.05
M8$_{VSM}$	-18.28± 0.70 N = 10 P < 0.05	8.27± 0.39 N = 10 P < 0.05	59.05± 11.62 N = 4 NS	1983.37± 700.53 N = 4 NS	228.00± 23.82 N = 13 NS
M2$_{VSM}$	-18.96± 0.67 N = 8 P < 0.05	7.80± 0.21 N = 8 P < 0.05	94.20± 31.57 N = 5 NS	1866.39± 495.92 N = 5 NS	166.69± 11.91 N = 10 P < 0.05
P1$_{VSM}$	-19.58± 0.77 N = 12 P < 0.001	7.81± 0.35 N = 12 P < 0.05	66.05± 6.70 N = 2 NS	960.73± 307.83 N = 2 NS	204.79± 14.30 N = 16 NS
5b$_{VSM}$	-16.31± 1.05 N = 11 NS	7.41± 0.44 N = 11 NS	ND	ND	273.28± 29.23 N = 13 NS
M7$_{VSM}$	-17.61± 1.30 N = 9 NS	8.35± 0.53 N = 9 P < 0.05	ND	ND	249.53± 17.14 N = 11 NS

Tab.8

Next we investigated the effect of Diltiazem and the five analogs on the **time course of recovery of I_{Ba} from inactivation** assessed using a standard two-pulse protocol. The recovery from inactivation induced by a 3s depolarization (prepulse) to +10mV from a holding potential of -80mV and it was measured using 350ms test pulses to +10mV after various intervals (25ms to 28s). Between the subsequently applied pulses trains the membrane voltage was held for 3min at -100mV, resulting in complete unblock of the channels (dissociation of the drug from its binding site). After returning to a negative potential following a voltage step, it takes a finite amount of time for the channels to recover from inactivation and be available to conduct for the next depolarizing pulse. Peak $I_{Ba,}$ elicited by the test pulses were normalized with respect to the peak I_{Ba} of the prepulse, which should be constant. The fraction of current recovered is plotted against the recovery interval. The time course of recovery was well fitted with a double exponential equation (Figure 23, 24).

Control and drug data were averaged from different groups of cells. As shown in Figure 23, recovery of HHT-$Ca_v1.2$ channels from inactivation in the absence of drug follows a biexponential time course, reflecting a fast and a slow time course of recovery from inactivation. In the absence of Diltiazem, the fraction of current was recovering with a fast (τ_f) and slow (τ_s) time constant of 48.98±4.20ms and 1823.74±221.71ms, respectively. In the presence of 100μM Diltiazem, the fast phase of HHT-$Ca_v1.2$ recovery is substantially slowed (τ_f=442.34±151.85ms) and the time constant of slow recovery is virtually unchanged (τ_s=1951.32±241.70ms). Slow recovery enhances the use-dependent block. These results are in good agreement with the data presented by Dilmac *et al.* [99]. However, the recovery from inactivation in 100μM M8 was not changed prominently compared with control. There was a slight difference in the fast time constant of recovery in presence of P1 (τ_f=94.14 ± 17.97ms; τ_s=1350.73 ± 314.01ms) compared with control (Table 6, 7). The slow time constant was not significantly accelerated. The absence of use-dependent block of the Diltiazem analogs during pulse trains is probably due to an affect on channel recovery rather than causing decreased inactivation. Therefore, it allows fewer channels to bind since M2, M8 and P1 accelerated the inactivation time in oocytes experiments. In summary, M8, M2, 5b and M7 did not show any relevant effects on the times of recovery from inactivation of the

channel. In the case of the VSM-α_{1Cb} no difference was found with regard to time constants compared with results with HHT-α_{1C} (Figure 24).

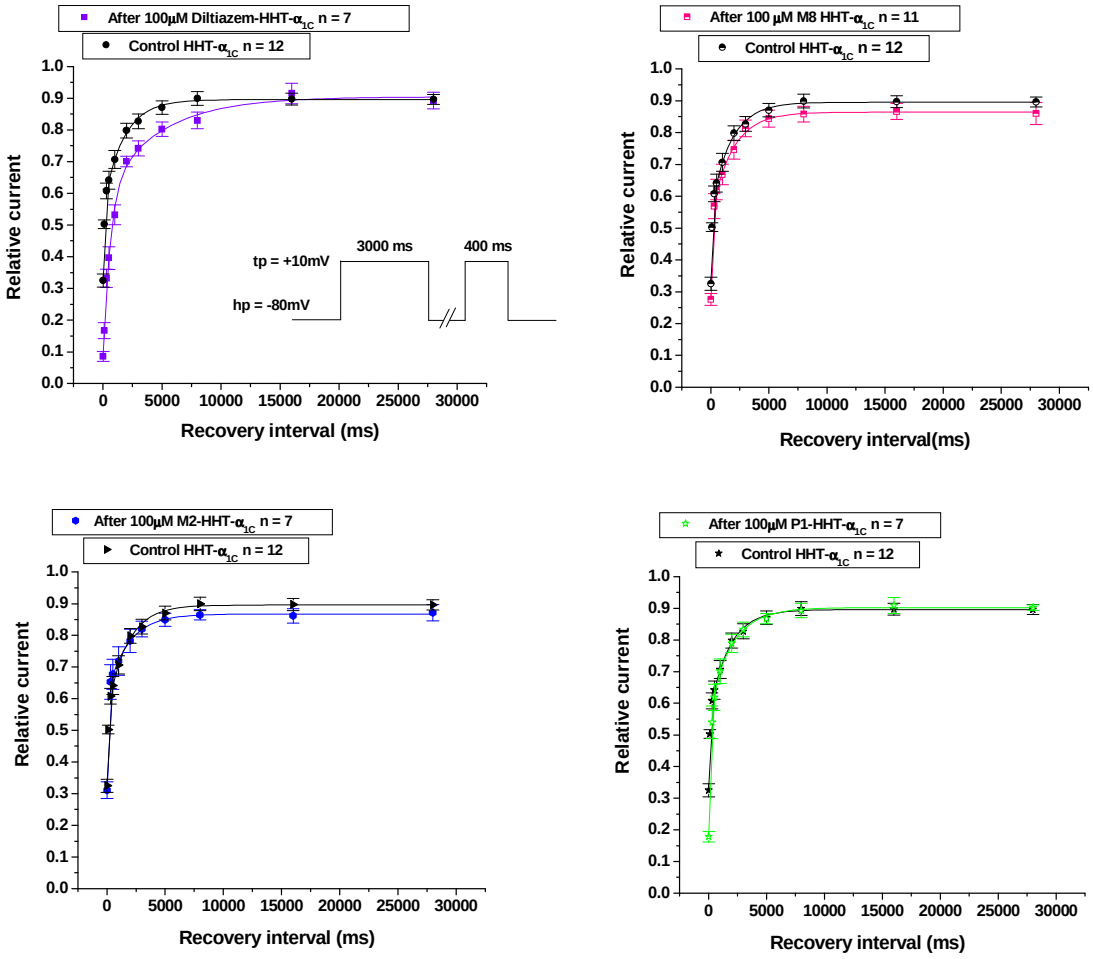

Figure 23. Kinetics of I_{Ba} recovery from inactivation after treatment with Diltiazem and M2, M8 and P1. The time constant are summarized in Table 6, 7. The time course of recovery from inactivation at -80mV was determined by subsequent test pulses applied at various times (recovery interval) after the prepulse as described under "Methods".

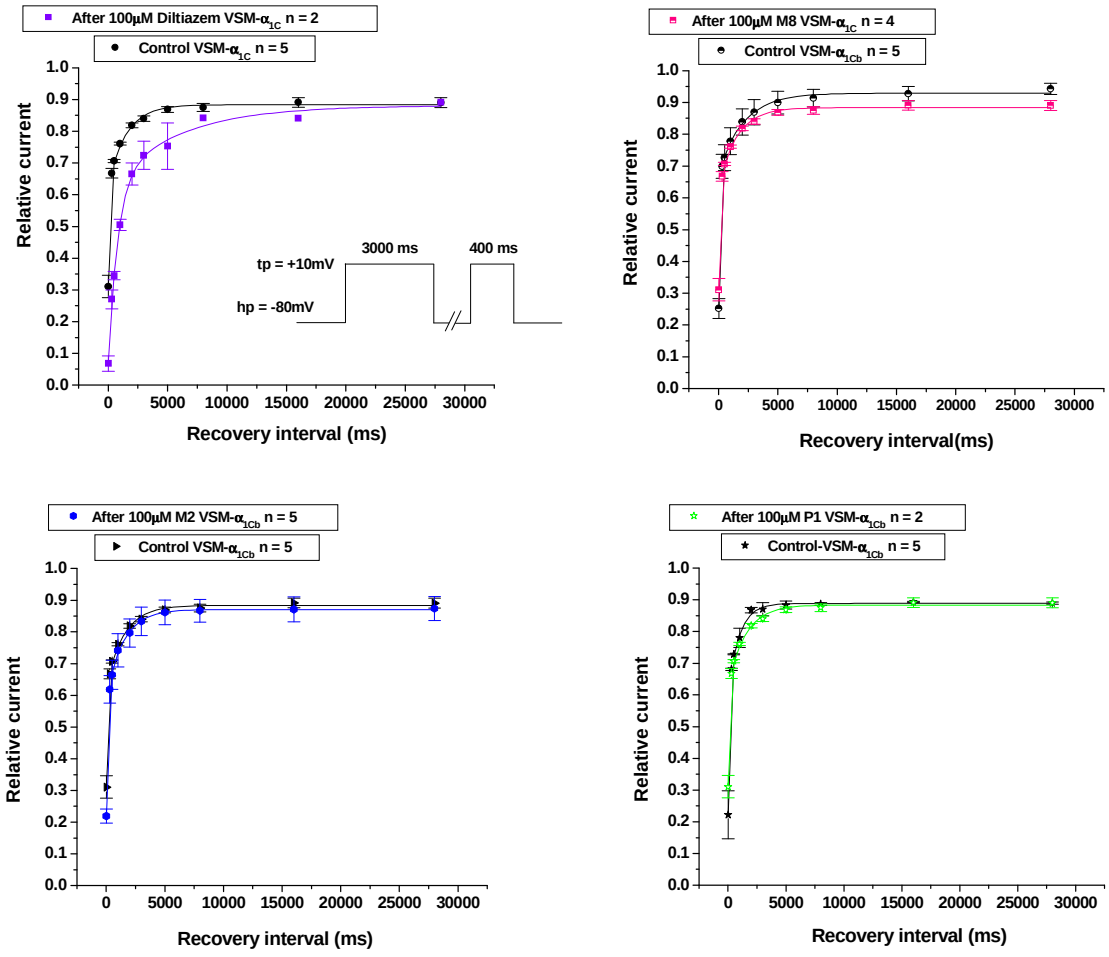

Figure 24. Kinetics of I_{Ba} recovery from inactivation of VSM-α_{1Cb} ($Ca_v1.2$) channel, after treatment with Diltiazem and M2, M8 and P1. The time constant are summarized in Table 8.

In all cases, recovery could be described by two phases. I_{Ba} rapidly recovered monoexponentially to 80-90% of control within 15s (termed "fast recovery"), and the remaining current which did not recover within the 15s period arbitrarily defined as "slow recovery" [100].

Effects of Diltiazem and a novel Diltiazem analog M8 on mouse ventricular cardiomyocytes

The aim of this study was to characterize the pharmacological effects of Diltiazem and M8 on native cardiac Ca^{2+} channels, to check if the drugs actually function differently in native environment. It was assumed that the drug sensitivity on the cardiac calcium channel described in the oocytes system would be corroborated on cardiomyocytes. The whole cell configuration of the patch-clamp technique was used to measure I_{Ca}. From published data, it appears that in oocytes usually a five-to tenfold higher concentration of antiarrhythmic drugs are required to get an effect comparable with that of mammalian cell lines or native cells. It is possible that, the charged hydrophobic yolk in the intact oocytes complicate the drug equilibrium. Furthermore, it was found that that the follicle cell layer surrounding the oocytes after incomplete digestion process can interfere with the drug effects drastically and can result in up to 30-fold increase in IC_{50} values, probably due to a reduced access of the substances to the oocytes membrane. Based on the results derived from the oocytes expression study effect of M8 was chosen to be studied on cardiomyocytes. Diltiazem and M8 were applied in concentrations of 10μM (corresponding to an intracellular concentration of ~100μM) in cardiomyocytes in 1.8mM Ca^{2+} containing recording solution. Diltiazem stock solution (10mM) was made in double distilled water, M8 (10μM) in dimethyl sulfoxide (DMSO) and this solution was used to make the appropriate dilution using the recording solution. Use-dependency was investigated using holding potential of -60mV, the same as in oocytes. We have to note that the development of UDB by Diltiazem is not simply dependent on the number of opening of channels (holding potential), but is dependent on the frequency and the duration of the test pulse. The results clearly show that block of Ca^{2+} channel current by Diltiazem can be modulated by changes in the duration of the test pulse. The effect of use-dependency after exposure of Diltiazem was most prominent when longer test pulse (320ms) was used in the train instead of the shorter pulse (80ms) (Figure 25).

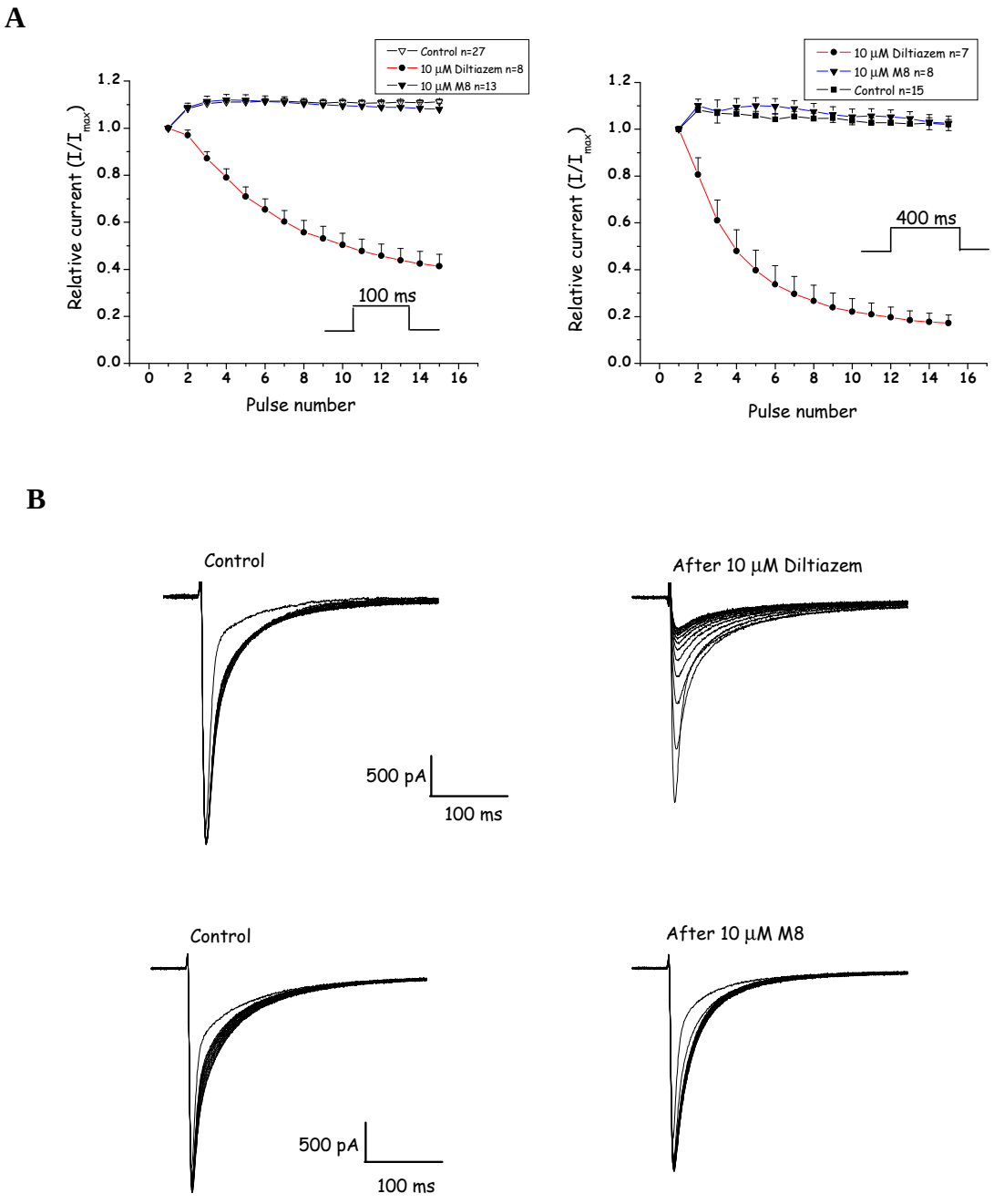

Figure 25. Use dependent blockade of I_{Ca}. **(A)** Stimulation trains consist of 15 consecutive depolarizing voltage pulses were applied from a holding potential of -60mV to 10mV at 0.5Hz in the absence (control) and in the presence of Diltiazem and M8. The pulse durations were 80ms and 320ms, respectively. Trains were applied before and after a rest period of about 3min. at -60mV. I_{Ca} amplitudes were normalized to the amplitude of I_{Ca} elicited by the first pulse in a train. **(B)** Use-dependent peak I_{Ca} decay in the presence of Diltiazem and M8. Original current traces illustrating the use-dependent block during a pulse train in control and in presence of 10µM Diltiazem and M8.

The UDB was studied only at frequency of 0.5Hz under this EP protocol. Diltiazem suppressed I_{Ca} in a use-dependent manner without a significant tonic component (-4.6±4.1 % during 80ms pulse train and -7.4±5.2 % during 480ms pulse train,). It is clear from the representative figure that more channels are blocked when Ca^{2+}, instead of Ba^{2+} is the charge carrier. Using both train pulses (80ms and 320ms), M8 produced a slightly bigger tonic block compared with Diltiazem (-10.9±3.5 % vs. -11.2±3.3 %, respectively). However, in good agreement with results obtained from oocytes, M8 failed to produce any use-dependent inhibition on the I_{Ca}.

In conclusion, these results with Diltiazem and M8 in cardiomyocytes confirmed the findings in heterologous expression system using the two electrode voltage clamp.

It is a well known phenomenon that a train of repetitive depolarizations [101] drives the L-VDCCs from their normal gating pattern into a mode of gating characterized by long opening and high open probability [102], a process that has been termed "facilitation". The facilitation can be clearly seen in Figure 25. In cardiomyocytes, as a consequence of using Ca^{2+} as a charge carrier, calcium channels have evolved in the voltage and Ca^{2+}-dependent inactivation mechanism. Therefore, in cardiomyocytes we have to take into consideration both inactivation processes. Both Ca^{2+} dependent inactivation and facilitation require high affinity binding of calmodulin (CaM) to the IQ motif (See Figure 1) located in the carboxyl terminal tail of the $Ca_v1.2$ channel [103]. Ca^{2+} dependent facilitation has been attributed to the action of Ca^{2+}/calmodulin-dependent protein kinase II.

The effect of Diltiazem and M8 on I_{Ca} inactivation rate was also examined. As expected, M8 revealed faster time and voltage dependent inactivation compared with that of Diltiazem. In contrast, Diltiazem in 10μM of concentration did not accelerate the Ca^{2+} channel inactivation [60,99]. The effects of Diltiazem and M8 on the voltage-dependence of the availability of L-VDCC are shown in Figure 26. The $V_{0.5}$ of steady state inactivation was significantly shifted by -7.4mV. The slope factor between control and M8 are similar in steady-state inactivation (4.7±0.33mV vs. 4.8±0.03mV, respectively) [104].

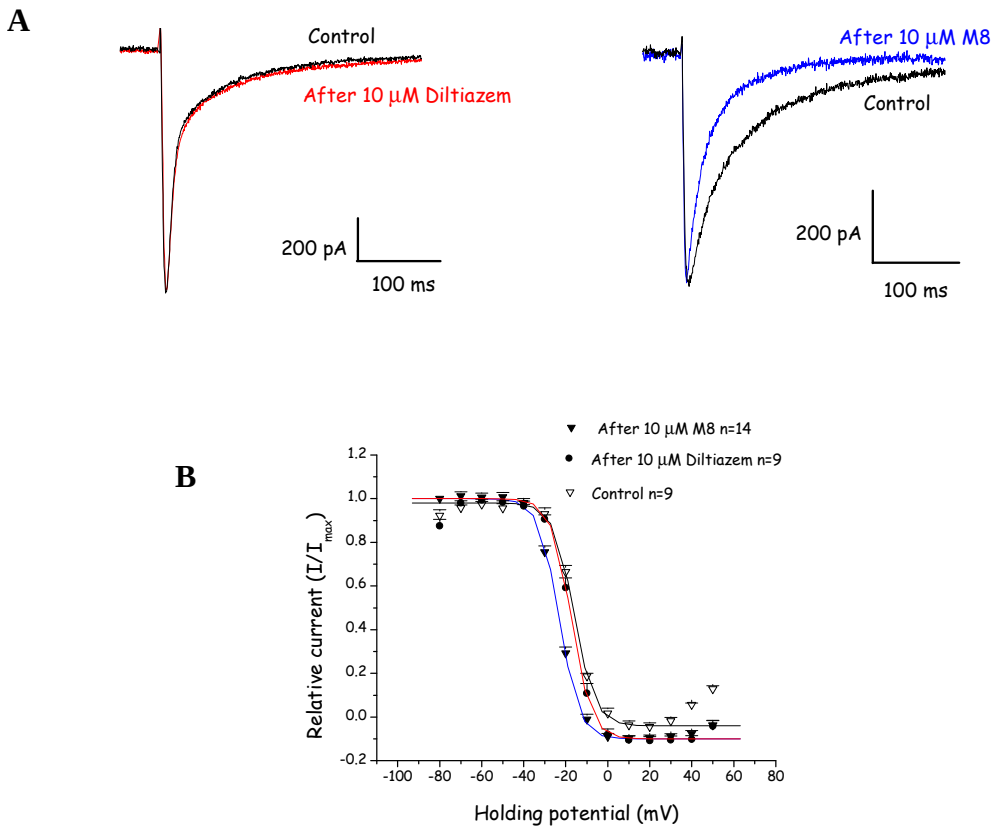

Figure 26. Time course of Diltiazem and M8 block of depolarized wild-type $Ca_v1.2$ channels. **(A)** Representative traces of Ca^{2+} current through HHT-$Ca_v1.2$ channels measured during a 380ms depolarization from -60mV to +10mV in controls (black line) and after M8 (blue) and after Diltiazem (red), respectively. **(B)** Voltage dependence of inactivation in wild-type $Ca_v1.2$ channels. Peak Ca^{2+} current elicited by depolarization to +10mV immediately after 1s conditioning pulses to the indicated potentials from a holding potential of -80mV are plotted against the amplitude conditioning pulse voltage in the presence or absence of M8 and Diltiazem, respectively.

5.2. Langendorff hearts

The present experiments aimed to elucidate whether the Diltiazem analogs in mouse hearts affect ventricular contractility (inotropism) and relaxation (lusitropic) within a wild range of concentrations. For this purpose we utilized the isolated mouse heart perfused according to Langendorff. The Langendorff system represents a good approach to analyze lusitropism and inotropism at the same time. This is because the ventricular systole occurs at isovolumic conditions; therefore the relaxation performance is not influenced by the contraction [105]. Cumulative concentration-response curves (from 10^{-10} to 10^{-5}M) of Diltiazem and the Diltiazem analogs were generated by exposing the cardiac preparations after taking baseline values to increasing concentrations of drugs. Cardiac parameters were measured at 2.5min. As seen in Figure 27 the negative inotropic effect of Diltiazem up to 10^{-6}M was not statistically significant [106]. The observed relative sharp decrease after starting the drug perfusion process is considered an artifact due to switching to a perfusion pump therefore causing the perfusion pressure to decrease. Additionally, temporary temperature decrease could be also a factor and should be taken into consideration during the interpretation of the data. Usually, it takes 4-5min to stabilize the left ventricular pressure to the new setting in the perfusion rate. In retrospect, we should have begun the perfusion through the perfusion pump in addition to the retrograde perfusion with Tyrode solution and used these recordings as baseline values. Following administration of Diltiazem at 1μM, results were that the maximum rate of contraction (+dP/dt) showed only 6% reduction (from 2541.32±111.0 to 2404.35±93.69 mmHg/s), whereas 10^{-5}M caused sudden decrease in +dP/dt (1676.55±182.04 mmHg/s), probably due to the compound toxic effect on the heart. M8, P1 and 5b in the tested concentration ranges showed very similar tendency to Diltiazem regarding the effect on +dP/dt. M8 and P1 in 10^{-6}M increased +dP/dt by 5%, however it was not significant (from 2703.84±122.31mmHg/s to 2859.76±261.29mmHg/s vs. from 2826.25±74.24mmHg/s to 2955.65±181.82mmHg/s, respectively). Interestingly, M2 and M7 displayed a statistically significant ($p<0.05$) increase in +dP/dt after both 10^{-6} and 10^{-5}M concentrations. M2 caused a concentration-dependent increase (~10%) in +dP/dt which begun at a low concentration (10^{-9}M) and persisted up throughout the higher doses (10^{-6} and 10^{-5}M). After perfusion of 10^{-6}M M2 the +dP/dt increased from 2617.52±78.84mmHg/s to 2910.87±104.42mmHg/s ($p<0.05$). M7 also induced a concentration dependent (~20%)

increase in +dP/dt, from 2709.55±114.56mmHg/s to 3139.25±144.26mmHg/s ($p<0.05$) in 10^{-6}M concentration. Original recordings before and after 1µM Diltiazem or the five Diltiazem analogs are shown in Figure 28.

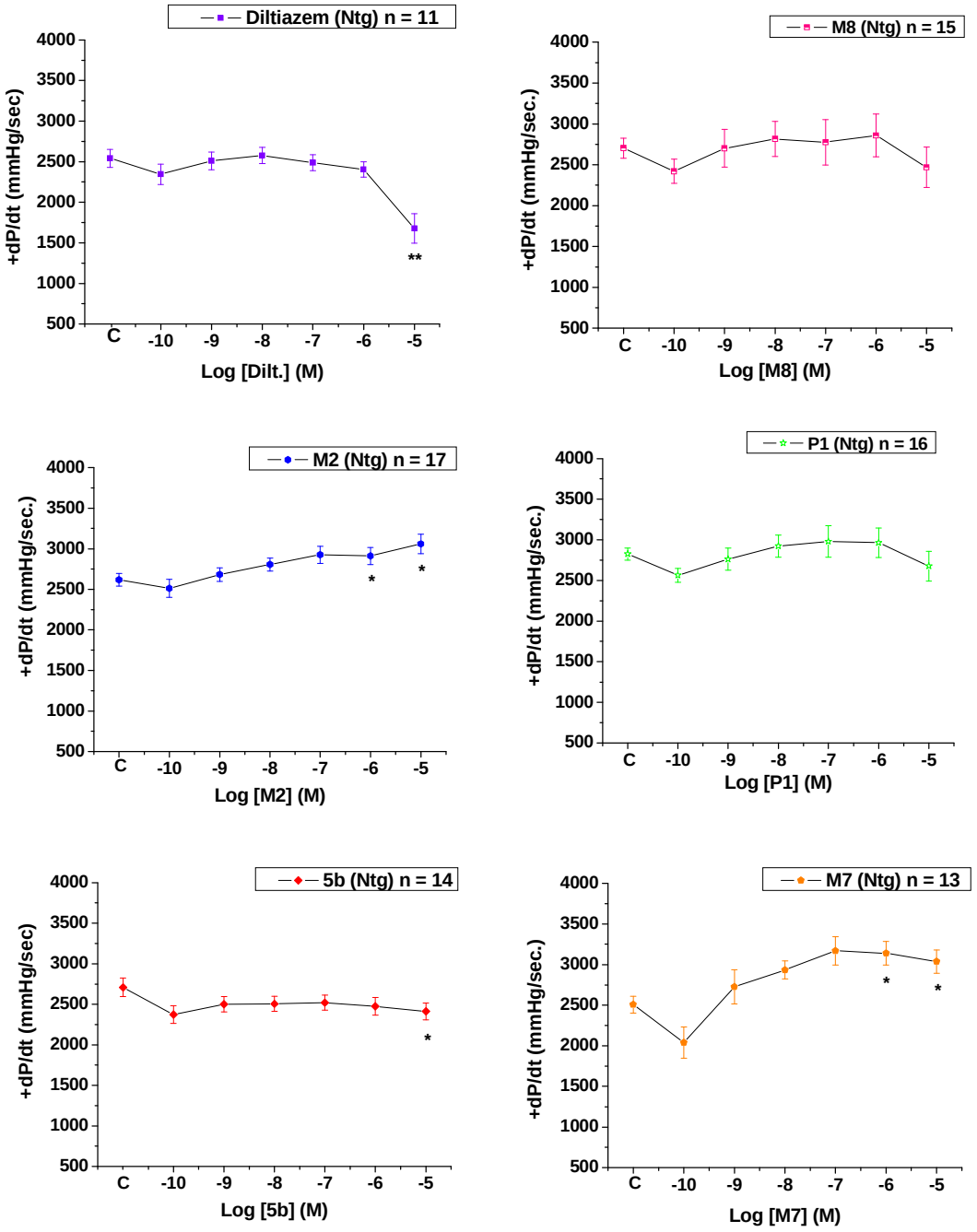

Figure 27. Concentration-response curves for the effect of Diltiazem, M8, M2, P1, 5b, M7 (10nM to 10µM) in the isolated retrograde perfuse heart at 2mM [Ca^{2+}] in the perfusion solution. +dP/dt was used as a indices of contractility and is displayed. Each symbol and vertical bar represents the mean ± S.E.M. (*, $p < 0.05$, **, $p < 0.001$, unpaired Student's *t*-test).

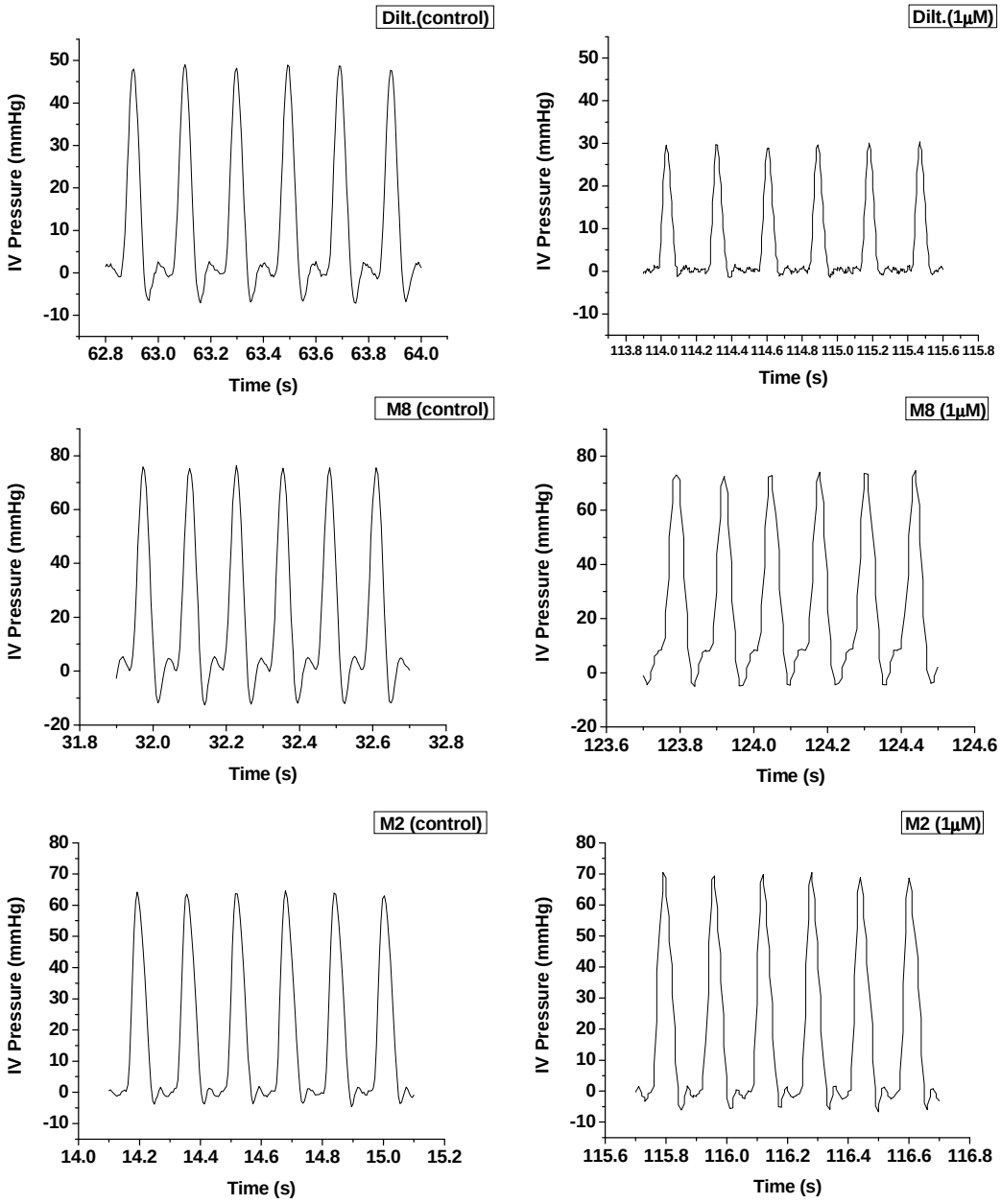
Dilt.(control)
IV Pressure (mmHg)
50
40
30
20
10
0
-10
62.8 63.0 63.2 63.4 63.6 63.8 64.0
Time (s)
Dilt.(1μM)
IV Pressure (mmHg)
50
40
30
20
10
0
-10
113.8 114.0 114.2 114.4 114.6 114.8 115.0 115.2 115.4 115.6 115.8
Time (s)
M8 (control)
IV Pressure (mmHg)
80
60
40
20
0
-20
31.8 32.0 32.2 32.4 32.6 32.8
Time (s)
M8 (1μM)
IV Pressure (mmHg)
80
60
40
20
0
-20
123.6 123.8 124.0 124.2 124.4 124.6
Time (s)
M2 (control)
IV Pressure (mmHg)
80
70
60
50
40
30
20
10
0
-10
14.0 14.2 14.4 14.6 14.8 15.0 15.2
Time (s)
M2 (1μM)
IV Pressure (mmHg)
80
70
60
50
40
30
20
10
0
-10
115.6 115.8 116.0 116.2 116.4 116.6 116.8
Time (s)

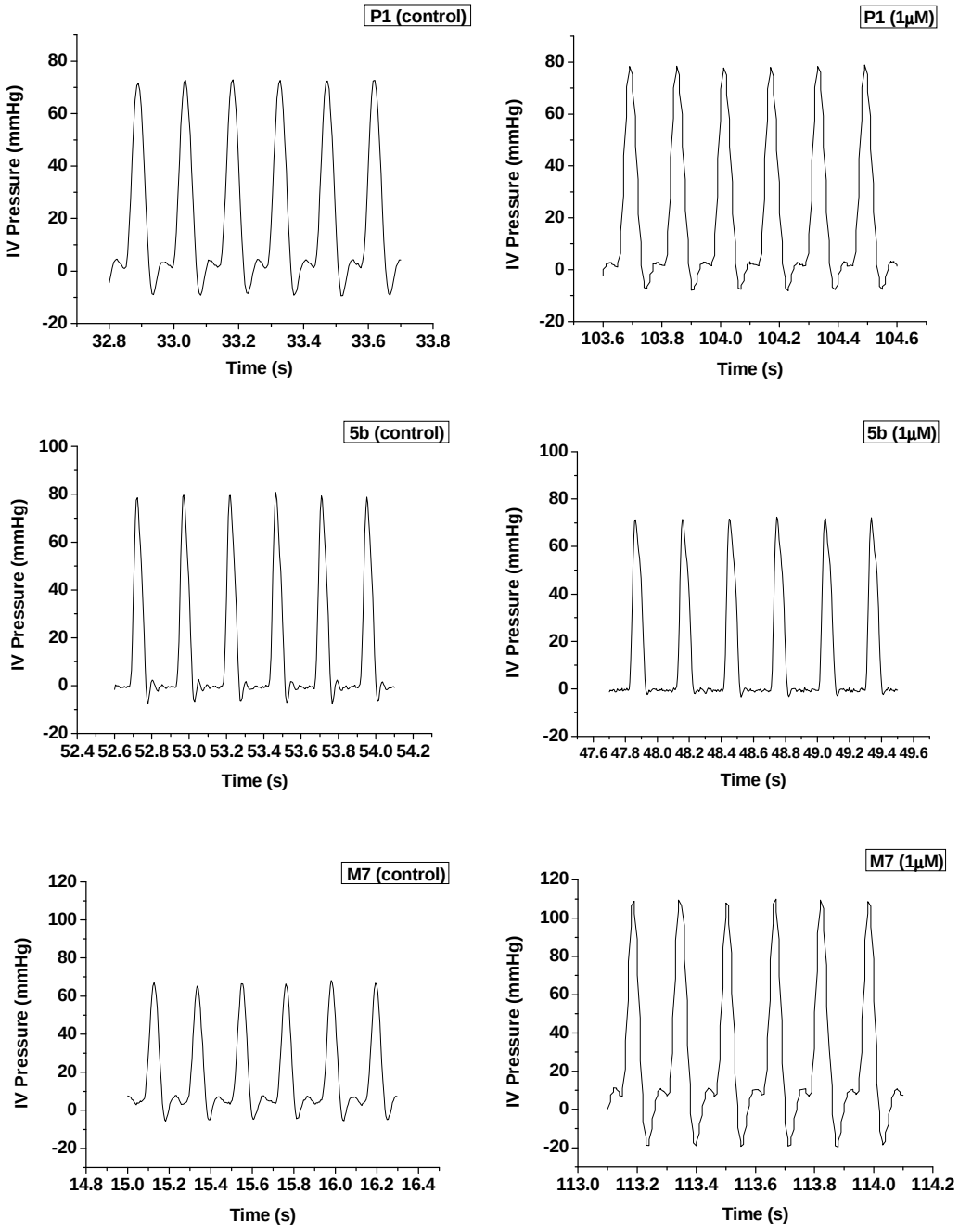

Figure 28. Representative Intra Ventricular pressure traces before and after the exposition of the cardiac preparations to 1µM of Diltiazem, M8, M2, P1, 5b and M7.

Analysis of the myocardial effects of Diltiazem, P1 and 5b elicited a positive lusitropic effect, represented by a significant reduction in –dP/dt only in 10^{-5}M concentration. After perfusion of M8, M2 and M7 a slight negative lusitropic (hastening) tendency was observed at the concentration tested, however, these variations were not significantly different from the control values in parallel with the change in dP/dt (Figure 29).

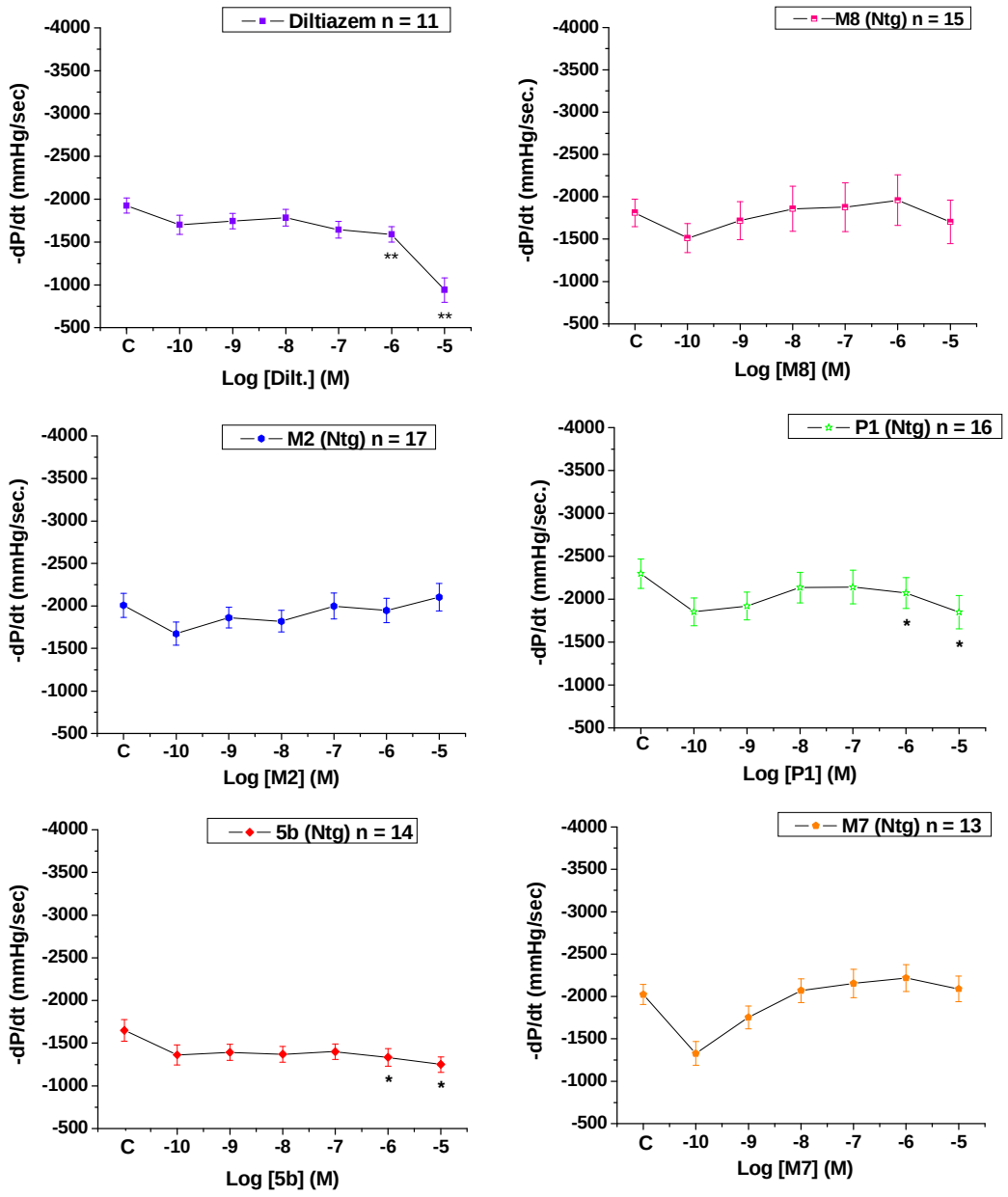

Figure 29. Concentration-response curves for the effect of Diltiazem, M8, M2, P1, 5b, M7 (10nM to 10μM) in the isolated retrograde perfuse heart at 2mM [Ca^{2+}] in the perfusion solution. -dP/dt was used as a indices of relaxation and is displayed. Each symbol and vertical bar represents the mean ± S.E.M. (*, $p < 0.05$, **, $p < 0.001$, unpaired Student's *t*-test).

All of the compounds slightly decreased the heart rate in 10^{-5}M and 10^{-6}M concentrations, however only Diltiazem, P1 and 5b showed a significant decrease (Figure 30).

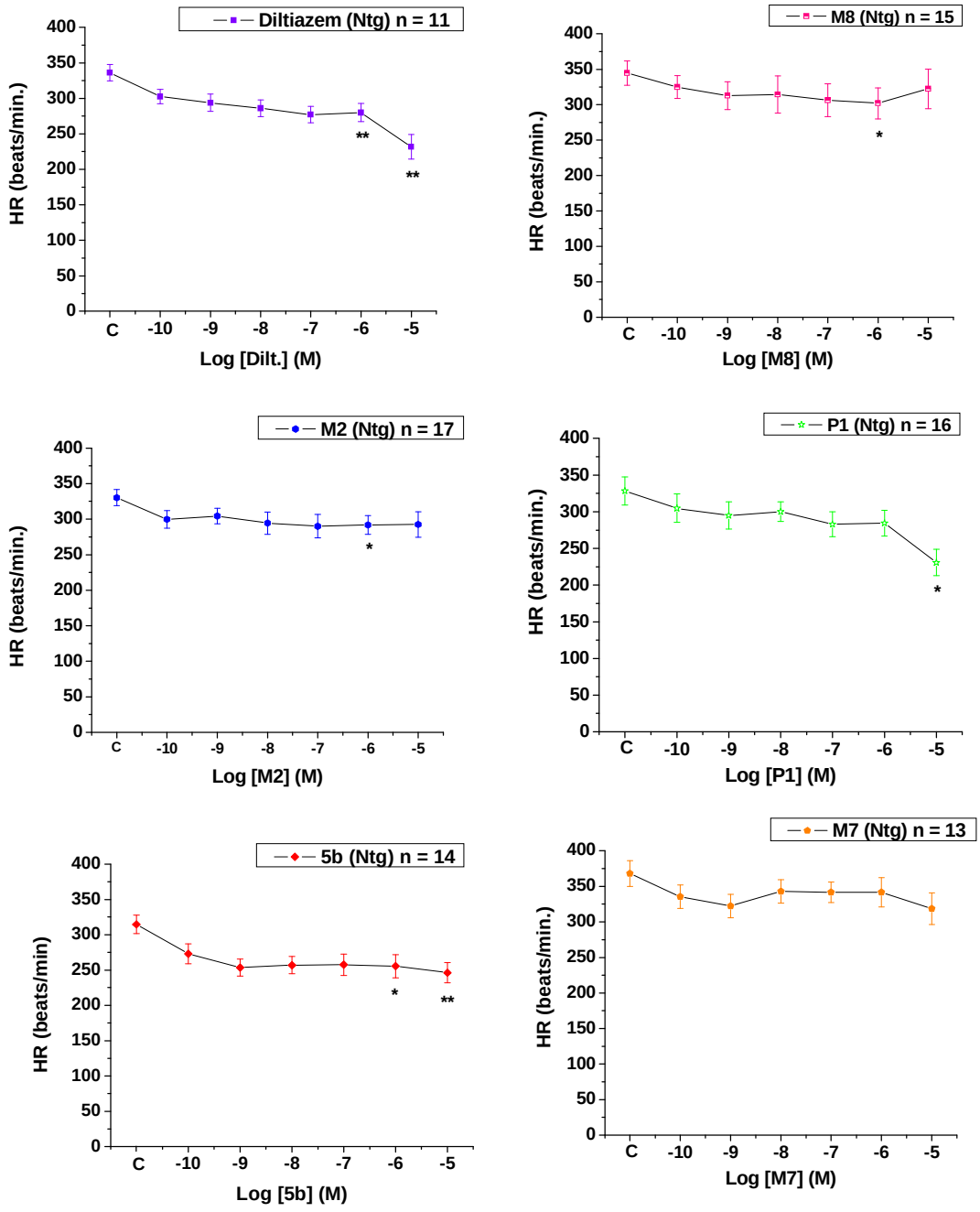

Figure 30. Concentration-response curves for the effect of Diltiazem, M8, M2, P1, 5b, M7 (10 nM to 10μM) in the isolated retrograde perfuse heart at 2 mM [Ca^{2+}] in the perfusion solution. HR was used as a indices of cronotropy and is displayed. Each symbol and vertical bar represents the mean ± S.E.M. (*, $p < 0.05$, **, $p < 0.001$, unpaired Student's *t*-test).

5.2.1. Antiarrhythmic effect of Diltiazem and the selected Diltiazem analogs

In addition to the hemodynamic measurements, we tried to access the antiarrhythmic effect of Diltiazem and the selected Diltiazem analogs in Langendorff–perfused mouse hearts. We took advantage of a transgenic mouse model which was previously developed in Dr. Schwartz's laboratory [107]. In this transgenic mouse model, the L-VDCC HHT-α_{1C} subunit was overexpressed (α_{1C}-Tg) in a cardiac specific manner using the α-myosin heavy chain promoter. Increasing gene expression of the α_{1C} subunit induces a sustained increase in $[Ca^{2+}]_i$ causing significant changes in critical intracellular factors that trigger cardiac hypertrophy and eventual failure. The cellular electrophysiological changes include prolonged action potential duration, downregulation of potassium currents, and alterations in Ca^{2+} homeostasis. In general, sudden death occurrence could be due to ventricular arrhythmias associated with cardiac hypertrophy and failure. This is the result of remodeling processes that occurs in both the myocyte and interstitial compartments of the heart and creates a substrate that is vulnerable for triggering potentially lethal ventricular arrhythmias.

Therefore, this α_{1C}-Tg mouse model was utilized to investigate the possible antiarrhythmic property of two of the newly synthesized Diltiazem analogues, M8 and M2, compared with Diltiazem. It is well established that when this mouse model reaches 7-10 months of age, they develop cardiac hypertrophy associated with spontaneous ventricular extrasystoles, tachycardia or bradycardia. The arrhythmia occurrence was accessed from the left ventricular pressure. After recording the baseline conditions with "arrhythmia phenotype", 10μM Diltiazem, M8 and M2 were perfused, respectively. After drug (Diltiazem, M8 or M2) administration the persisting arrhythmia was suspended or completely suppressed. These preliminary experiments implicate that M8 and M2 have some antiarrhythmic effect despite the absence of use-dependency (Figure 31) since use-dependent-block is thought to be a particularly important mechanism of antiarrhythmic drug action. To further elucidate the antiarrhythmic aspect of the Diltiazem analogs is beyond the scope of this study and would require additional experiments.

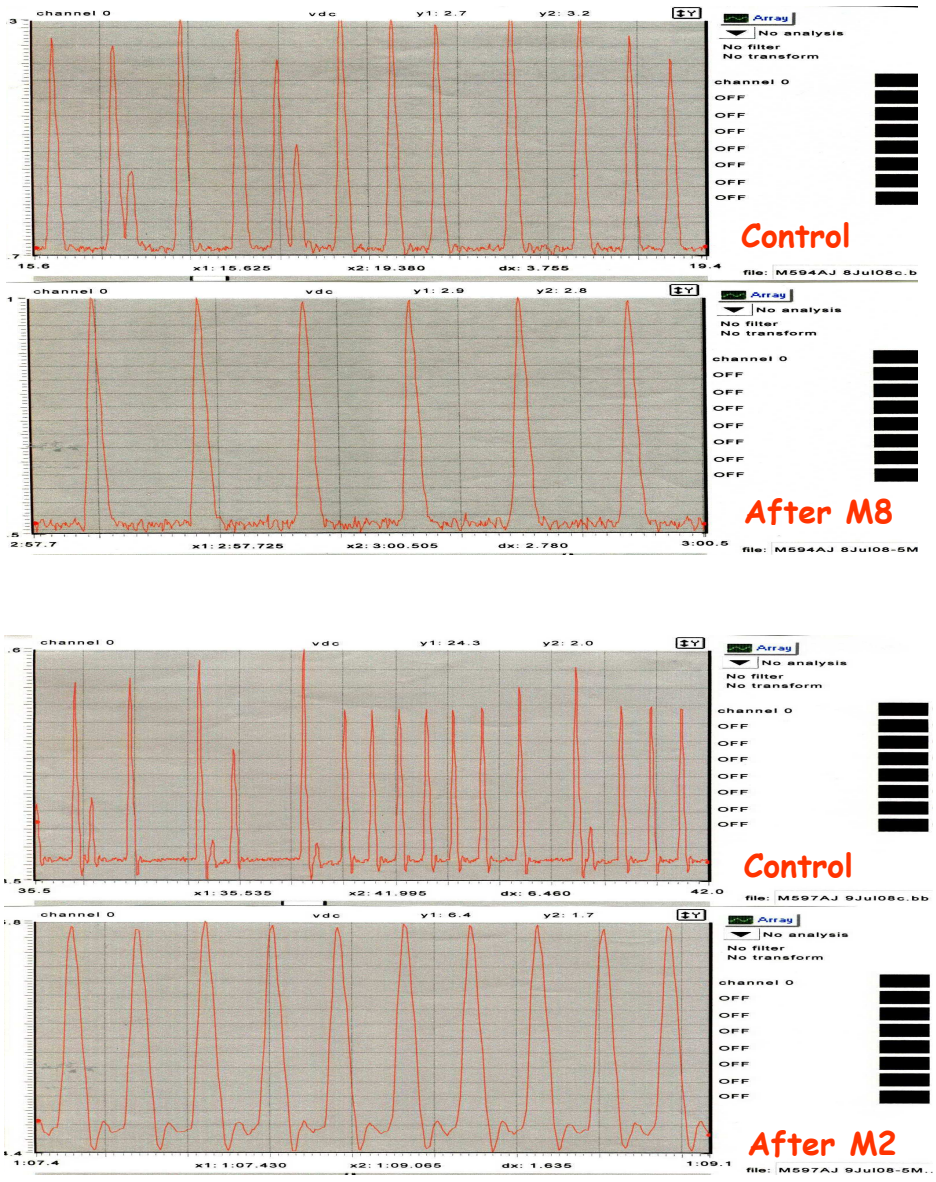

Figure 31. Antiarrhytmic effects in transgenic hearts (HHT-α_{1C} subunit over expressed) of 10μM M8 and M2, on Langendorff-perfused mouse hearts.

5.3. Electrically evoked cystolic Ca^{2+} transients in single cardiac mouse myocytes

The previous experiments in the whole heart (Langendorff) indicated that M2 and M7 had a positive inotropic effect (+dP/dt). To correlate this finding on single cell level and provide a feasible explanation for the *ex vivo* results, the Ca^{2+} transients were measured in Fura-2 loaded cardiomyocytes. Table 9 summarizes the effect of Diltiazem analogs compared with Diltiazem on the Ca^{2+} transients. In our analyses we were focusing on three parameters: the amplitude of Ca^{2+} transients (ΔR 340/380), which was measured as the difference between diastolic and maximal systolic fluorescence ratio (ΔR 340/380); TRC 50%, is time to 50% relaxation in $[Ca^{2+}]_i$ and the time constant of recovery to baseline (τ). After adding 1μM Diltiazem to the perfusion buffer during continuous pacing, fluorescence ratio was significantly decreased by 16 % without changing TRC 50% and the τ. This result is good agreement with published data by others [108]. In contrast to Diltiazem, M8, M2 and M7 produced a slight increase in the $[Ca^{2+}]_i$ amplitude. This correlated with results generated from the *ex vivo* experiments (increased +dP/dt). During the present study we obtained supportive evidence (*ex vivo* and *in vitro*) that both M2 and M7, and in some instances M8, slightly increased the contractility at higher concentrations and was also accompanied by an increased decay of the Ca^{2+} transients (Table 9, Figure 32). One possible interpretation of this finding is that these drugs facilitate the coupling process between the L-VDCC and RyR-2 (increased EC gain). This process, called Ca^{2+}-induced Ca^{2+} release (CICR) by A. Fabiato, causes a rapid increase in intracellular Ca^{2+} concentration to a level required for optimal binding of Ca^{2+} to troponin C and induction of contraction [8]. However, according to the electrophysiological measurements, these drugs did not increase I_{Ba} or I_{Ca}. The newly synthesized Diltiazem analogs might have an allosterical binding site beside the BTZ, or bind to an internal site producing increased levels of intracellular Ca^{2+}. It is a known fact that Diltiazem is capable of stimulating the binding of dihydropyridines to T-tubular sites [92,109]. Interestingly, the action of DHPs can be related to the modulatory mode shift. In response to depolarization, the L-type channel opens. In the basal, unphosphorylated mode 0, the probability of the channel being open is very low. Moderate phosphorylation, typically by stimulation of the β-adrenergic receptors, increases the probability of being open after depolarization (mode 1). More extensive phosphorylation leads to mode 2, where prolonged

channel openings occur, greatly increasing the current. Mode 0 is also favored by binding of the Ca^{2+}-antagonist drugs, and mode 2 is produced by agonist, for example BayK8644. "It is possible that the allosteric effects of phosphorylation are the reverse of those induced by drug binding, so they may bias the same molecular mechanism in opposite directions" by H. Fozzard (Foundation of cardiac arrhythmias Edited by Peter M. Spooner & Michael R. Rosen, Marcel Dekker, Inc. 2001). In summary, our results are consistent with the idea that M2, M7 and M8 in lower concentrations have Ca^{2+}-agonist effect without influencing the Ca^{2+} current through the L-VDCC.

	Amplitude, 340/380 nm (Systolic-diastolic)	TRC 50% (s)	Time constant of recovery to baseline (s)
Control	0.43 ±0.17 N = 4	0.46 ± 0.07 N = 4	0.47 ± 0.12 N= 4
Isoproterenol	0.60 ±0.24 N = 4 P <0.05	0.32 ±0.01 N = 4 NS	0.20 ± 0.01 N= 4 NS
Control	0.56 ±0.04 N = 22	0.39 ± 0.02 N = 22	0.34 ± 0.03 N= 22
Diltiazem	0.47 ±0.03 N = 22 P <0.001	0.41 ± 0.01 N = 22 NS	0.34 ± 0.02 N= 22 NS
Control	0.52 ±0.03 N = 21	0.40 ± 0.02 N = 21	0.38 ± 0.04 N= 21
M8	0.59 ±0.03 N = 21 P <0.05	0.36 ±0.01 N = 21 P <0.05	0.30 ± 0.01 N= 21 P <0.05
Control	0.52 ±0.05 N = 21	0.37 ±0.01 N = 21	0.34 ± 0.02 N= 21
M2	0.58 ±0.04 N = 21 P <0.05	0.36 ±0.01 N = 21 NS	0.27 ± 0.01 N= 21 P <0.05
Control	0.54 ±0.04 N = 20	0.40 ± 0.02 N = 20	0.36 ± 0.03 N= 20
P1	0.57 ±0.04 N = 20 NS	0.39 ±0.01 N = 20 NS	0.33 ± 0.02 N= 20 NS
Control	0.51 ±0.03 N = 18	0.38 ±0.01 N = 18	0.32 ± 0.01 N= 18
M7	0.55 ±0.03 N = 18 P <0.05	0.39 ±0.01 N = 18 NS	0.34 ± 0.02 N= 18 NS
Control	0.55 ±0.10 N = 11	0.45 ± 0.02 N = 11	0.36 ± 0.03 N= 11
5b	0.50 ±0.07 N = 11 NS	0.44 ±0.01 N = 11 NS	0.36 ± 0.02 N= 11 NS

Table 9. $[Ca^{2+}]_i$ parameters in Fura-2 loaded cardiomyocytes.

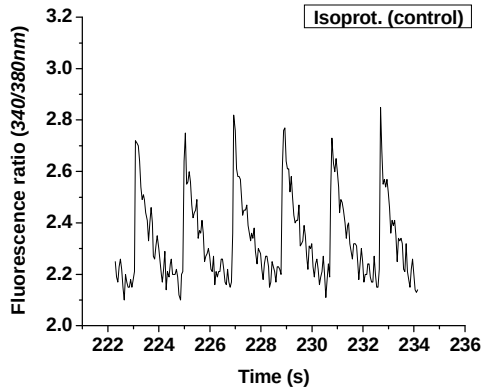
Isoprot. (control)
Fluorescence ratio (340/380nm)
Time (s)

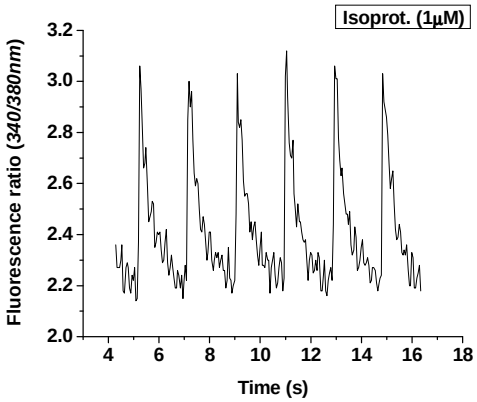
Isoprot. (1μM)
Fluorescence ratio (340/380nm)
Time (s)

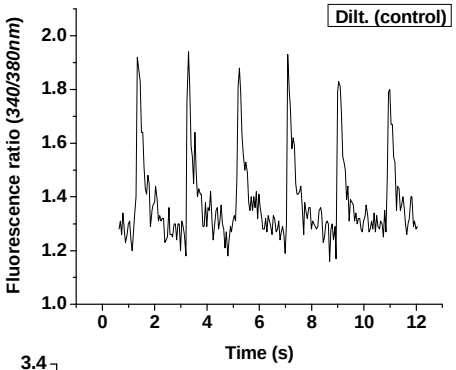
Dilt. (control)
Fluorescence ratio (340/380nm)
Time (s)

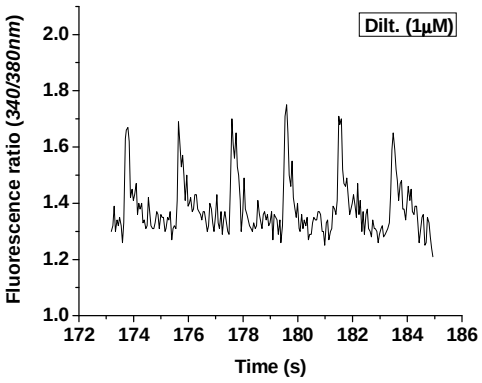
Dilt. (1μM)
Fluorescence ratio (340/380nm)
Time (s)

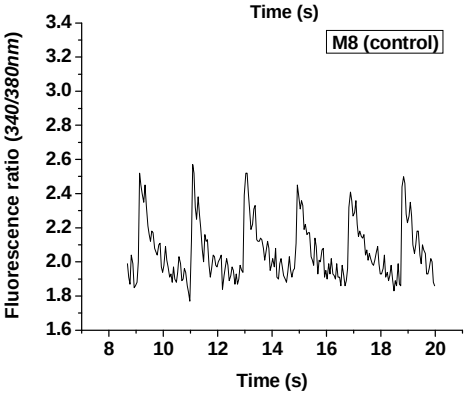
M8 (control)
Fluorescence ratio (340/380nm)
Time (s)

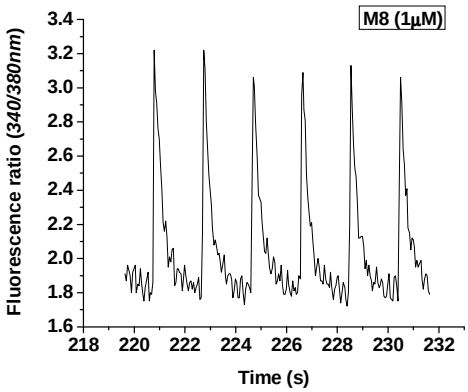
M8 (1μM)
Fluorescence ratio (340/380nm)
Time (s)

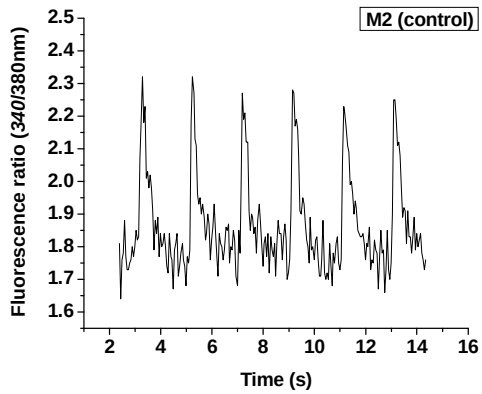
M2 (control)
Fluorescence ratio (340/380nm)
Time (s)

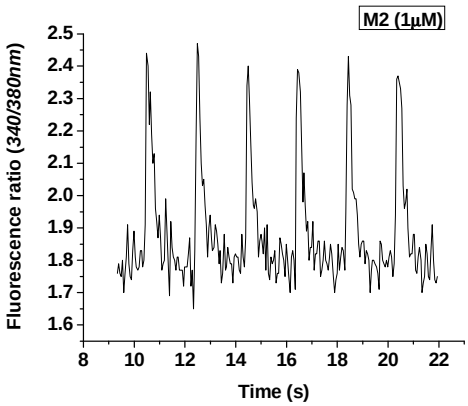
M2 (1μM)
Fluorescence ratio (340/380nm)
Time (s)

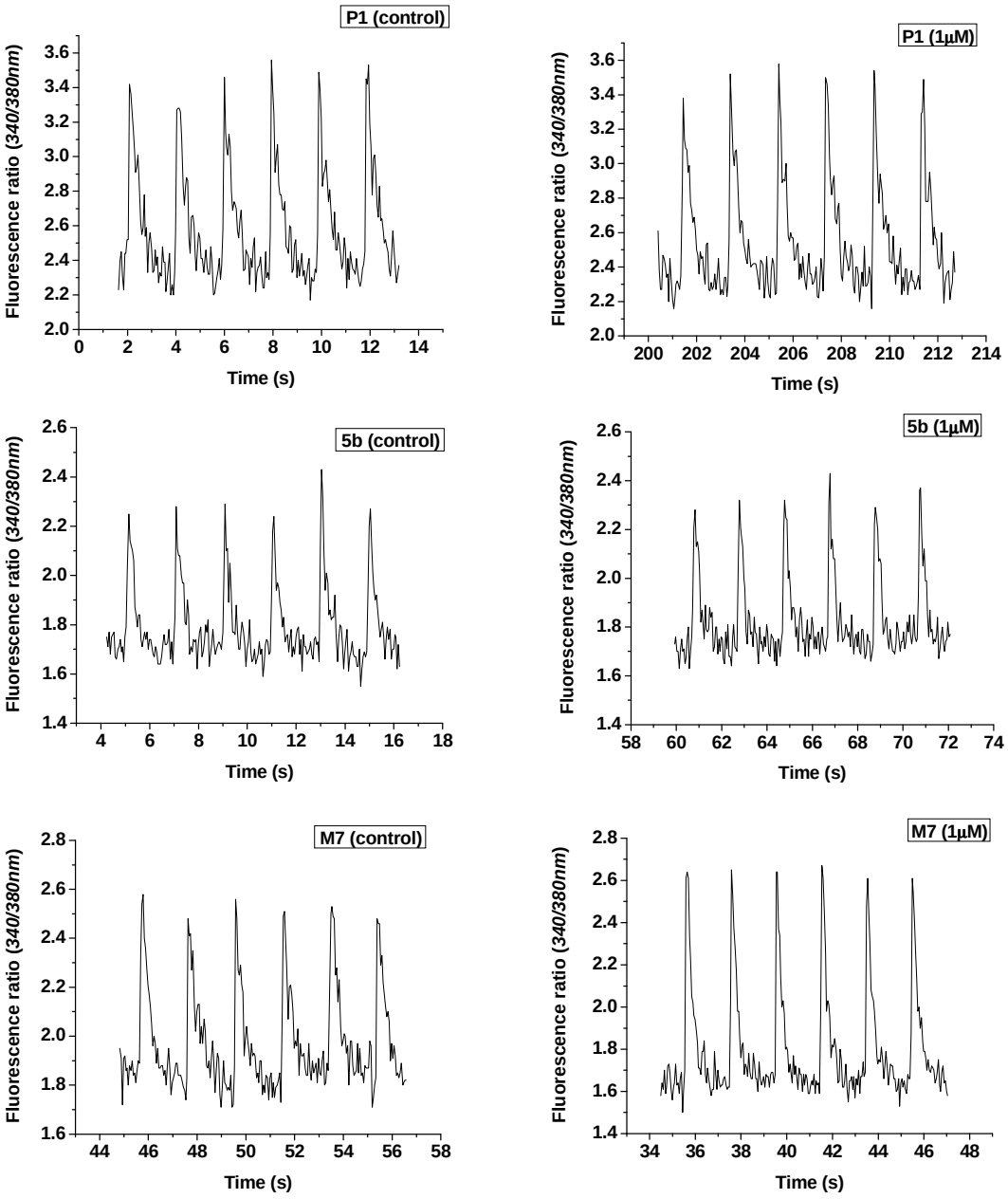

Figure 32. Effects of Diltiazem and Diltiazem analogs on intracellular Ca^{2+} transients. Representative recordings of Ca^{2+} transients in response to field stimulation at 0.5Hz obtained from a myocyte before and after bath application of drugs.

6. DISCUSSION

Previous studies showed that [1,4] thiazino[3,4-c] [1,2,4]oxadiazolones with a methyl group at position 5 of the thiazin-oxadiazolo ring, a free OH at C-8, and an unsubstituted or *p*-bromo-substituted 8-phenyl ring exhibited negative inotropic potency [110]. In this context, a series of acetals were designed and functionally assayed, and the series of oxadiazolones were optimized with an ethyl group at position 8 (8-(4-bromophenyl)-8-ethoxy-8H-[1,4]thiazino[3,4-c][1,2,4]-oxadiazol-3-one, coded as 5b) [111] (Figure 33).

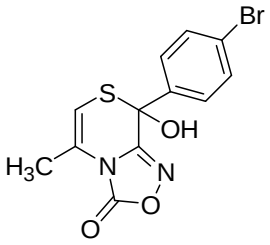

[1,4]thiazino[3,4-c][1,2,4]oxadiazolone
Left Atria
EC_{50} = 0.32μM (0.23-0.43)

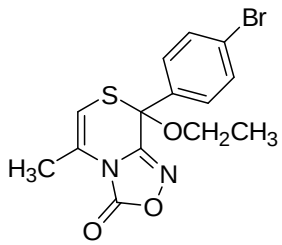

8 (8-(4-bromophenyl)-8-ethoxy-8H-[1,4]thiazino[3,4-c] [1,2,4]-oxadiazol-3-one (**5b**)
Left Atria
EC_{50} = 0.04μM (0.03-0.05)

Figure 33. Diltiazem structure compare with **5b** structure, one of the Diltiazem structurally related compounds with a better negative inotropic potency than Diltiazem.

However, important questions remained unsolved. Does 5b bind to the Diltiazem binding site or does it have its own site? Are both enantiomers of 5b active, or is only a single enantiomer active? Could 5b be used as a new template to search for novel calcium antagonists?

First, to evaluate the stereoactivity of 5b, the two enantiomers were resolved by semi preparative enantio-HPLC. The absolute configuration of 5b was assigned using vibrational circular dichroism (VCD) spectroscopy. Second, assays on rat cardiomyocytes with [^{3}H] Diltiazem as the radioligand were performed, and the direct interaction at the Diltiazem binding site was confirmed for 5b, although only at high concentrations. In addition, for 5b, the (-) isomer exhibited a more noticeable negative inotropic activity, demonstrating the stereo specificity of the binding site. Then, a ligand-based virtual screening (LBVS)

procedure was developed in order to search for novel chemotypes for calcium channel blockers, starting from the oxadiazolone series.

The virtual screening procedure was based upon the oxadiazolone 5b and a database of approximately 340.000 commercially available compounds assembled in-house from commercial catalogues.

Using different filters based on the selection of compounds with only C, H, O, S, N, P and halogens showing similarity in the active compound R(-) isomer 5b (i.e. similar structure and molecular weight) and devoid of toxicity and instability, only 20 representative virtual hits were selected for purchasing and further investigation (Figure 34).

Figure 34. Structures of Compounds Identified Using Virtual Screening

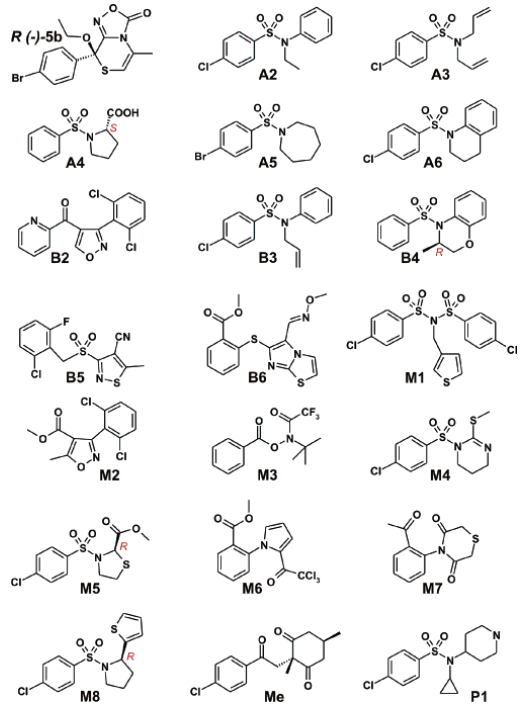

The pharmacological profile of all 20 compounds was tested on guinea-pig isolated left and right atria to evaluate their inotropic and chronotropic effects, respectively, and on K^+-depolarized (80mM) guinea pig aorta strips to assess vasorelaxant activity. The results were compared with those of reference compounds Diltiazem and 5b. Six out of 20 compounds (**M7, M8,** A2, A5, B2, **P1**) revealed a good inotropic profile, with negative inotropic EC_{50} values between 0.2 and 0.4μM. The structure of these compounds suggests that at least one bulky and lipophilic group is necessary for negative inotropic activity (i.e. the phenyl of A2, B3 and M7; the azepine ring of A5; the 2-thienyl-pyrrolidine of M8; the cyclopropyl in tandem with the 4-piperydinyl substituent of P1). Six other compounds revealed an inotropic potency of the same magnitude as the reference Diltiazem (B4, B6, B2, **M2,** M5, A4), whereas all of the remaining compounds (A3, A6, M4, M1, M3, M6, Me, B5) have very low negative inotropic potency.

On the basis of parameters like the selectivity and negative inotropic potency, four compounds have been selected (**M2, M7, M8 and P1**) and analyzed together with **5b** and **Diltiazem**, to investigate the affinity for the binding site of the latter (Figure 35).

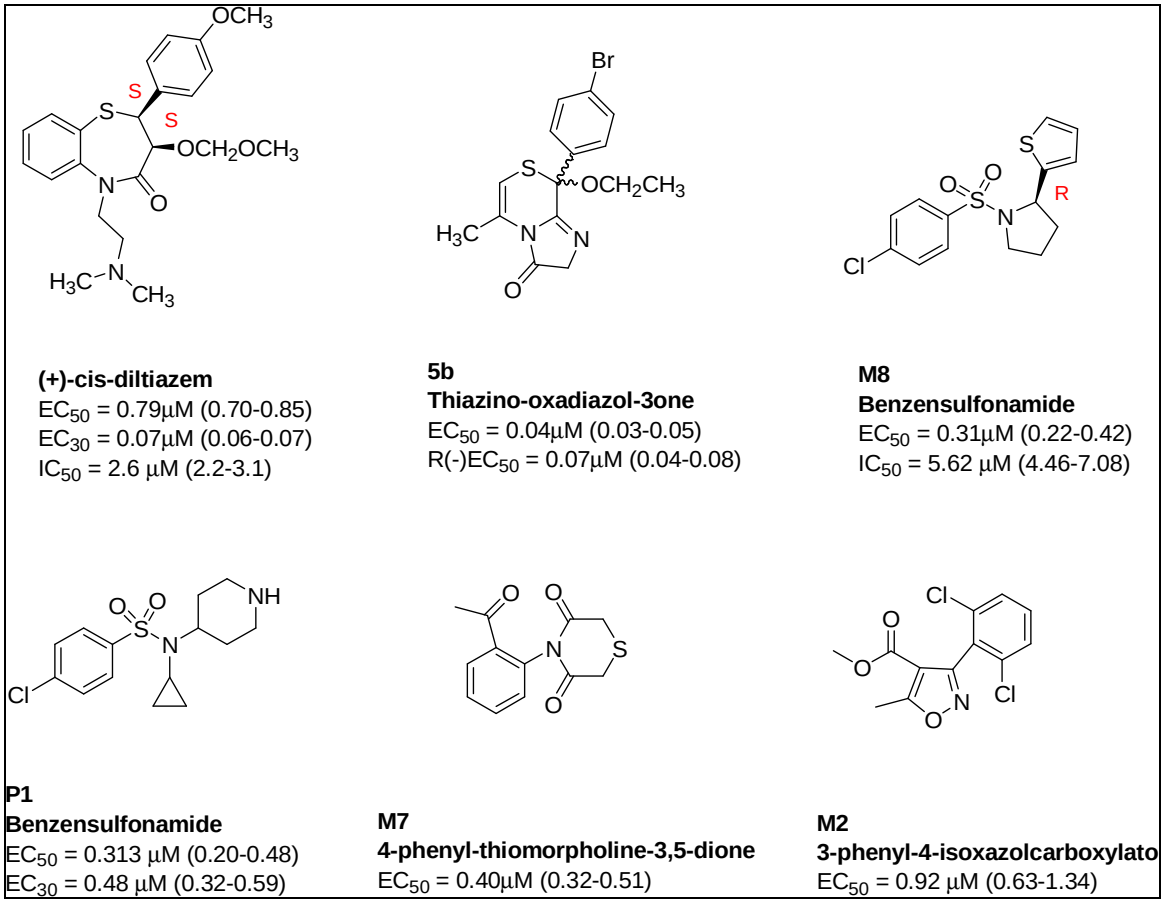

Figure 35. Structures, inotropic EC_{50}, chronotropic EC_{30} and vasorelaxant IC_{50} of Diltiazem and structurally related compounds (**5b**, **M8**, **P1**, **M7**, **M2**).

Further functional tests were carried out for these selected compounds on isolated tissues (left papillary muscle) to assess the ventricular inotropic effect and isolated organs (guinea-pig Langendorff perfused heart), to assess the cardiovascular profile.

Since the Ca^{2+} channel antagonists also have important inhibitory effects on vascular and nonvascular smooth muscle, further investigations examined the relaxant activity of these selected compounds on K^+ depolarized (80mM) guinea-pig ileum longitudinal smooth muscle. It is well-known that the Ca^{2+} influx may occur through two distinct pathways, one activated by membrane depolarization and the other by receptor-mediated events. The Ca^{2+} channel

antagonists appear to discriminate between these 2 processes, preferentially inhibiting mechanical responses of Ca^{2+} influx through the voltage-dependent Ca^{2+} channels (L-VDCC). For the newly synthesized Diltiazem analogs and the reference Diltiazem, the calcium channel antagonism was also determined as inhibition on the muscarinic receptor-mediated Ca^{2+}-dependent contraction of guinea-pig ileum longitudinal smooth muscle, induced by the muscarinic agonist carbachol.

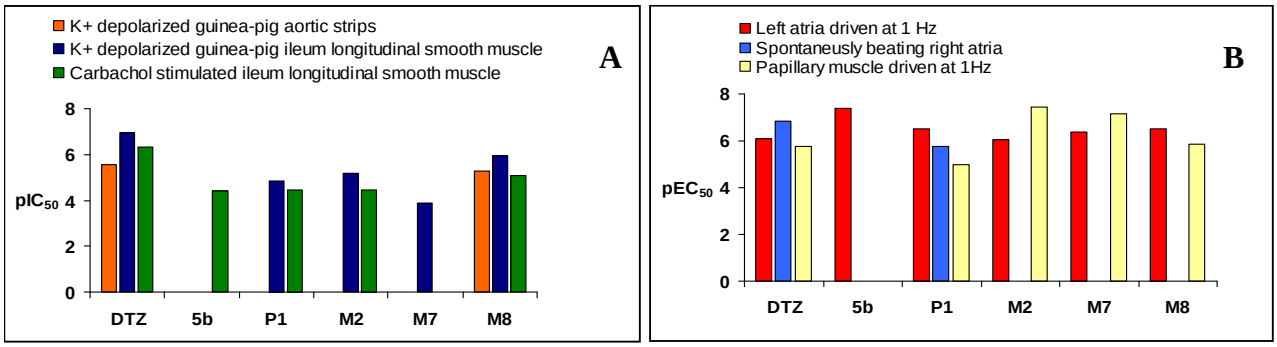

Figure 36. Potency of Diltiazem, **5b**, **P1**, **M2**, **M7** and **M8** in different guinea-pig preparations.

M8 was characterized by high activity and potency on vascular and non vascular tissue of the same order as that of Diltiazem. In this group, **M8** was the only compound showing vasorelaxant activity on both vascular and non-vascular smooth muscle similar to that of Diltiazem (Figure 36A). **P1, M2, M7** and **5b** possessed vasorelaxant effect only on non-vascular smooth muscle (guinea pig ileum longitudinal smooth muscle) with lower potency than Diltiazem. **P1** and **M2** inhibited both the membrane potential and muscarinic receptor-mediated Ca^{2+} dependent contraction. Interestingly, **M7** and **5b** showed vasorelaxant activity on non-vascular smooth muscle at lower potency compared with that of Diltiazem. **M7** inhibited Ca^{2+} influx activated by membrane potential, while **5b** inhibited Ca^{2+} influx caused by activation of muscarinic receptors.

With regard to the positive inotropic and chronotropic effect of the selected compounds, three different guinea pig heart preparations were utilized (Figure 36B): (1) paced left atria for inotropy, (2) spontaneously beating right atria for chronotropy and (3) papillary muscle for ventricular inotropy. **P1** displayed negative inotropic activity in paced left atria and papillary muscle, and in addition showed negative chronotropic potency similar to that of Diltiazem. **M2, M7** and **M8** showed negative inotropic effect both in left atria and

ventricular papillary muscle, and their potencies were higher than Diltiazem. The oxadiazolone **5b** was found to have negative inotropic potency only in left atria.

For the series of selected candidates, binding assay on rat cardiomyocytes was carried out in order to get information about their potential binding site. [^{3}H]Diltiazem (5nM) was incubated with increasing concentrations (0.1nM-100μM) of the selected compounds to generate a dose-response curve.

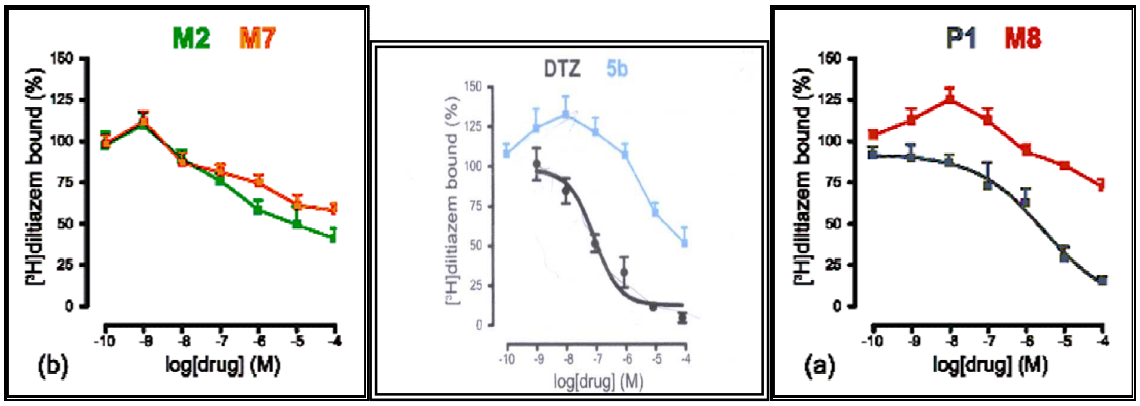

Figure 37. Effect of M2, M7, Diltiazem, 5b, P1 and M7 on ^{3}[H]Diltiazem binding.

Compounds **5b, M2, M7** and **M8** affected the binding of [^{3}H]Diltiazem, in a different manner. In fact, only **P1** caused a concentration-dependent inhibition of [^{3}H]Diltiazem binding. In contrast, **5b, M2, M8** and **M7** revealed a complex interaction with the benzothiazepine binding site producing a small stimulation of [^{3}H]Diltiazem binding at lower concentration, followed by partial inhibition at higher concentrations (Figure 37). The highest stimulation was observed with M8 (24.8% of control at 10nM), whereas the highest inhibition was displayed by M2 (59.6% at 100μM).

P1 completely inhibited [^{3}H]Diltiazem binding to rat cardiomyocytes, indicating a non benzothiazepine structure that can compete directly with Diltiazem at the benzothiazepine-binding site. This is consistent with the effects produced by **P1** on cardiac and non-vascular smooth muscle preparation where the molecule displayed the classical properties of a CCB. In addition, the minor effects displayed on vascular smooth muscle differentiated P1 from Diltiazem, suggesting that it might be classified as a unique CCB rather selective toward the cardiac tissue. The mixed pattern of modulation characteristics of the hits **M2, M7, M8** as well as **5b** is a preliminary indication that these compounds affect the benzothiazepine

receptor at low concentration by interacting at a distinct binding site, the occupation of which allosterically modulates Diltiazem binding in a positive manner. However, at higher concentrations, these molecules interact directly at the benzothiazepine binding site in the L-VDCC receptor complex [92].

Using the Langerdorff perfused guinea pig heart, only Diltiazem showed a significant influence on the left ventricular contractile force (-59 ± 4.2mmHg/s), heart rate (-25 ± 1.9beats/min), and coronary perfusion pressure (-51 ± 3.1mmHg).

Having these previously published results in evidence, we tried to focus in our studies on techniques which were not utilized before in terms of characterization of the selected Diltiazem analog compounds. For the comprehensive electrophysiological investigation of the newly developed compounds, the *Xenopus* oocytes heterologous expression system was used, mainly since this system is well established and routinely used in Dr. Schwartz's laboratory to study structure-function relationship of the L-VDCCs. Secondly, it is proven to be a very convenient system, relatively straightforward in terms of the technique and a good deal of valuable data can be generated within a year. Of course, as described in the "Methods" section in details, this system has advantages and disadvantages. One of the biggest disadvantages with respect to our study is that we were supposed to use a much higher concentration from the reference Diltiazem (and the newly synthesized compounds) than the therapeutic concentration which is in the single micromole range (Ref). However, we have to point out that the selected concentration of the BTZ Diltiazem used in our experiments is comparable with the concentration used by others, in many heterologous expression systems (both *Xenopus* oocytes and mammalian cell lines) and native cells (e.g. cardiomyocytes) [60,82,99,100,104,112-114]. It is well known that only the (+) cis-Diltiazem is the active enantiomer. In all of our experiments including the EP measurements, the racemic Diltiazem was used, commercially available from Sigma Chemical. In the *Xenopus* oocytes experiments, all of the compounds were applied in concentrations of 100μM for better comparisons with Diltiazem.

We examined the new Diltiazem analog compounds including **M2, M7, M8, P1** and **5b** and compared them with Diltiazem using *ex vivo* and *in vitro* methodologies also.

Ca^{2+} influx via voltage-dependent L-type Ca^{2+} channels ($Ca_v1.2$), found in cardiac and vascular smooth muscle, initiates contraction. Diltiazem, as the reference compound, is also used to

treat some types of supraventricular arrhythmias since it preferentially blocks channels that are activated at high frequency, a property known as frequency dependent block [115]. In some complementary experiments we took advantage of a mouse model overexpressing the HHT-α_{1C} subunit of the L-VDCC in mouse heart, which was developed in Dr. Schwartz's laboratory in 1998. This mouse model offered both a physiological and pharmacological tool to test the potential antiarrhythmic property of two newly synthesized compounds since this transgenic mouse (named α_{1C}-Tg) at 7-11 months of age (mo) develops cardiac remodeling with signs of arrhythmia. Overexpression of the α_{1C}-subunit increases inward I_{Ca} and this would indirectly increase SR Ca^{2+} uptake, potentially to levels that could produce spontaneous SR Ca^{2+} release and causes arrhythmias as a consequence. The action potential duration was also prolonged in older mice resulting from a reduced transient outward potassium current (I_{to}) and the increased inactivation time of I_{Ca}, all of which can increase the likelihood of arrhythmogenic tendency. In younger mice when the heart performed better than wild-type due to early signs of the hypertrophy phenotype with overexpressed calcium channels, mostly spontaneous extrasystoles occurred but in older age the cardiac function became impaired (heart failure) and tachycardia combined with compromised atrial-ventricular conduction (e.g. bradycardia) appeared in many animals. The arrhythmia signs were reflected by the recording of the left ventricular pressure. The "pressure-arrhythmia" incidence was around 50% in the α_{1C}-Tg mice at 7-10 mo and lasted sometimes 5-10min and thereafter returned spontaneously to normal sinus rhythm but in some instances, was continuous throughout the experiments (20min). Interestingly, perfusion of M2 and M8 to the Langendorff-heart reduced and in some cases completely suspended the incidence and the appearance of arrhythmia compared with those of DMSO-containing Tyrode solution perfused control group. However, this aspect of the study was not pursued in detail due to time limitations. The results are therefore considered to be preliminary and have been presented with caution. The observed "antiarrhythmic" effect of the two Diltiazem analogs is quite surprising since these compounds did not exert any use-dependency and had very little tonic block on both I_{Ba} and I_{Ca} (however, it was significant for M8 and M2; around 10%). We have not investigated the effect of these drugs on action potential duration mediated by sodium and potassium channels at different phases of the

repolarization process and hence have no definite explanation for this effect. It is assumed that these compounds might have an inhibitory effect on Na^+ or K^+ channels or perhaps the moderate inhibition of I_{Ca} by M2 and M8 might contribute to their anti-arrhythmic action in the present model.

The electrophysiological studies were performed in a heterologous expression system. Inward barium currents (I_{Ba}) (using 40mM Ba^{2+} as the charge carrier) were measured using two microelectrode voltage-clamp of *Xenopus* oocytes 3-4 days after microinjection of mRNA mixtures of human $\alpha_{1C}/\beta_3/\alpha_2/\delta$ [84] subunits. The voltage dependence and the kinetics of block by Diltiazem and M8 on L-VDCC (I_{Ca}) were investigated in mouse ventricular cardiomyocytes using the whole-cell patch clamp technique with 1.8 mM Ca^{2+} as charge carrier. The results, derived from the oocytes expression indicate that Diltiazem and the selected Diltiazem analogs in concentration of 100μM did not cause any substantial inhibition in I_{Ba} amplitude. Overall, there was no fundamental difference in the effect on the voltage-dependence of the *I-V* relationships between the selected compounds. The fitting yielded nearly identical values for either the half maximal potential or the slope factor.

Conditioned ("use-dependent") inhibition by Diltiazem is a characteristic property of L-type voltage dependent calcium channels. In the clinical setting, use-dependent drug action is therapeutically desirable property of the CCB antiarrhythmics. During repetitive depolarizations, the block by Diltiazem accumulates in a frequency and voltage-dependent manner because additional drug binds during each depolarization and fails to unbind completely at the resting potential between depolarizations. Such use-dependent block (UDB) is important for the clinical efficacy of the BTZ Diltiazem. As expected, I_{Ba} was efficiently blocked in a use-dependent manner by Diltiazem; in contrast, the selected Diltiazem analogs had no pronounced use-dependent block. In some recordings at 3 minutes (after perfusion with the compounds), progressive changes in Ba^{2+} currents were small and could be explained simply by combination of Ba^{2+} current "run-down" and the accumulation of Ca^{2+} channels in an inactivated state. Regarding the state-dependent Ca^{2+} channel block after exposure of the compounds, as stated above, very little change was observed except for M8 and M2. These compounds caused significant decrease in the peak I_{Ba} amplitude.

For comparison, and in order to confirm the results on native Ca^{2+}-channels, EP measurements were performed on mouse cardiomyocytes using EP protocols similar to those used in oocytes. Using a lower concentration of Diltiazem (10μM) in cardiomyocytes for block of I_{Ca} through $Ca_v1.2$ channels, it is obvious that more channels are blocked with Ca^{2+}, rather than with Ba^{2+} as the charge carrier. However, results by Dilmac [99] suggest that Ca^{2+}-dependent inactivation of $Ca_v1.2$ does not play a crucial role in the potentiation of Diltiazem block by Ca^{2+}. In contrast, in the presence of M8, no use-dependence block was observed and the current amplitude at the 15th pulse was not significantly different from control. The results might imply that these compounds are somewhat different from Diltiazem regarding their binding properties. The classic calcium antagonist such as Diltiazem binds to the same site between transmembrane segments IIIS6 and IVS6 in both opened and inactivated conformational states of the L-VDCC, with the inactivated state having a higher affinity for Diltiazem. Of course, this hypothesis already has been proven by the binding experiments previously published by Carosati *et al.* [92]. The use-dependent block depends on many factors: membrane potential, frequency and duration of the test pulse. In mouse cardiomyocytes the prolongation of the test pulse from 80ms to 400ms led to a more rapid and profound steady level of use-dependent block after application of Diltiazem but use-dependency was still absent for M8. Also, both Diltiazem and M8 produced slight tonic (resting-state-dependent) block in cardiomyocytes, however no significant differences were found in the mean values. The lack of appreciable tonic block indicates that the resting state has no significant affinity for these drugs.

Calcium channel inactivation is an important determinant of use-dependent Ca^{2+} channel block by Diltiazem (BTZ) and Verapamil (PAA). Hering *et al.* [81] were the first to suggest a close link between inactivation properties of the channel and use-dependent block by phenylalkylamines. Their data convincingly demonstrated that inactivation plays a key role in Ca^{2+} channel block by PAA. However, accelerated inactivation *per se* does not promote use-dependent PAA block of chimeric channels lacking the high affinity determinants in IVS6.

In cardiomyocytes, Lee *et al.* [115] found that faster inactivating Ca^{2+} currents are more efficiently blocked by PAA than slowly inactivating Ba^{2+} currents. In our experiments we had an unexpected finding: in spite of the diminished use-dependency by the new Diltiazem analogs, three compounds (**M8, M2 and P1**) accelerated the voltage dependence

inactivation in a time dependent manner. Comparatively, in *Xenopus* oocytes Diltiazem also accelerated the decay of the I_{Ba} current (inactivation time) during maintained step depolarization. We further calculated the time constant (τ values) with a single exponential equation. Effect of compound M8 on the voltage-dependent inactivation was also confirmed in cardiomyocytes. However, Diltiazem at a concentration of 10μM in cardiomyocytes did not show any effect on inactivation time despite its pronounced use-dependent block. According to the literature, Diltiazem displayed faster inactivation rate only in higher concentration even in the mammalian heterologous expression system using the enantiomer (+)-cis-Diltiazem [99]. The other feasible explanation for the discrepancy between the oocytes and native cells with regard to the effect of Diltiazem on the inactivation time of recombinant and native L-VDCC could be the co expression of HHT-α_{1C} with the β_3 subunit in oocytes. In heterologous expression system it is a well accepted procedure to co-express the auxiliary subunits with the pore forming α_{1C} subunit to increase channel expression.

It is well established that $Ca_v1.2$ inactivates in a Ca^{2+}-dependent and voltage-dependent manner. The rapid Ca^{2+} dependent component in the current decay is absent if Ba^{2+} served as charge carrier. The data by Dilmac *et al.* [99] suggest that Ca^{2+} dependent inactivation of $Ca_v1.2$ may involve Ca^{2+} binding in the pore that is modulated by conformational changes in the C-terminal tail. Diltiazem preferentially inhibits the channel when it resides in or near the open and/or inactivated state however, the underlying mechanism of the tonic block may also include blockade of channels in resting state. Such preferential inhibition of open/inactivated states could underlie the substantial use-dependent component of block observed in $Ca_v1.2$ channels in presence of BTZs and PAAs. Many compounds that show use-dependent block have an open-channel blocking action. The accelerated inactivation both in cardiomyocytes and oocytes after application of M8, M2 and P1 suggest that these drugs may act through blocking the open channels. However, we observed in cardiomyocytes, the Ca^{2+}-dependent I_{Ca} facilitation which is characterized by a stepwise increase of I_{Ca} amplitude and a slowing of inactivation during train of repetitive depolarizations. It requires CaMKII-dependent phosphorylation, presumably of the α_{1C}-subunit or an associated protein [116]. The facilitation did not interfere with the EP measurements since the use-dependent block by Diltiazem was very obvious.

In order to further determine the extent of inactivation of I_{Ba} or I_{Ca} a double-pulse protocol was applied. The steady state inactivation curves of wild-type (Wt) $Ca_v1.2$ channels before and after application of 100μM Diltiazem, M8,M2, M7, P1 and 5b were fitted to Boltzmann's equation. Diltiazem, M2, M8 and P1 displayed a slight, but significant negative shift in steady-state inactivation potentials compared with control (before drug). Especially, in cardiomyocytes, perfusion with 10μM M8 induced a more profound shift in the $V_{0.5}$ value compared to oocytes due to the use of Ca^{2+} as a charge carrier instead of Ba^{2+}. However, Diltiazem in a concentration of 10μM did not evoke significant change in the voltage-dependence of the availability of L-VDCC, in agreement with the unchanged inactivation decay of I_{Ca} at this concentration [115]. The finding that three newly synthesized benzothiazepine analogs caused a hyperpolarizing shift of the inactivation curve suggests that these compounds can interact with the inactivated channels in a special way. More importantly, the high affinity of M8, M2 and P1 (and Diltiazem) for the inactivated channels may cause these agents to act preferentially, on partially depolarized tissues in pathological conditions. Consequently, the potential reduction of Ca^{2+} influx under such conditions may contribute to a beneficial effect against arrhythmia.

We have characterized the Diltiazem and the new Diltiazem analogs on the VSM-α_{1Cb} channel expressed in *Xenopus* oocytes with a view to provide some information about the effect of the compounds on recombinant vascular smooth muscle Ca^{2+}-channels. It is of interest that the VSM-α_{1Cb} exhibited a slight left shift in its steady-state inactivation compared with that of HHT-α_{1C} (-15.8mV vs. -12.0mV, respectively). This rather small difference is important given the fact that for the generation of vascular tone, the smooth muscle $Ca_v1.2$ channel activates at more hyperpolarized potential as already discussed in the "Results" section. Noticeably, the only biophysical difference found in our study, as mentioned above is that, the VSM-α_{1Cb} channel inactivated closer to the resting potential compared with that of HHT-α_{1C}. According to the functional profile studies performed and published with the new Diltiazem analogs by Carosati *et al.* [92], M8 had a vasorelaxant activity in guinea pig aorta strips with EC50 value of 5.62μM compared with that of Diltiazem 2.6μM. Based on these EC50 values, M8 is 2 fold less sensitive on vascular smooth

muscle Ca^{2+}-channel than Diltiazem. Regarding the negative inotropic activity in left ventricular papillary muscle the EC50 values for Diltiazem and M8 were much different, 0.11μM vs. 1.18μM, respectively. This is a clear indication that racemic compound M8 has 10 fold less sensitivity to the ventricular L-VDCC compared with that of Diltiazem. In fact, based on our present results we do not have enough experimental evidence to delineate the contribution of Diltiazem and M8 to vascular and cardiac selectivity. Nevertheless, our results are somewhat consistent with the results published previously as no difference was found with regard to I_{Ba} inhibition through VSM-α_{1Cb} Ca^{2+} channel after application of M2, M7, P1 and 5b. At the same time, there is some discrepancy with the previous results described on the rat aorta strips, because in our experiments as mentioned above, neither Diltiazem nor M8 (100μM) displayed any substantial tonic block on the VSM-α_{1Cb} channel despite their effect on use-dependency/inactivation or both. The I_{Ba} block by Diltiazem and Diltiazem analogs in VSM-α_{1C} channels, in many respects is quite similar to the state dependence of Diltiazem blockade with HHT-α_{1C} channels. The discrepancy between our data and the published results may be due to the differences mainly in experimental conditions (like interspecies differences). First of all, we used recombinant channels instead of native channels. To be able to explain our findings on the *Xenopus* expression system we have to take into consideration several other factors. With an application time of 180 sec only acute effects can be studied. It is not absolutely sure that this perfusion time is sufficiently enough to induce all effects of the drugs. Therefore, it might be possible that due to problems in intracellular drug equilibrium, some of the described effects are not steady state and might increase at longer application time. However, to be able to increase the application time it would require an extremely good condition of oocytes and very good voltage clamp electrodes (to avoid clogging and damaging the oocytes). Based on the experience with the two-electrode voltage clamp on oocytes, it would require a tremendous amount of time and effort to comply with these two requirements. In addition, we have to take into consideration the Ca^{2+}-induced Cl^- current also in oocytes, when expressing Ca^{2+} channels. Therefore, before I_{Ba} measurements BAPTA is supposed to be injected into the oocytes in order to eliminate the Cl^--current and avoid its interference with the I_{Ba}-measurements. The other important issue as emphasized earlier is that oocytes require

much higher concentration of drugs to block ion channels than native cells. For example, single arterial vascular smooth muscle cells produced lower I_{Ca} amplitude in presence of Ca^{2+} containing recording solution (>2mM Ca^{2+}) compared with cardiomyocytes (or I_{Ba} in oocytes), and it is conceivable that such low I_{Ca} amplitude would enhance the effects of the drug. It will be interesting to check if differences in drug sensitivity of $Ca_v1.2$ (in heart and smooth muscle mRNAs) are related to a different subunit composition. Under physiological conditions the precise β-subunit composition of VSM-$Ca_v1.2$ is, however mostly unknown. Data from Colecraft *et al.* [51] suggests that β_{2b} is a good candidate for the endogenous cardiac β-subunit. As it was pointed out earlier, in our heterologous expression system, we have co-expressed the β_3 subunit with both HHT-α_{1C} and VSM-α_{1Cb}. It is possible that using double concentration from the racemic Diltiazem or using the active enantiomer (+) of Diltiazem we would have quite likely been able to see an increase in I_{Ba} block and as well as to distinguish between Diltiazem and M8 in terms of "vascular selectivity" that was observed in rat aorta tissue. However, more detailed knowledge about the β-subunit composition of VSM-$Ca_v1.2$ is required before our data on the recombinant VSM-α_{1Cb} Ca^{2+} channel can be correlated with pharmacological data obtained from native tissues. To address these problems the most potent Diltiazem analog compound should be investigated on native smooth muscle cells.

Furthermore, we have to note, that no functional consequences associated with the VSM splicing variants were observed so far, with one exception. The DHP Nisoldipine produced a marked inhibition of recombinant smooth muscle [85] inward calcium channel current in CHO cells, as shown by Welling [93]. However, DHPs exhibit a high affinity for the VSM-α_{1Cb} channels in the resting state. In a recent study, published in 2007, a novel smooth muscle $Ca_v1.2$ splice variant was reported ($Ca_v1.2$SM) that differs from the Biel *et al.* smooth muscle $Ca_v1.2$b [85] which was used for this study. The $Ca_v1.2$SM channel demonstrated a large hyperpolarizing shift in voltage-dependent inactivation and this gating property confers on the smooth muscle channel variant enhanced sensitivity to nifedipine compared with the $Ca_v1.2$b channel. In the future it would be interesting to test the effect of the novel compounds including the reference Diltiazem on this recombinant novel smooth muscle $Ca_v1.2$ splice variant.

Apart from the above discussed uncertainties and restrictions of our study on the oocytes expression system, in general, the present results reveal clear evidence and mechanism for drug effects on distinct calcium channel types.

In order to clarify the voltage-dependence of the use-dependent effect of M8 and Diltiazem, recovery of I_{Ba} from inactivation was measured by use of a double-pulse protocol. Both the pre- and test- pulse were stepped to +10mV and the pulse interval was varied between 20ms-28s. The ratio of I_{Ba} obtained by the test pulse to that elicited by the prepulse (fraction of recovery) is plotted as a function of the interpulse interval. After returning to a deep resting state (-100mV) following a voltage step, it takes a definite amount of time for the channels to recover from inactivation and conduct for the next depolarizing pulse. In some of our experiments, the kinetics of the slow component of I_{Ba} recovery from block after Diltiazem could not have been resolved because contamination by current "rundown" during long lasting measurements could not be excluded. As we described above, the recovery could be described by two phases: I_{Ba} rapidly recovered mono-exponentially to 80-90% of control within 10s (termed "fast recovery"), and the remaining current did not recover within the 10s period analyzed (termed "slow recovery"). From the total recoverable current, Kraus *et al.* [100] arbitrarily defined the contribution of "slow recovery" as the I_{Ba} not recovered after 15s. One model suggests that the channel opens on depolarization (state O) and then subsequently enters two inactivated states: I1 and I2. Two inactivated states were required to fit the bioexponential recovery from inactivation after 3s depolarization to +10mV, in the absence of drug. In this model, the rapidly recovering component arises from drug-bound open channels that are blocked during depolarizations and the slowly recovering component representing the drug bound inactivated channels. In the HHT-$Ca_v1.2$ channels, the slow recovery from block by Diltiazem was also predominantly caused by a slow rate of recovery of drug-bound, inactivated channels. The effect of Diltiazem resulted in a dramatic overall slowing of the recovery time course in wild type $Ca_v1.2$ channel. The unbinding rates suggest that Diltiazem bound to the channel receptors of open or inactivated channel more tightly and became trapped during the interval when the resting potential is held at -80mV. A delay in recovery from inactivation was previously observed for sodium channel inactivation and attributed to transition of channels to an additional (slow) inactivated state. Accumulation of sodium

channels in a slow inactivated state (for example by Lidocain) is induced by long lasting depolarization. The recovery from inactivation is described by exponential fit and the time constant for the recovery from the slow inactivated state ranging from several seconds to minutes. By analogy to sodium channels, interaction with local anesthetics slow inactivation time which may have a very important role in the antiarrhythmic effect of Ca^{2+}-antagonists. This delayed recovery was mainly due to an increase in the fast recovering component in good agreement with data by Dilmac *et al.* obtained on human tsA-201 (Human Embryonic Kidney) cells; however Diltiazem delayed the time course of the "slow recovering" component in some of our experiments which is also consistent with previous data [82]. Since Diltiazem promotes both fast and slowly recovering channel state, this explains the development of use-dependent block at a higher depolarization frequency [82]. It is believed that the time course of recovery from channel block is critically determined by the steric factors governing the rate of dissociation of the drug trapped within inactivated channel states. The size of the drug itself affects the rate of inactivation. Interestingly, the recovery from block by M8 was much faster than by Diltiazem, and it was comparable to control (absence of drug). In conclusion, our data demonstrate that the lack of use-dependent block after application of M8, M2, P1 and M7 during pulse trains is probably due to a change in recovery from inactivation and not the decreased inactivation during test pulses, since we observed faster inactivation times allowing more channels to enter a drug-bound state during the test train. The accelerated recovery from inactivation after **M8 and M2** in Wild type $Ca_v1.2$ (HHT and VSM) channel compared to that of Diltiazem indicates either that these compounds have decreased binding affinity for the binding site or have more rapid dissociation rate from the binding site after being trapped in a blocked channel state. Based on our EP data, it can be assumed that M8 has a steric structure that partially removes a dissociation barrier and facilitates dissociation of M8 from blocked (presumably open/inactivated) channel states. Therefore, we propose that the dramatic loss of use-dependency after introduction of M8 is due to the rapid dissociation of the drug from the binding site since recovery from inactivation after drug application was comparable to control or even slightly faster (**P1**).

The EP data also implies that **M8, M2, M7** and **5b** have a specific behavior and unique binding sites in close proximity and allosterically linked to the BTZ binding pocket and result

in a distinct effect from the classical representative benzothiazepine Diltiazem on L-VDCCs. Our hypothesis, that the newly developed compounds allosterically modulate the BTZ binding site, is supported by the previously reported binding studies [92], confirmed and indirectly supported by our results in Langendorff-perfused mouse heart preparations as well as in calcium transient measurements on isolated mouse ventricular cardiomyocytes. **M8, M2, M7** and **5b** produced a stimulatory effect on [^{3}H]Diltiazem binding at low concentration which was converted to an inhibitory at higher concentration. This finding correlates well with our results that some of the newly developed Diltiazem analogs produced biphasic effect *ex vivo and in vitro*: In lower concentrations (1μM or less), they evoked positive inotropic effect and at higher concentration this declined.

" The Ca^{2+} antagonistic potency of bezothiazepines is critically dependent on the presence of two pharmacophores, i.e., the basic amino group in ethyl linkage at position N-1 and hydrogen bond acceptor (preferentially a methoxy group) at position 4' on the 4-aryl ring. The affinity of BZT also increases with their hydrophobicity, indicating partitioning into a hydrophobic environment. This suggests that the benzothiazepine binding domain consists of a hydrophobic pocket that accommodates the hydrophobic substituted benzothiazepine ring next to a polar region that interacts with the basic amine"[63].

Taken together, our data convincingly show that the new Diltiazem analogs especially **M8, M2** and **P1** accelerated the inactivation decay of both recombinant Ca^{2+} channels in the *Xenopus* oocyte expression system and in cardiomyocytes without developing any evidence for use-dependent block which is very characteristic of the Diltiazem. The experiments described here suggest that depolarization of the membrane and opening of the channels were required for Diltiazem and the other Diltiazem analogs to exert their blocking action.

7. Limitations of the study future plans and final conclusion

In this study five newly developed Diltiazem analogs were systematically characterized and compared with the reference Diltiazem with regard to their inhibition on two classes of Ca^{2+} channels (cardiac α_{1C} and vascular smooth muscle α_{1Cb}) expressed in *Xenopus* oocytes and native mouse cardiomyocytes. In complementary experiments, we studied the effect of these compounds on the cardiac performance using Langendorff perfused mouse hearts and

on Ca^{2+} transients in isolated mouse cardiomyocytes. Previous data revealed several important properties of these compounds [92]. Among them, the [^{3}H]Diltiazem binding data provided strong indication that M8, M2 and M7 have a very specific profile resembling the characteristics of DHPs with respect to their positive allosteric modulation at the benzothiazepine binding sites. The dihyropyridine Ca^{2+} channel blockers are allosteric modulators and may act on the L-VDCC as either agonist favoring the open state or antagonist favoring inactivated state. The typical organic Ca^{2+} channel blockers including the DHPs, PAAs and BTZs bind to distinct, allosterically coupled, high affinity binding domains on the α_1 subunit of the L-VDCC (motifs IIIS6 and IVS5). During this study, independent lines of evidence confirmed this hypothesis: in lower concentrations (up to 1μM) some of these compounds elicited positive inotropic effect *ex vivo* accompanied with slight, but significant increase in Ca^{2+} transients in fura-2 loaded cardiomyocytes. An attempt was made to further elucidate the detailed mechanism of the interaction of these drugs with their receptor sites on recombinant Ca^{2+}-channels using electrophysiological measurements. Together with previous pharmacological and drug binding data the electrophysiological results generated in this study, provide some insight into the molecular mechanism that underlies the regulation of Ca^{2+} channel gating by these compounds.

Considering the restrictions of the oocyte system, our findings suggest that these compounds exert significant effect on channel inactivation but lack the use-dependent effect that is very characteristic of the BTZs. UDB is a "hallmark" of the antiarrhythmic activity. We used Diltiazem as a reference drug for comparison which exerts UDB associated with slowed recovery from inactivation process. During the use-dependency protocol, blocked channels accumulate because of incomplete recovery of drug-bound channels during diastole. The slowed recovery of drug bound channels can be explained by combination of the modulated receptor hypothesis [78,79] and the guarded receptor model [117]. The modulated receptor hypothesis proposes that antiarrhythmic drugs like Diltiazem have higher affinity for their binding sites during activated and inactivated gating states of the Ca^{2+} channel. Therefore, the unbinding of the drug and consequently, the recovery of the drug-bound channels is slowed down. The guarded receptor model emphasizes that the drug appears to bind to the channel protein when it assumes a specific conformation. Furthermore, based on this model, "*the state-dependent availability of the drug access path*

to and from their binding sites influences the binding and unbinding kinetics" [118]. Our findings with the Diltiazem analogs suggest that there must be other distinct structural elements in repeats III and IV, different from the amino acids most critical to Diltiazem binding (Y1490, A1494, I1497), that are involved in the drug effect. The existence of a physically distinct binding region controlling drug binding and access to the receptor fits naturally with a guarded receptor mechanism of drug inhibition.

According to our results the Ca^{2+}-channel block by Diltiazem and the new Diltiazem analogs on VSM-α_{1Cb} Ca^{2+} channels in *Xenopus* oocytes was quite similar to that of HHT-α_{1C} Ca^{2+} channels. The novel Diltiazem analog M8, M2 and P1, like Diltiazem, have little tonic block (significant block was observed only after application of M8 and M2), but accelerated the inactivation of I_{Ba}. These results are interpreted as resulting from the higher affinity of the drug for the open and inactivated Ca^{2+} channels.

In contrast, no change in the inactivation time constant of I_{Ca} was observed after Diltiazem was exposed in isolated mouse cardiomyocytes. It has been described for PAAs that the amount of block of cardiac I_{Ca} was dependent on the duration of a preceding depolarization. For Diltiazem, the blockade of inactivated channels may be particularly important because open channel block is not prominent even at the relatively high concentration of 50μM under certain experimental conditions. We superfused the cardiomyocytes with 10μM Diltiazem in the patch clamp experiments. In oocytes expression, M8, M2 and P1 significantly shifted the steady-state inactivation curves toward negative potential, suggesting that these compounds shift the Ca^{2+}-channels to the inactivated states as also observed with Diltiazem. In correlation with the unchanged inactivation time after Diltiazem exposure in cardiomyocytes, the steady-state inactivation curve was overlapped with the curve generated before drug. Diltiazem exhibited a slower recovery from inactivation in oocytes suggesting that this drug can interact with the inactivated channels with a slow dissociation rate. In contrast, M8, M2 and P1 demonstrated a fast recovery from inactivation which is possible due to the fast dissociation of these drugs from the Ca^{2+} channels, allowing the drug to dissociate before the next depolarizing test pulse is given. In general, drugs with very fast time constant of recovery have a very small effect on and block the calcium channel for too little time. Hondeghem named the type of antiarrhythmic drugs that showed

fast recovery from block "No effect" drugs. These agents "*might provide ideal competitive displacers to treat an overdose"* [119]. The other possible explanation for the fast recovery from inactivation, which is comparable with control, is that these newly synthesized compounds shift the Ca^{2+} channel into a rapidly recovering inactivated state. This hypothesis is partially supported by the fact that these drugs abolish use-dependent effect. Since M8 and M2 caused the biggest tonic block on recombinant cardiac Ca^{2+} channels, it is attractive to speculate that these compounds might exert some vasorelaxant effect. However, in our experimental design, no significant differences were obtained among the compounds using the VSM-α_{1Cb} compared with those of HHT-α_{1C} L-VDCCs. The explanation for that is quite complex and it was elaborated on this issue in the "Discussion" section. One feasible explanation for that is the importance of the L-VDCC subunits. Increasing evidence indicates that the drug sensitivity is affected by the composition of subunits in different expression system. The possibility that the same auxiliary subunits were coexpressed with the different α_1 subunits cannot be excluded and this contributed to our results. It would have been interesting to compare the biophysical properties of the novel smooth muscle $Ca_v1.2SM$ splice variant with the HHT-α_{1C} channel using the new Diltiazem analogs and Diltiazem applying the same EP protocols as in the present study. According to Liao *et al.* [97] data, the $Ca_v1.2SM$ channel demonstrated a large hyperpolarized shift in the voltage dependent inactivation curve and the gating property, modeling the native vascular smooth muscle L-VDCC. However, the relevance of $Ca_v1.2SM$ channels to the function of the smooth muscle in vessels requires additional proof but can potentially be used as a tool in future studies. However, due to the uncertainties of the oocytes expression system detailed in the "Methods" section, the most reliable information about the vasoselectivity and the gating properties of the novel compounds could be derived from experiments using native smooth muscle cells.

Some calcium channel blockers also have other mechanisms of action, such as interaction with α-adrenoreceptors, inhibition of intracellular Ca^{2+} release or influx of Ca^{2+} through receptor operated calcium channels [120]. The pharmacological properties of some Ca^{2+} channel blocking compounds are consistent with those of Diltiazem and Verapamil. These experiments are out of the scope of this study. These newly developed Diltiazem analogs

could extend our knowledge about the three dimensional structure of the benzothiazepine binding sites of the L-VDCCs. However, we can not be positive with regard to the potential clinical aspect of their usage.

8. BIBLIOGRAPHY

1. Splawski I, Timothy KW, Sharpe LM, Decher N, Kumar P, et al. (2004) Ca(V)1.2 calcium channel dysfunction causes a multisystem disorder including arrhythmia and autism. Cell 119: 19-31.
2. Bodi I, Mikala G, Koch SE, Akhter SA, Schwartz A (2005) The L-type calcium channel in the heart: the beat goes on. J Clin Invest 115: 3306-3317.
3. Catterall WA (2000) Structure and regulation of voltage-gated Ca^{2+} channels. Annu Rev Cell Dev Biol 16: 521-555.
4. Catterall WA, Goldin AL, Waxman SG (2005) International Union of Pharmacology. XLVII. Nomenclature and structure-function relationships of voltage-gated sodium channels. Pharmacol Rev 57: 397-409.
5. Perez-Reyes E (2003) Molecular physiology of low-voltage-activated t-type calcium channels. Physiol Rev 83: 117-161.
6. Yokoyama CT, Myers SJ, Fu J, Mockus SM, Scheuer T, et al. (2005) Mechanism of SNARE protein binding and regulation of Ca_v2 channels by phosphorylation of the synaptic protein interaction site. Mol Cell Neurosci 28: 1-17.
7. Lee JH, Cribbs LL, Perez-Reyes E (1999) Cloning of a novel four repeat protein related to voltage-gated sodium and calcium channels. FEBS Lett 445: 231-236.
8. Carafoli E, Santella L, Branca D, Brini M (2001) Generation, control, and processing of cellular calcium signals. Crit Rev Biochem Mol Biol 36: 107-260.
9. Takahashi M, Catterall WA (1987) Dihydropyridine-sensitive calcium channels in cardiac and skeletal muscle membranes: studies with antibodies against the alpha subunits. Biochemistry 26: 5518-5526.
10. Cataldi M, Perez-Reyes E, Tsien RW (2002) Differences in apparent pore sizes of low and high voltage-activated Ca2+ channels. J Biol Chem 277: 45969-45976.
11. Klockner U, Mikala G, Schwartz A, Varadi G (1996) Molecular studies of the asymmetric pore structure of the human cardiac voltage- dependent Ca^{2+} channel. Conserved residue, Glu-1086, regulates proton-dependent ion permeation. J Biol Chem 271: 22293-22296.
12. Mikala G, Bahinski A, Yatani A, Tang S, Schwartz A (1993) Differential contribution by conserved glutamate residues to an ion-selectivity site in the L-type Ca2+ channel pore. FEBS Lett 335: 265-269.
13. Koch SE, Bodi I, Schwartz A, Varadi G (2000) Architecture of Ca(2+) channel pore-lining segments revealed by covalent modification of substituted cysteines. J Biol Chem 275: 34493-34500.
14. Bezanilla F (2002) Voltage sensor movements. J Gen Physiol 120: 465-473.
15. De Jongh KS, Warner C, Catterall WA (1990) Subunits of purified calcium channels. Alpha 2 and delta are encoded by the same gene. J Biol Chem 265: 14738-14741.
16. Ellis SB, Williams ME, Ways NR, Brenner R, Sharp AH, et al. (1988) Sequence and expression of mRNAs encoding the alpha 1 and alpha 2 subunits of a DHP-sensitive calcium channel. Science 241: 1661-1664.
17. Qin N, Yagel S, Momplaisir ML, Codd EE, D'Andrea MR (2002) Molecular cloning and characterization of the human voltage-gated calcium channel alpha(2)delta-4 subunit. Mol Pharmacol 62: 485-496.

18. Muth JN, Varadi G, Schwartz A (2001) Use of transgenic mice to study voltage-dependent Ca2+ channels. Trends Pharmacol Sci 22: 526-532.
19. Mori Y, Mikala G, Varadi G, Kobayashi T, Koch S, et al. (1996) Molecular pharmacology of voltage-dependent calcium channels. Jpn J Pharmacol 72: 83-109.
20. Hofmann F, Biel M, Flockerzi V (1994) Molecular basis for Ca^{2+} channel diversity. Annu Rev Neurosci 17: 399-418.
21. Varadi G, Lory P, Schultz D, Varadi M, Schwartz A (1991) Acceleration of activation and inactivation by the beta subunit of the skeletal muscle calcium channel. Nature 352: 159-162.
22. Sutton KG, Martin DJ, Pinnock RD, Lee K, Scott RH (2002) Gabapentin inhibits high-threshold calcium channel currents in cultured rat dorsal root ganglion neurones. Br J Pharmacol 135: 257-265.
23. Marais E, Klugbauer N, Hofmann F (2001) Calcium channel alpha(2)delta subunits-structure and Gabapentin binding. Mol Pharmacol 59: 1243-1248.
24. Luo ZD, Calcutt NA, Higuera ES, Valder CR, Song YH, et al. (2002) Injury type-specific calcium channel alpha 2 delta-1 subunit up-regulation in rat neuropathic pain models correlates with antiallodynic effects of gabapentin. J Pharmacol Exp Ther 303: 1199-1205.
25. Ivanov SV, Ward JM, Tessarollo L, McAreavey D, Sachdev V, et al. (2004) Cerebellar ataxia, seizures, premature death, and cardiac abnormalities in mice with targeted disruption of the Cacna2d2 gene. Am J Pathol 165: 1007-1018.
26. Abernethy DR, Soldatov NM (2002) Structure-functional diversity of human L-type Ca2+ channel: perspectives for new pharmacological targets. J Pharmacol Exp Ther 300: 724-728.
27. Letts VA, Felix R, Biddlecome GH, Arikkath J, Mahaffey CL, et al. (1998) The mouse stargazer gene encodes a neuronal Ca^{2+}-channel gamma subunit. Nat Genet 19: 340-347.
28. Kang MG, Campbell KP (2003) Gamma subunit of voltage-activated calcium channels. J Biol Chem 278: 21315-21318.
29. Chen L, Chetkovich DM, Petralia RS, Sweeney NT, Kawasaki Y, et al. (2000) Stargazin regulates synaptic targeting of AMPA receptors by two distinct mechanisms. Nature 408: 936-943.
30. De Waard M, Pragnell M, Campbell KP (1994) Ca^{2+} channel regulation by a conserved beta subunit domain. Neuron 13: 495-503.
31. Pragnell M, De Waard M, Mori Y, Tanabe T, Snutch TP, et al. (1994) Calcium channel beta-subunit binds to a conserved motif in the I-II cytoplasmic linker of the alpha 1-subunit. Nature 368: 67-70.
32. Opatowsky Y, Chomsky-Hecht O, Kang MG, Campbell KP, Hirsch JA (2003) The voltage-dependent calcium channel beta subunit contains two stable interacting domains. J Biol Chem 278: 52323-52332.
33. Van Petegem F, Clark KA, Chatelain FC, Minor DL, Jr. (2004) Structure of a complex between a voltage-gated calcium channel beta-subunit and an alpha-subunit domain. Nature 429: 671-675.
34. Chen YH, Li MH, Zhang Y, He LL, Yamada Y, et al. (2004) Structural basis of the alpha1-beta subunit interaction of voltage-gated Ca^{2+} channels. Nature 429: 675-680.

35. Bichet D, Cornet V, Geib S, Carlier E, Volsen S, et al. (2000) The I-II loop of the Ca^{2+} channel alpha1 subunit contains an endoplasmic reticulum retention signal antagonized by the beta subunit. Neuron 25: 177-190.
36. Singer D, Biel M, Lotan I, Flockerzi V, Hofmann F, et al. (1991) The roles of the subunits in the function of the calcium channel. Science 253: 1553-1557.
37. Muth JN, Bodi I, Lewis W, Varadi G, Schwartz A (2001) A Ca(2+)-dependent transgenic model of cardiac hypertrophy: A role for protein kinase Calpha. Circulation 103: 140-147.
38. Chien AJ, Zhao X, Shirokov RE, Puri TS, Chang CF, et al. (1995) Roles of a membrane-localized beta subunit in the formation and targeting of functional L-type Ca^{2+} channels. J Biol Chem 270: 30036-30044.
39. Mikala G, Klockner U, Varadi M, Eisfeld J, Schwartz A, et al. (1998) cAMP-dependent phosphorylation sites and macroscopic activity of recombinant cardiac L-type calcium channels. Mol Cell Biochem 185: 95-109.
40. Schuhmann K, Voelker C, Hofer GF, Pflugelmeier H, Klugbauer N, et al. (1997) Essential role of the beta subunit in modulation of C-class L-type Ca^{2+} channels by intracellular pH. FEBS Lett 408: 75-80.
41. Cens T, Mangoni ME, Richard S, Nargeot J, Charnet P (1996) Coexpression of the beta2 subunit does not induce voltage-dependent facilitation of the class C L-type Ca channel. Pflugers Arch 431: 771-774.
42. Tareilus E, Roux M, Qin N, Olcese R, Zhou J, et al. (1997) A Xenopus oocyte beta subunit: evidence for a role in the assembly/expression of voltage-gated calcium channels that is separate from its role as a regulatory subunit. Proc Natl Acad Sci U S A 94: 1703-1708.
43. Yamaguchi H, Hara M, Strobeck M, Fukasawa K, Schwartz A, et al. (1998) Multiple modulation pathways of calcium channel activity by a beta subunit. Direct evidence of beta subunit participation in membrane trafficking of the alpha1C subunit. J Biol Chem 273: 19348-19356.
44. Viard P, Butcher AJ, Halet G, Davies A, Nurnberg B, et al. (2004) PI3K promotes voltage-dependent calcium channel trafficking to the plasma membrane. Nat Neurosci 7: 939-946.
45. Gregg RG, Messing A, Strube C, Beurg M, Moss R, et al. (1996) Absence of the beta subunit (cchb1) of the skeletal muscle dihydropyridine receptor alters expression of the alpha 1 subunit and eliminates excitation-contraction coupling. Proc Natl Acad Sci U S A 93: 13961-13966.
46. Ball SL, Powers PA, Shin HS, Morgans CW, Peachey NS, et al. (2002) Role of the beta(2) subunit of voltage-dependent calcium channels in the retinal outer plexiform layer. Invest Ophthalmol Vis Sci 43: 1595-1603.
47. Murakami M, Yamamura H, Murakami A, Okamura T, Nunoki K, et al. (2000) Conserved smooth muscle contractility and blood pressure increase in response to high-salt diet in mice lacking the beta3 subunit of the voltage-dependent calcium channel. J Cardiovasc Pharmacol 36 Suppl 2: S69-73.
48. Hullin R, Singer-Lahat D, Freichel M, Biel M, Dascal N, et al. (1992) Calcium channel beta subunit heterogeneity: functional expression of cloned cDNA from heart, aorta and brain. Embo J 11: 885-890.

49. Chien AJ, Carr KM, Shirokov RE, Rios E, Hosey MM (1996) Identification of palmitoylation sites within the L-type calcium channel beta2a subunit and effects on channel function. J Biol Chem 271: 26465-26468.
50. Qin N, Platano D, Olcese R, Costantin JL, Stefani E, et al. (1998) Unique regulatory properties of the type 2a Ca^{2+} channel beta subunit caused by palmitoylation. Proc Natl Acad Sci U S A 95: 4690-4695.
51. Colecraft HM, Alseikhan B, Takahashi SX, Chaudhuri D, Mittman S, et al. (2002) Novel functional properties of Ca(2+) channel beta subunits revealed by their expression in adult rat heart cells. J Physiol 541: 435-452.
52. Hullin R, Khan IF, Wirtz S, Mohacsi P, Varadi G, et al. (2003) Cardiac L-type calcium channel beta-subunits expressed in human heart have differential effects on single channel characteristics. J Biol Chem 278: 21623-21630.
53. Singh BN (2001) Morbidity and mortality in cardiovascular disorders: impact of reduced heart rate. J Cardiovasc Pharmacol Ther 6: 313-331.
54. Jessup M, Brozena S (2003) Heart failure. N Engl J Med 348: 2007-2018.
55. Hajjar RJ, MacRae CA (2002) Adrenergic-receptor polymorphisms and heart failure. N Engl J Med 347: 1196-1199.
56. Marks AR (2003) A guide for the perplexed: towards an understanding of the molecular basis of heart failure. Circulation 107: 1456-1459.
57. Hoshijima M, Chien KR (2002) Mixed signals in heart failure: cancer rules. J Clin Invest 109: 849-855.
58. He M, Bodi I, Mikala G, Schwartz A (1997) Motif III S5 of L-type calcium channels is involved in the dihydropyridine binding site. A combined radioligand binding and electrophysiological study. J Biol Chem 272: 2629-2633.
59. Hockerman GH, Johnson BD, Abbott MR, Scheuer T, Catterall WA (1997) Molecular determinants of high affinity phenylalkylamine block of L-type calcium channels in transmembrane segment IIIS6 and the pore region of the alpha1 subunit. J Biol Chem 272: 18759-18765.
60. Hering S, Aczel S, Grabner M, Doring F, Berjukow S, et al. (1996) Transfer of high sensitivity for benzothiazepines from L-type to class A (BI) calcium channels. J Biol Chem 271: 24471-24475.
61. Schuster A, Lacinova L, Klugbauer N, Ito H, Birnbaumer L, et al. (1996) The IVS6 segment of the L-type calcium channel is critical for the action of dihydropyridines and phenylalkylamines. Embo J 15: 2365-2370.
62. Hockerman GH, Johnson BD, Scheuer T, Catterall WA (1995) Molecular determinants of high affinity phenylalkylamine block of L-type calcium channels. J Biol Chem 270: 22119-22122.
63. Hering S, Savchenko A, Strubing C, Lakitsch M, Striessnig J (1993) Extracellular localization of the benzothiazepine binding domain of L-type Ca^{2+} channels. Mol Pharmacol 43: 820-826.
64. Channer KS (2001) Current management of symptomatic atrial fibrillation. Drugs 61: 1425-1437.
65. Lim SH, Anantharaman V, Teo WS (2002) Slow-infusion of calcium channel blockers in the emergency management of supraventricular tachycardia. Resuscitation 52: 167-174.

66. Echt DS, Liebson PR, Mitchell LB, Peters RW, Obias-Manno D, et al. (1991) Mortality and morbidity in patients receiving encainide, flecainide, or placebo. The Cardiac Arrhythmia Suppression Trial. N Engl J Med 324: 781-788.
67. Packer M, O'Connor CM, Ghali JK, Pressler ML, Carson PE, et al. (1996) Effect of amlodipine on morbidity and mortality in severe chronic heart failure. Prospective Randomized Amlodipine Survival Evaluation Study Group. N Engl J Med 335: 1107-1114.
68. Boden WE, Ziesche S, Carson PE, Conrad CH, Syat D, et al. (1996) Rationale and design of the third vasodilator-heart failure trial (V-HeFT III): felodipine as adjunctive therapy to enalapril and loop diuretics with or without digoxin in chronic congestive heart failure. V-HeFT III investigators. Am J Cardiol 77: 1078-1082.
69. Dunselman PH, Kuntze CE, van Bruggen A, Hamer JP, Scaf AH, et al. (1989) Efficacy of felodipine in congestive heart failure. Eur Heart J 10: 354-364.
70. Elkayam U, Amin J, Mehra A, Vasquez J, Weber L, et al. (1990) A prospective, randomized, double-blind, crossover study to compare the efficacy and safety of chronic nifedipine therapy with that of isosorbide dinitrate and their combination in the treatment of chronic congestive heart failure. Circulation 82: 1954-1961.
71. Furberg CD, Psaty BM, Meyer JV (1995) Nifedipine. Dose-related increase in mortality in patients with coronary heart disease. Circulation 92: 1326-1331.
72. (1992) Improved diastolic function with the calcium antagonist nisoldipine (coat-core) in patients post myocardial infarction: results of the DEFIANT study. Doppler Flow and Echocardiography in Functional cardiac Insufficiency: Assessment of Nisoldipine Therapy. Eur Heart J 13: 1496-1505.
73. (1990) Effect of verapamil on mortality and major events after acute myocardial infarction (the Danish Verapamil Infarction Trial II--DAVIT II). Am J Cardiol 66: 779-785.
74. Black HR, Elliott WJ, Grandits G, Grambsch P, Lucente T, et al. (2003) Principal results of the Controlled Onset Verapamil Investigation of Cardiovascular End Points (CONVINCE) trial. Jama 289: 2073-2082.
75. (1988) The effect of diltiazem on mortality and reinfarction after myocardial infarction. The Multicenter Diltiazem Postinfarction Trial Research Group. N Engl J Med 319: 385-392.
76. Kostis JB, Lacy CR, Cosgrove NM, Wilson AC (1997) Association of calcium channel blocker use with increased rate of acute myocardial infarction in patients with left ventricular dysfunction. Am Heart J 133: 550-557.
77. Ibrahim OA, Dunlap ME (2005) Combination pharmacologic therapies for heart failure: what next after angiotensin-converting enzyme inhibitors and beta-blockers? Curr Heart Fail Rep 2: 89-93.
78. Hille B (1977) Local anesthetics: hydrophilic and hydrophobic pathways for the drug-receptor reaction. J Gen Physiol 69: 497-515.
79. Hondeghem LM, Katzung BG (1977) Time- and voltage-dependent interactions of antiarrhythmic drugs with cardiac sodium channels. Biochim Biophys Acta 472: 373-398.
80. Hering S, Berjukow S, Aczel S, Timin EN (1998) Ca^{2+} channel block and inactivation: common molecular determinants. Trends Pharmacol Sci 19: 439-443.

81. Hering S, Aczel S, Kraus RL, Berjukow S, Striessnig J, et al. (1997) Molecular mechanism of use-dependent calcium channel block by phenylalkylamines: role of inactivation. Proc Natl Acad Sci U S A 94: 13323-13328.
82. Motoike HK, Bodi I, Nakayama H, Schwartz A, Varadi G (1999) A region in IVS5 of the human cardiac L-type calcium channel is required for the use-dependent block by phenylalkylamines and benzothiazepines. J Biol Chem 274: 9409-9420.
83. Bezanilla F (2000) The voltage sensor in voltage-dependent ion channels. Physiol Rev 80: 555-592.
84. Schultz D, Mikala G, Yatani A, Engle DB, Iles DE, et al. (1993) Cloning, chromosomal localization, and functional expression of the alpha 1 subunit of the L-type voltage-dependent calcium channel from normal human heart. Proc Natl Acad Sci U S A 90: 6228-6232.
85. Biel M, Ruth P, Bosse E, Hullin R, Stuhmer W, et al. (1990) Primary structure and functional expression of a high voltage activated calcium channel from rabbit lung. FEBS Lett 269: 409-412.
86. Collin T, Wang JJ, Nargeot J, Schwartz A (1993) Molecular cloning of three isoforms of the L-type voltage-dependent calcium channel beta subunit from normal human heart. Circ Res 72: 1337-1344.
87. Miledi R, Parker I, Sumikawa K (1983) Recording of single gamma-aminobutyrate- and acetylcholine-activated receptor channels translated by exogenous mRNA in Xenopus oocytes. Proc R Soc Lond B Biol Sci 218: 481-484.
88. Dascal N (1987) The use of Xenopus oocytes for the study of ion channels. CRC Crit Rev Biochem 22: 317-387.
89. Cole KS (1949) Some physical aspects of bioelectric phenomena. Proc Natl Acad Sci U S A 35: 558-566.
90. Hodgkin AL, Huxley AF, Katz B (1952) Measurement of current-voltage relations in the membrane of the giant axon of Loligo. J Physiol 116: 424-448.
91. Petrashevskaya NN, Bodi I, Rubio M, Molkentin JD, Schwartz A (2002) Cardiac function and electrical remodeling of the calcineurin-overexpressed transgenic mouse. Cardiovasc Res 54: 117-132.
92. Carosati E, Cruciani G, Chiarini A, Budriesi R, Ioan P, et al. (2006) Calcium channel antagonists discovered by a multidisciplinary approach. J Med Chem 49: 5206-5216.
93. Welling A, Kwan YW, Bosse E, Flockerzi V, Hofmann F, et al. (1993) Subunit-dependent modulation of recombinant L-type calcium channels. Molecular basis for dihydropyridine tissue selectivity. Circ Res 73: 974-980.
94. Hu H, Marban E (1998) Isoform-specific inhibition of L-type calcium channels by dihydropyridines is independent of isoform-specific gating properties. Mol Pharmacol 53: 902-907.
95. Lacinova L, Klugbauer N, Hofmann F (2000) State- and isoform-dependent interaction of isradipine with the alpha1C L-type calcium channel. Pflugers Arch 440: 50-60.
96. Koch WJ, Ellinor PT, Schwartz A (1990) cDNA cloning of a dihydropyridine-sensitive calcium channel from rat aorta. Evidence for the existence of alternatively spliced forms. J Biol Chem 265: 17786-17791.
97. Liao P, Yu D, Li G, Yong TF, Soon JL, et al. (2007) A smooth muscle $Ca_v1.2$ calcium channel splice variant underlies hyperpolarized window current and enhanced state-dependent inhibition by nifedipine. J Biol Chem 282: 35133-35142.

98. Liao P, Yu D, Lu S, Tang Z, Liang MC, et al. (2004) Smooth muscle-selective alternatively spliced exon generates functional variation in Cav1.2 calcium channels. J Biol Chem 279: 50329-50335.
99. Dilmac N, Hilliard N, Hockerman GH (2003) Molecular determinants of Ca^{2+} potentiation of diltiazem block and Ca^{2+}-dependent inactivation in the pore region of $Ca_v1.2$. Mol Pharmacol 64: 491-501.
100. Kraus RL, Hering S, Grabner M, Ostler D, Striessnig J (1998) Molecular mechanism of diltiazem interaction with L-type Ca^{2+} channels. J Biol Chem 273: 27205-27212.
101. Noble S, Shimoni Y (1981) The calcium and frequency dependence of the slow inward current 'staircase' in frog atrium. J Physiol 310: 57-75.
102. Pietrobon D, Hess P (1990) Novel mechanism of voltage-dependent gating in L-type calcium channels. Nature 346: 651-655.
103. Zuhlke RD, Pitt GS, Deisseroth K, Tsien RW, Reuter H (1999) Calmodulin supports both inactivation and facilitation of L-type calcium channels. Nature 399: 159-162.
104. Cai D, Mulle JG, Yue DT (1997) Inhibition of recombinant Ca^{2+} channels by benzothiazepines and phenylalkylamines: class-specific pharmacology and underlying molecular determinants. Mol Pharmacol 51: 872-881.
105. Vittone L, Mundina-Weilenmann C, Mattiazzi A, Cingolani H (1994) Physiologic and pharmacologic factors that affect myocardial relaxation. J Pharmacol Toxicol Methods 32: 7-18.
106. DePover A, Grupp IL, Grupp G, Schwartz A (1983) Diltiazem potentiates the negative inotropic action of nimodipine in heart. Biochem Biophys Res Commun 114: 922-929.
107. Muth JN, Yamaguchi H, Mikala G, Grupp IL, Lewis W, et al. (1999) Cardiac-specific overexpression of the alpha(1) subunit of the L-type voltage-dependent Ca(2+) channel in transgenic mice. Loss of isoproterenol-induced contraction. J Biol Chem 274: 21503-21506.
108. Balasubramaniam R, Chawla S, Mackenzie L, Schwiening CJ, Grace AA, et al. (2004) Nifedipine and diltiazem suppress ventricular arrhythmogenesis and calcium release in mouse hearts. Pflugers Arch 449: 150-158.
109. Walsh KB, Bryant SH, Schwartz A (1984) Diltiazem potentiates mechanical activity in mammalian skeletal muscle. Biochem Biophys Res Commun 122: 1091-1096.
110. Budriesi R, Cosimelli B, Ioan P, Lanza CZ, Spinelli D, et al. (2002) Cardiovascular characterization of [1,4]thiazino[3,4-c][1,2,4]oxadiazol-1-one derivatives: selective myocardial calcium channel modulators. J Med Chem 45: 3475-3481.
111. Budriesi R, Carosati E, Chiarini A, Cosimelli B, Cruciani G, et al. (2005) A new class of selective myocardial calcium channel modulators. 2. Role of the acetal chain in oxadiazol-3-one derivatives. J Med Chem 48: 2445-2456.
112. Rolf S, Haverkamp W, Borggrefe M, Musshoff U, Eckardt L, et al. (2000) Effects of antiarrhythmic drugs on cloned cardiac voltage-gated potassium channels expressed in Xenopus oocytes. Naunyn Schmiedebergs Arch Pharmacol 362: 22-31.
113. Niimi Y, Hino N, Ochi R (2003) Diltiazem facilitates inactivation of single L-type calcium channels in guinea pig ventricular myocytes. Jpn Heart J 44: 1005-1014.
114. Berjukow S, Gapp F, Aczel S, Sinnegger MJ, Mitterdorfer J, et al. (1999) Sequence differences between alpha1C and alpha1S Ca^{2+} channel subunits reveal structural determinants of a guarded and modulated benzothiazepine receptor. J Biol Chem 274: 6154-6160.

115. Lee KS, Tsien RW (1983) Mechanism of calcium channel blockade by verapamil, D600, diltiazem and nitrendipine in single dialysed heart cells. Nature 302: 790-794.
116. Xiao RP, Cheng H, Lederer WJ, Suzuki T, Lakatta EG (1994) Dual regulation of Ca^{2+}/calmodulin-dependent kinase II activity by membrane voltage and by calcium influx. Proc Natl Acad Sci U S A 91: 9659-9663.
117. Starmer CF, Grant AO, Strauss HC (1984) Mechanisms of use-dependent block of sodium channels in excitable membranes by local anesthetics. Biophys J 46: 15-27.
118. Lee PJ, Sunami A, Fozzard HA (2001) Cardiac-specific external paths for lidocaine, defined by isoform-specific residues, accelerate recovery from use-dependent block. Circ Res 89: 1014-1021.
119. Hondeghem LM (1987) Antiarrhythmic agents: modulated receptor applications. Circulation 75: 514-520.
120. Godfraind T, Miller R, Wibo M (1986) Calcium antagonism and calcium entry blockade. Pharmacol Rev 38: 321-416.